Chem Soc Rev

REVIEW ARTICLE

View Article Online
View Journal | View Issue

Flexible metal–organic frameworks

Cite this: *Chem. Soc. Rev.*, 2014, 43, 6062

A. Schneemann,[a] V. Bon,[b] I. Schwedler,[a] I. Senkovska,[b] S. Kaskel*[b] and R. A. Fischer*[a]

Advances in flexible and functional metal–organic frameworks (MOFs), also called soft porous crystals, are reviewed by covering the literature of the five years period 2009–2013 with reference to the early pertinent work since the late 1990s. Flexible MOFs combine the crystalline order of the underlying coordination network with cooperative structural transformability. These materials can respond to physical and chemical stimuli of various kinds in a tunable fashion by molecular design, which does not exist for other known solid-state materials. Among the fascinating properties are so-called breathing and swelling phenomena as a function of host–guest interactions. Phase transitions are triggered by guest adsorption/desorption, photochemical, thermal, and mechanical stimuli. Other important flexible properties of MOFs, such as linker rotation and sub-net sliding, which are not necessarily accompanied by crystallographic phase transitions, are briefly mentioned as well. Emphasis is given on reviewing the recent progress in application of *in situ* characterization techniques and the results of theoretical approaches to characterize and understand the breathing mechanisms and phase transitions. The flexible MOF systems, which are discussed, are categorized by the type of metal-nodes involved and how their coordination chemistry with the linker molecules controls the framework dynamics. Aspects of tailoring the flexible and responsive properties by the mixed component solid-solution concept are included, and as well examples of possible applications of flexible metal–organic frameworks for separation, catalysis, sensing, and biomedicine.

Received 3rd March 2014

DOI: 10.1039/c4cs00101j

www.rsc.org/csr

[a] *Anorganische Chemie II – Organometallics and Materials, Ruhr-Universität Bochum, Universitätsstr. 150, D-44801 Bochum, Germany. E-mail: Roland.Fischer@rub.de*

[b] *Department of Inorganic Chemistry, Technische Universität Dresden, Bergstr. 66, D-01069 Dresden, Germany. E-mail: stefan.kaskel@chemie.tu-dresden.de*

1. Introduction

The analogy between metal–organic frameworks and porous network compounds based on purely inorganic building units, such as aluminosilicates (zeolites) or aluminophosphates, is

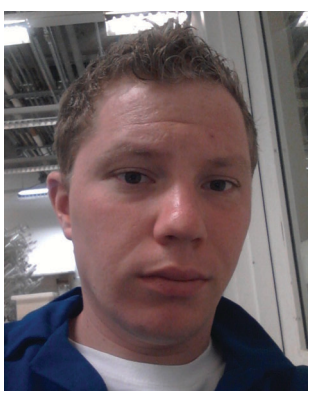

A. Schneemann

Andreas Schneemann originates from Sprockhövel, Germany. He achieved his BSc in Industrial Chemistry in 2009 under the supervision of Prof. W. Grünert at the Ruhr-University Bochum and his MSc in Inorganic Chemistry under the guidance of Prof. R. A. Fischer in 2011. He spent time abroad in the labs of Dr I. A. Fallis at Cardiff University (Erasmus scholarship) and Prof. S. M. Cohen at the University of California, San Diego (DAAD fellowship). He is currently a graduate student in the group of Prof. R. A. Fischer at the Ruhr-University Bochum, working on flexible and functionalized metal–organic frameworks.

V. Bon

Volodymyr Bon, 32 years old, received his PhD in 2008 from the Institute of General and Inorganic Chemistry, National Academy of Sciences of Ukraine. In 2011, he joined the group of Prof. Kaskel, Dresden University of Technology, as a postdoctoral researcher. His current research focuses on the design, synthesis, and crystal structure analysis of new MOF materials, as well as in situ X-ray diffraction during gas adsorption on flexible crystalline porous solids.

much related to reticular synthesis aiming at the control of the pore structure and coordination space in such kind of materials. Chemical and thermal robustness of MOFs, including structural rigidity during reversible adsorption/desorption, have been key features in terms of possible industrial applications in catalysis and gas storage/separation[1–3] and herein MOFs are challenging established porous materials. During the last decade, however, it has become increasingly evident that there is much room for discoveries and design beyond the concept of looking at MOFs just as more or less zeolite-like materials. Exploiting the advantage of a wide expanded set of modular molecular building units of virtually unlimited combinatorial possibilities[4] and thus going much beyond the limitations of zeolites (at least from the view-point of synthesis and structural chemistry) is crucial. A so-called third-generation of functional MOFs has been rising since its prediction in 1998.[5] These materials are characterized by dynamic features of the framework structure and may be called "soft porous crystals" (SPCs).[6] Obviously, the pre-requisite of structural responsivity of a crystalline solid towards external stimuli is non-rigidity, *i.e.* "flexibility". In a way, some disadvantages of the first-generation of porous coordination network compounds, namely the collapse upon guest (solvent) removal, can be turned into a unique functional advantage, if the building units and the structure are properly chosen or designed:

I. Schwedler

Inke Schwedler obtained her MSc in 2013 at the Ruhr-University of Bochum, concentrating on MOFs under the supervision of Prof. R. A. Fischer. From her early Bachelor studies on, she was a fellow of the German National Academic Foundation. During the course of her studies she spent 6 months at Cardiff University (Erasmus scholarship). Part of her master thesis was performed in the group of Prof. A. K. Cheetham at the University of Cambridge (funded by the German National Academic Foundation). She joined the group of Prof. Fischer in November 2013 for her doctoral studies. Her research concentrates on functionalized metal–organic frameworks.

I. Senkovska

Irena Senkovska was born and raised in Ukraine. She received her diploma in Chemistry from Ivan Franko National University of Lviv, Ukraine. In 2004, she obtained her PhD degree in natural sciences from the Ulm University, Germany. Since 2005 she has been a research assistant in the Institute of Inorganic Chemistry at Dresden University of Technology. Her research interests involve design, synthesis and applications of metal–organic frameworks.

S. Kaskel

Prof. Dr Stefan Kaskel studied chemistry and received his PhD in Tübingen in 1997. After a post-doctoral stay as a Feodor Lynen fellow of the Alexander von Humboldt foundation in the group of J. D. Corbett, he obtained his habilitation degree in 2003 at Bochum University on the design and functionality of new porous materials when he also worked as a group leader at the Max Planck Institute for Coal Research from 2002 to 2004. Since June 2004, he has been Professor of Inorganic Chemistry at Dresden University of Technology and, from 2008 on, also the head of Department of Thin-film Technology at the Fraunhofer Institute for Material and Beam Technology (IWS), Dresden. Stefan Kaskel is the coordinator of the German MOF program (2008–2014, www.metal-organic-frameworks.de) with 36 groups in Germany supported by DFG in the area of MOFs.

R. A. Fischer

Roland A. Fischer studied chemistry at Technische Universität München (TUM) and received his Dr rer. nat. in 1989 under the guidance of Wolfgang A. Herrmann. After a postdoctoral collaboration with Herb D. Kaesz at the University of California, Los Angeles (UCLA), he returned to TUM in 1990, where he obtained his Habilitation in 1995. In 1996 he was appointed Associate Professor at Ruprecht-Karls Universität Heidelberg. In 1998 he moved to Ruhr-Universität Bochum where he took the chair in Inorganic Chemistry II. He was Dean of the Ruhr University Research School (2006–2009). His research interests focus on group 13/transition metal compounds, precursor chemistry for inorganic materials, chemical vapour deposition (CVD), thin films, nanoparticles, colloids and in particular the supramolecular chemistry and property tailoring of porous coordination network compounds (MOFs).

"Soft porous crystals are defined as porous solids that possess both a highly ordered network and structural transformability. They are bistable or multistable crystalline materials with long range structural ordering, a reversible transformability between states, and permanent porosity. The term porosity means that at least one crystal phase possesses space that can be occupied by guest molecules, so that the framework exhibits reproducible guest adsorption" (cited from S. Horike *et al.*[6]).

This definition of SPCs refers to reversible structural transformations of the type crystal-to-crystal or crystal-to-amorphous (or less crystalline), which are essentially phase transitions. So-called breathing MOFs, which feature a drastic change in unit cell volume (pore volume) upon external stimuli (*e.g.* guest molecule adsorption/desorption), are prominent examples of SPCs.[7] These materials transform between open pore and closed pore (**cp**) or narrow pore (**np**) and large pore (**lp**) forms. The field has been pioneered by the groups of S. Kitagawa and G. Ferey and has been expanding since the first major conceptual article has appeared in 2004.[8] However, among the about 20 000 coordination network structures, which may be classified as MOFs and are listed in the Cambridge Structural Database (CSD), only less than 100 compounds reveal substantial breathing (**np** ↔ **lp**) transitions or related stimuli responsive properties. The progress has been reviewed continuously and we explicitly refer to these excellent previous articles.[5–13] The latest article by D. M. Jenkins and co-authors refers to breathing MOFs based on categorizing breathing modes or mechanisms by the concept of dimensional rigidity, *i.e.* analyzing which part of the framework is (more) rigid and which part is (more) flexible.[12] Herein, we will build upon these previous reviews and provide a collection of representative examples for discussion of the various modes of flexibility of MOFs, which are important for the progress of the field. Therefore, we will not restrict our definition of "flexibility" or "softness" to phase-transitions and breathing phenomena in a narrow sense, rather we will include some examples of dynamic features of MOFs, which are not connected with larger changes of the unit cell volume. Reviewing the recent literature published after the last comprehensive review in 2009,[7] it was striking that there are numerous examples of MOF systems showing structural flexibility. However, only a few systematic studies are conducted, which mostly concentrate on MIL-53 (Materiaux Institute Lavoisier), MIL-88 or paddle-wheel based pillared-layered frameworks. In our review we will cover several flexible MOF systems beyond those, nonetheless, also focusing on the archetypal systems. Also we will include sections on *in situ* analysis, computational modeling and applications of flexible properties of MOFs (Fig. 1). The various forms of applications and conceptual visions around flexible MOFs viewed as soft porous crystals have been discussed in the perspective review by S. Kitagawa and co-workers.[6]

The advantages and potential application fields of flexible materials were recognized very early. For example, by exploiting the flexible properties of the human hair to absorb and release water from air with slight changes in its dimensions and weight, Leonardo da Vinci was able to build the first hygrometer. The diversity of envisioned applications of flexible MOFs is remarkable, however, most of the investigations performed up to now concern gas separation (pressure-swing adsorption) and sensor technology.[14] For the adsorptive gas separation process, high capacity and highly selective adsorbents are key factors to realize the energy-efficient adsorption separation. In principle, flexible MOFs can combine these two requirements due to the general high adsorption capacity on one side, and the ideal selectivity in the pressure region, where one of the components can open the framework and the second one cannot, on the other side. Therefore, the challenge is to engineer a flexible MOF in a way that only specific interactions dominate the recognition and pore opening for a targeted adsorptive. Furthermore, for pressure swing adsorption, materials with small volume changes associated with gate opening (for example linker rotation caused adsorption) would be beneficial. For the application of MOFs as adsorbents for adsorptive gas storage, the so called working capacity is crucial. It is the difference in adsorption capacity at maximum storage pressure and the residual amount of gas at the lowest pressure allowed into the storage tank. Microporous MOFs show excellent overall uptake of gas, but quite low pressure (usually below 5, or even below 1 bar) should be applied to remove the gas from the MOF completely. The gate pressure MOFs with "gate closing pressure" in the right pressure region (above 1 bar) can help to overcome this problem. The vision is to go beyond host–guest interaction related stimuli, and expand the functional concept of framework responsiveness to factors causing the structural changes being dependent on general physical stimuli, such as light, mechanical deformation, thermal, electrical or magnetic stimuli. The reversible and controllable change of the materials density, dimensions, and optical, magnetic, and electrical properties is a requirement for using a flexible MOF as a sensor or a switching device. Combination of fundamental physical properties of stimuli responsive frameworks with host–guest interactions will create novel perspectives for unique functions. Eventually, the integration of such materials into a working system must be solved. The latter would greatly facilitate system integration in established technology fields, such as microsensors, micromechanical devices, and nanomedicine. For instance, using unique properties of selective adsorption, flexible MOFs could be used as catalytic nanoreactors, adsorbing exclusively educts from a mixture and then releasing the reaction products from the pores by applying an external stimulus. An enormous change in cell volume during adsorption could be used for the construction of micromechanical devices by transformation of volume expansion into mechanical energy.

2. General aspects of framework flexibility

For a systematic discussion of flexible MOFs in the following chapters, we need to classify the different modes of framework flexibility. One widely accepted possible distinction of the different modes of flexibility was presented by Bousquet *et al.* and Coudert *et al.* (Fig. 2).[15,16] Usually, framework flexibility is connected with supramolecular host–guest interactions. However, MOFs as soft porous crystals may show framework flexibility also

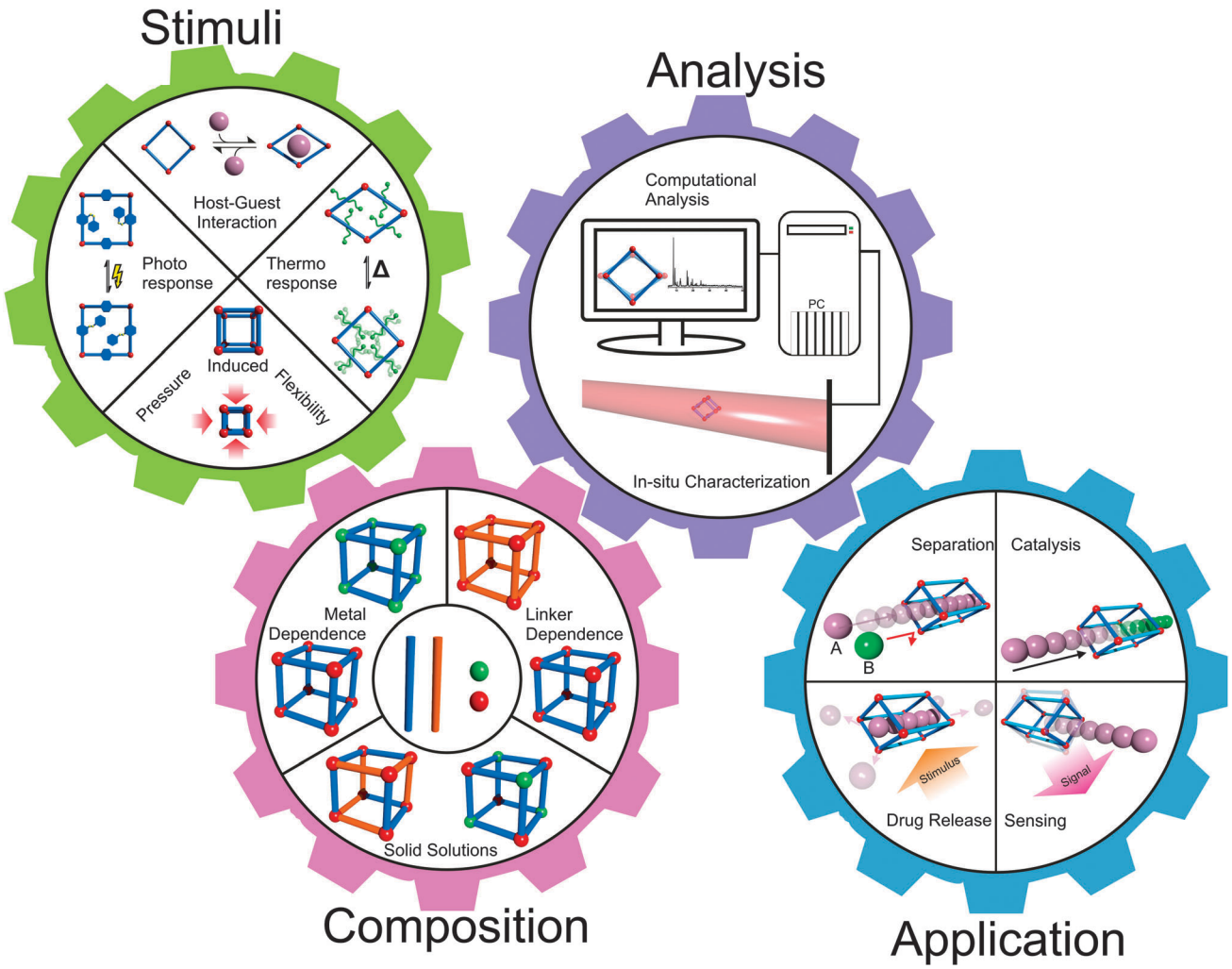

Fig. 1 Schematic overview of the content of this review, focusing on the stimuli used to trigger phase transitions, methods to control the composition of MOFs, *in situ* analysis methods and possible future applications.

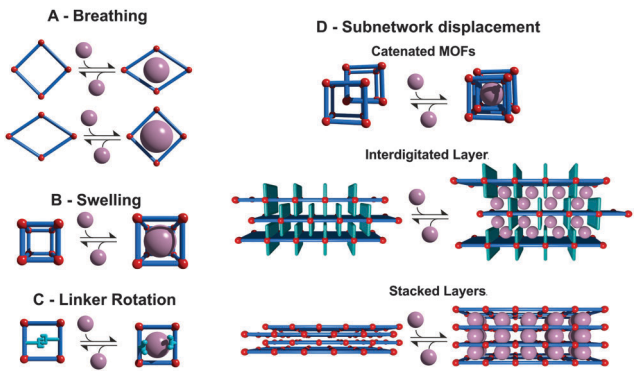

Fig. 2 Classification of different flexibility modes of MOFs. One class is characterized by the change in unit cell volume ($\Delta V \neq 0$; A, B and D) while in the other case the unit cell volume does not change ($\Delta V = 0$; C, D).

in the absence of guests or without the involvement of adsorption and desorption phenomena. Flexibility or responsivity may be triggered by an external stimulus in general (by guests and external force fields, such as mechanical stress, temperature and interactions with light, *etc.*; furthermore electrical and magnetic interactions are predicted to be further possible stimuli).

2.1. Breathing, swelling, linker rotation and subnetwork displacement

As *breathing* we want to entitle (reversible) transitions of metal–organic frameworks, during which the (substantial) displacement of atoms of the framework is accompanied by a change in unit cell volume ($\Delta V \neq 0$). Characteristic distances and angles of the unit cell change and the crystallographic space groups of the two distinct phases (**np** and **lp**) may be different. The prototypical example for this kind of flexibility is the MIL-53(M) family ($[M(bdc)(OH)]_n$ with bdc = 1,4-benzenedicarboxylate, and M = Al,[17] Fe,[18] Cr,[19,20] Sc,[21] Ga,[22] In[23]). Because of the wide variety of structure forming metals and linker derivatives, the influence of different structure building units on the framework flexibility has been extensively studied from a theoretical and experimental point of view, with more than 400 publications published up to date.

The *swelling* mode is characterized by a (gradual) enlargement of the MOF unit cell volume ($\Delta V \neq 0$) without a change in

the unit cell shape and typically without a change in the space group.

The most representative material possessing the swelling mode of flexibility is MIL-88.[24] The crystal structure is based on a trimeric $M_3O(H_2O)_2X^{6+}$ (M = Fe^{3+}, Cr^{3+}; X = F^-, OH^-) SBU (Secondary Building Unit) that consists of three truncated tetrahedra that are interconnected by dicarboxylic acids: fumaric acid (MIL-88A), bdc (MIL-88B), 2,6-ndc (2,6-naphthalenedicarboxylate; MIL-88C) or bpdc (4,4′-biphenyldicarboxylate; MIL-88D).[25] The changes in the unit cell parameters and cell volume are found to be strongly guest dependent. Thus, starting from the evacuated structure (423 K) of MIL-88A, the volume of the unit cell increases from 1135 Å^3 to 1840 Å^3 in the case of *n*-butanol adsorption, to 1970 Å^3 after adsorption of ethanol, to 2090 Å^3 for the methanol filled material, and to 2110 Å^3 after soaking in water.[24]

A flexibility mode which is also related to swelling is thermal expansion or shrinking in the absence of guest molecules (or not triggered by guest adsorption/desorption), which is found for some of the most archetypal "rigid" MOFs, *e.g.* MOF-5 (also known as IRMOF-1; $[Zn_4O(bdc)_3]_n$)[26] or HKUST-1 (Hong Kong University of Science and Technology; $[Cu_3(btc)_2]_n$ btc = 1,3,5-benzenetricarboxylate).[27] The phenomenon of thermal expansion of such MOFs will not be the focus of this article.

Linker rotation is defined as a (continuous) transition where the spatial alignment of a linker is changed by turning around a rotational axis. A simple prototype of this flexibility mode is ZIF-8 (Zeolitic Imidazolate Framework, $[Zn(mIm)_2]_n$, mIm = 2-methylimidazole).[28] The inconsistence of the crystallographically determined pore windows size with the adsorption properties of the material forced the MOF community to explain this phenomenon. The combined experimental and theoretical studies have led to the conclusion that the rotational linker movement causes the expansion of the pore windows and the adsorption of molecules larger than expected.[29,30] Framework flexibility based on linker rotation can be used to engineer special functions. One interesting example was presented by Seo *et al.* The framework $[Cd_2(pzdc)_2(BHE\text{-}bpb)]_n$ (pzdc = 2,3-pyrazinedicarboxylate; BHE-bpb = 2,5-bis(2-hydroxyethoxy)-1,4-bis(4-pyridyl)benzene) consists of $[Cd_2(pzdc)_2]_n$ layers interconnected by alkyloxy functionalized pyridyl linkers.[31] At the end of the alkyloxy side chains of the pyridyl pillars an OH group is situated, which can interact with the OH groups of neighboring pyridyl pillars. These interactions lead to a gating of the pore, which triggers selectivity in adsorption of certain guest molecules. If polar molecules approach the gate, they can interact with the metal center. This leads to a rotation of the pillar, which eventually ends up in the opening of the pore space (Fig. 3).

Subnetwork displacement is a phenomenon restricted to systems having individual frameworks, which are not connected to each other by (strong) chemical bonds, but interact only by rather weak forces (van der Waals interactions) and thus the subnets can drift, relocate, or shift in regard to each other. This includes interpenetrated three dimensional (3D) frameworks, as well as interdigitated and stacked two dimensional (2D) frameworks.[8,32–34] For instance, the 2D MOF $[Cu(dhbc)_2(bipy)]$

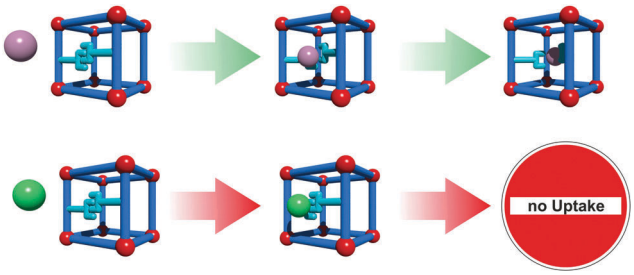

Fig. 3 Concept of guest selective gate-opening based on linker rotation. Blue rods represent linkers, red spheres SBUs and purple/green spheres potential adsorptive molecules. Only the molecule which owns the appropriate chemical property, the key to unlock the gate, can enter the pore.

(Hdhbc = 2,5-dihydroxybenzoic acid, 4,4′-bipy = 4,4′-bipyridine) shows a gate-opening/closing after a certain threshold pressure of nitrogen, oxygen or methane is applied.[35] Interpenetration has been considered for a long time as a drawback in the design of porous materials. There have been many strategies developed to avoid catenation to achieve ultra large pore spaces *e.g.* the use of topologies that cannot interpenetrate (*e.g.* **rht**),[36] bulky side chains[37,38] or template addition.[39] However, the adsorption of small molecules (*e.g.* H_2) can benefit from interpenetration. By confining the pore space, the number of adsorption sites increases and also the specific matching of the cavity of the MOF to the target molecule can increase.[40,41]

Within the concept of taking advantage of softness and flexibility, the interest connected with catenation and interdigitation is the possibility of inducing sorption selectivity (guest recognition) by guest selective, induced subnetwork movements. An outstanding example of the usefulness of catenation for sorption selectivity was given by Maji *et al.*[32] with a pillared-layer framework consisting of two dimensional $[Ni(bpe)_2]_n$ (bpe = 1,2-bis(4-pyridyl)ethane) sheets, which are connected by dicyanamide pillars ($N(CN)_2^-$). The as-synthesized (**as**) onefold interpenetrated framework has the composition $[(Ni(bpe)_2(N(CN_2)))(N(CN_2))(H_2O)_5]_n$, accommodating water, as well as $N(CN)_2^-$ anions. The two interpenetrated nets are positioned in such a way that there are two different types of channels. One small channel (2.81 × 0.61 Å^2), incorporating the $N(CN)_2^-$ anions and one large channel (6.50 × 4.74 Å^2), incorporating the water. After activation at elevated temperatures, the water is removed, yielding $[Ni(bpe)_2(N(CN_2))][(N(CN_2))]_n$, which retains the pore structure of the **as** form with only small changes. The permanently porous framework can undergo a subnetwork shifting transition by exchange of $N(CN)_2^-$ with N_3^-. A second interesting example was given by Yang *et al.*[42] The MOF $[(Me_2\text{-}NH_2)_{1.75}[In(BTPC)]_{1.75}]_n$ (NOTT-202a; University of NOTTingham) based on the tetratopic linker biphenyl-3,3′,5,5′-tetra(phenyl-4-carboxylate) (BTPC) is interpenetrated and consists of two crystallographically independent nets (A and B). Net A has binodal diamondoid topology. In contrast to net A, net B is composed of two disordered equally occupied nets (B1 and B2) that are interwoven into each other. The overall structure can be viewed as a partially interpenetrated framework with the ratio of two nets, A and B, of 1 : 0.75.

This compound is highly flexible, but so far it is not clarified if the flexibility arises from subnetwork mobility or transitions within the respective independent frameworks.

2.2. Photoresponsivity

If organic molecules, which change their conformation or structure upon interaction with light, known as photoswitches, are implemented into MOFs, the pore size and shape, and hence the ability to adsorb certain guests, can be controlled by light irradiation. The most common way to introduce photoswitches is their addition as a functional side group to the linker. Even though there is a wide range of different photoswitchable molecules, only the prototypical azobenzene group has been incorporated into MOFs so far. In most cases the azobenzene photoswitch dangles into the pore and after light exposure (365 nm) changes its conformation from *trans* to *cis*. This is usually accompanied by a change in the accessibility of the pore space. The switch to the initial state can be triggered by either absorption of light of a higher wavelength (*i.e.* 440 nm) or by heating (Fig. 4). An example of a photoswitchable linker was first given by Modrow *et al.*[43] In their work, an azobenzene functionalized bipyridine derivative was used in the synthesis of the pillared-layer based framework $[Zn_2(2,6\text{-ndc})_2(\text{azo-bipy})]_n$ (azo-bipy = 3-azo-phenyl-4,4′-bipyridine). Exposure of the material to light of a wavelength of 365 nm triggers the transition of the linker from the thermodynamically stable *trans* to the *cis* isomer. A reversible switching back can be achieved by either irradiation with light of a wavelength of 440 nm or by thermal treatment. This concept was pursued by other groups and further exploited. Brown *et al.*[44] were able to prepare an azobenzene functionalized linker that can be introduced into IRMOF-74-III $[Mg_2(C_{26}H_{16}O_6N_2)]_n$. By switching from the *trans*-conformer to the *cis*-conformer, the pore aperture expands from 8.3 Å to 10.3 Å. Also the light-induced release of adsorbed dye was demonstrated by controlling the conformation of the azobenzene with the appropriate wavelength of light. Park *et al.* prepared an IRMOF-1 derivative containing azobenzene functionalized bdc-type linker.[45] Notably, when the azobenzene is in the *cis*-conformation, the material has a substantially lower CO_2 uptake in comparison to the material containing the linker in the *trans*-conformation.

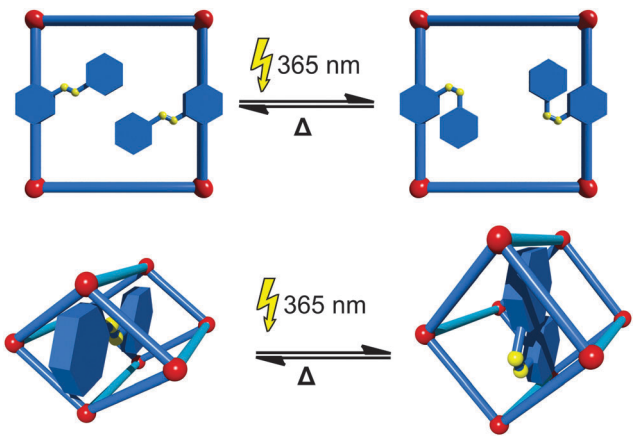

Fig. 4 Illustration of the photochemically induced phase transitions in metal–organic frameworks. Top: Linker functionalization with photoswitchable units in a rigid MOF. Bottom: employment of a photoswitch in a host–guest fashion into a flexible MOF.

A different approach was undertaken by Yanai and coworkers.[46] In their work the $[Zn_2(bdc)_2(dabco)]_n$ (dabco = 1,4-diazabicyclo-[2.2.2]octane) framework was loaded with azobenzene photoswitches as guest molecules. The $[Zn_2(bdc)_2(dabco)]_n$ framework is known to perform slight changes in the crystal structure upon exposure to different solvents.[47] Interestingly, the $[Zn_2(bdc)_2(dabco)]_n$ framework is also able to mimic the behavior of the photoswitch. When the azobenzene is present in the *cis* form, the MOF is contracted around the azobenzene guest. After exposure to light, the conformation of the guest is changed to the *trans* isomer and the framework expands to the **lp** form. Photoresponsive MOFs are still very scarce.

The third approach to incorporate photoswitchable behavior into a MOF is to use flexible linkers that undergo a reversible conformational change upon light exposure. Although the implementation of photoswitchable backbones into metal–organic frameworks could be achieved, light induced flexibility of the framework could be observed only in one case.

Lyndon *et al.*[48] prepared a triply interpenetrated pillared layered framework built up from an azobenzene containing pillar and a stilbene containing linker with the formula $[Zn_2(AzDC)_2(4,4'\text{-bpe})]_n$ (AzDC = azobenzene-4,4′-dicarboxylate; 4,4′-bpe = *trans*-1,2-bis(4-pyridyl)ethylene). The light-induced conversions between the two isomeric forms of the framework were confirmed by adsorption measurements: the structure changes are reflected in the large variation of CO_2 uptake. The transition between the *cis* and *trans* isomer is very rapid and local – no structure of the **lp** phase that triggers the CO_2 release could be determined.

2.3. Thermoresponsivity

Thermoresponsive MOFs are all those MOFs that show a reversible change in their lattice parameters after exposure to a temperature program without alteration of the molecular composition. Thus, materials that contain solvent guests are excluded from this class, since exposure to elevated temperature in this case would only lead to a phase transition induced by guest desorption. In this context we need to distinguish between two phenomena. Based on the structure at room temperature, (i) systems that after activation are present in their large pore form and (ii) systems that are contracted and possess narrow pores after activation. Systems in group (i) are most likely to undergo a phase transition when cooled and systems from group (ii) undergo a reversible phase transition when heated. Negative or positive thermal expansion (NTE or PTE, respectively) is a phenomenon that describes the expansion or shrinkage of a framework before a complete phase transition occurs. In other words, NTE and PTE are continuous processes.

Some representative materials, which show PTE or NTE, and respectively changes in their unit cell parameters during the heating/cooling from room temperature until the threshold temperature of the phase transition is reached, are listed in Table 1.

Table 1 Thermal expansion coefficients α of some metal–organic frameworks and metal–cyanide coordination polymers

MOF	Axis	α (MK^{-1})	Ref.
$Cd(im)_2$	*a*, *b*	+ 92.6, −22.5	51
MOF-5	*a*	−16	52
HKUST-1	*a*	−7.5	53
Ag(mIm)	*a*, *b*, *c*	+130, +44, −24.5	54
HMOF-1	*a*, *b*, *c*	+177, −21, +2.1	55
FMOF-1	*a*, *c*	+230, −170	56
$[Zn_2(BME\text{-}bdc)_2(dabco)]_n$	*a*, *b*	−380, +1161	57
$[Ni(H_2diol)(DMF)_2]_n$	*a*, *c*	+16, +323	58
$[Zn(NIY\text{-}bc)(OH)]_n$	*a*, *b*, *c*	−21, −21, +127	59
$Ag_3[Co(CN)_6]$	*a*, *b*	+150, −130	60
$Cd(CN)_2$	*a*	20.4	61
$Zn(CN)_2$	*a*	16.9	61

A common method to compare PTE and NTE of materials is to compare their thermal expansion coefficients α.

A prominent example is the well studied MIL-53 system. Upon cooling down *in vacuo* to low temperatures a **lp** → **np** phase transition is observed at approximately 125 K.[49] A large hysteresis (volume *vs.* *T*) is observed and the material transforms gradually back to the **lp** form above 325 K and the phase transition is finished at approximately 375 K. Theoretical calculations lead to the assumption that this behavior is caused by a decrease of the benzene rings motion. Their fast rotation is believed to help span the diamond shaped channels of MIL-53(Al). Walker *et al.*[50] took a closer look at the origins of the thermally induced flexibility of MIL-53(Al) and found that dispersive interactions stabilize the **np** at low temperatures. At increased temperatures the higher entropy of the rotating linker molecules leads to the formation of the **lp** phase.

Another example of a material that shows a **np** → **lp** transformation is a functionalized analogue of the $[Zn_2(bdc)_2(dabco)]_n$[62] system, namely $[Zn_2(BME\text{-}bdc)_2(dabco)]_n$ (BME-bdc = 2,5-bis(2-methoxyethoxy)benzenedicarboxylate).[57]

The pores of this material are filled with dangling side chains that can interact with each other (Fig. 5A). In the as-synthesized state, the pores additionally accommodate solvent molecules and the material is present in the **lp** form. Upon activation, contraction to the **np** form occurs. When the temperature is increased, the thermal movement of the linkers' side chains is increased (and hence the side chains require more space) inducing the pore swelling and phase transition to the **lp** form at 493 K. Interestingly, the temperature for this phase transition is highly dependent on the type of linker functionalization (fu-bdc = functionalized benzene-1,4-dicarboxylate) in a series of $[Zn_2(fu\text{-}bdc)_2(dabco)]_n$. When the BME-bdc linker is exchanged by the analogue DB-bdc (2,5-dibutoxybenzenedicarboxylate), a much lower transition temperature is observed (120 K). However, if this linker is used, the phase transition is not fully reversible. By preparing solid solutions containing both mentioned linkers, the transition temperature is tunable over a considerable range. Similar observations were made by Grobler *et al.*[59] for a zinc(II) containing MOF of the composition $[Zn(NIY\text{-}bc)(OH)]_n$. The used asymmetric (1*H*-naphtho[2,3-*d*]imidazol-1-yl)benzoate (NIY-bc) linker has a rotational degree of freedom along its bridging axis (Fig. 5B).

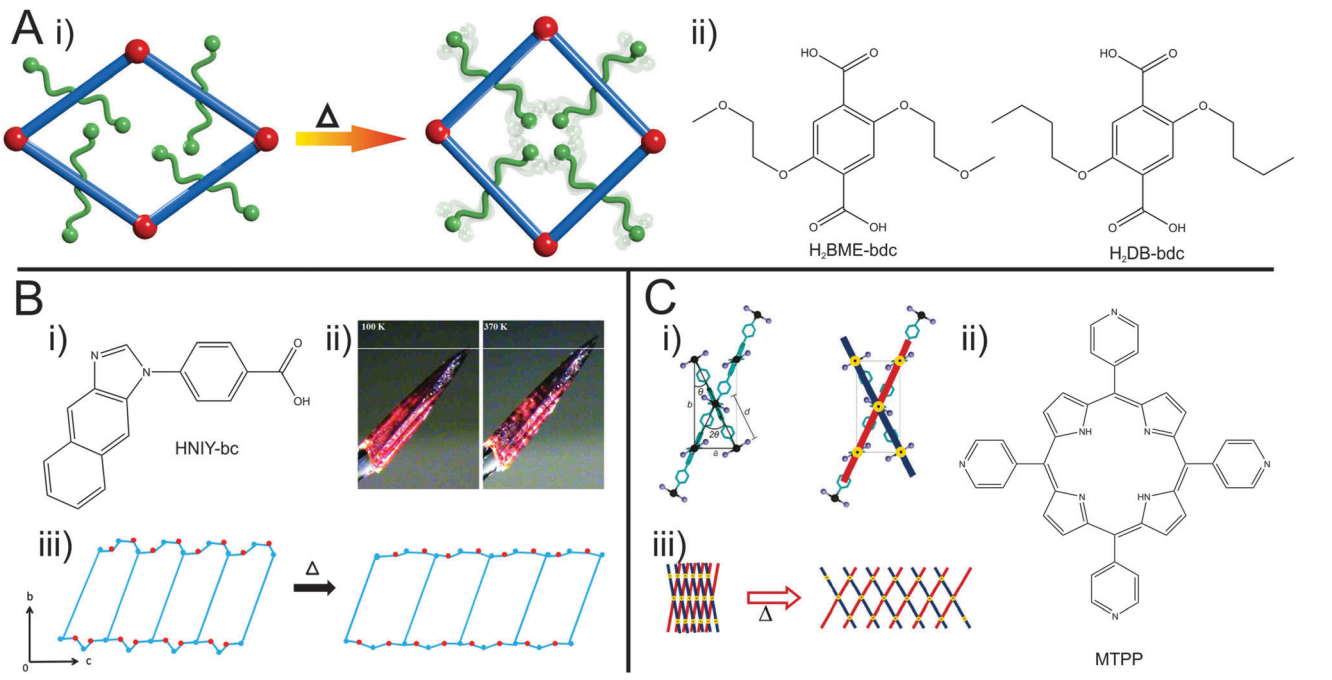

Fig. 5 (A) – (i) Schematic illustration of the pore re-opening of $[Zn_2(BME\text{-}bdc)_{2-x}(DB\text{-}bdc)_x(dabco)]_n$ upon exposure to heat; (ii) functionalized bdc-type linkers H_2BME-bdc and H_2DB-bdc; (B) – (i) linker used in the synthesis of $[Zn(NIY\text{-}bc)(OH)]_n$. (ii) Photograph of a single crystal of the compound at different temperatures (100 K left and 370 K right); (iii) depiction of the phase transition occurring in the framework. (C) – (i) Schematic representation of the hinge in HMOF; (ii) illustration of the porphyrin linker (MTPP) incorporated into HMOF. (iii) Representation of the "lattice-fence-like" expansion of HMOF upon heating. (Reprinted with permission.[55,57,59] Copyright 2013. American Chemical Society.)

When heated until a certain threshold temperature, the rotation is so strong that the pores open in order to avoid energetically non-beneficial collision of naphthalene groups from neighboring NIY-bc molecules.

A further example of a MOF featuring a phase transition upon heating was shown by DeVries *et al.*[55] The framework called HMOF (Hinged Metal–Organic Framework; Fig. 5C) was prepared from CdI_2 and a *meso*-tetra(4-pyridyl)porphine linker (MTPP). Each cadmium ion possesses an octahedral coordination sphere, with 4 pyridyl groups of different porphine linkers coordinating to the Cd in the equatorial position and two iodines coordinating in the axial position. Two of the equatorially coordinating porphines contribute to the formation of a 2D sheet. The other two porphines belong to the second grid, skewed to the initial grid. This leads to a lattice-fence like topology, where parallel grids are linked by grids skewed to them. In this arrangement, the axially coordinating iodine ions of adjacent grids are in close proximity to each other. By heating, the iodines' thermal movement increases and neighbouring iodine molecules start to repulse each other, leading to a swinging out of the lattice fence-like structure. The common motif of these examples of *guest independent* thermal responsiveness is most likely entropy based motions of the linkers. If dangling (and flexible) side groups are pinned to the backbone of the linkers, the effect of their motions is transduced to the framework.

Thermal amorphization is another phenomenon observed for some materials. Bennett *et al.*[63] presented a series of ZIF like materials that undergo an amorphization after heating to 300 °C. Interestingly, when the material is heated to 450 °C the formation of a new, dense, high temperature phase is observed. The amorphous phase and the high temperature phase are recoverable to room temperature.

2.4. Mechanical properties, elasticity

The mechanical property of MOFs, their "softness", is associated with a highly anisotropic elastic behavior of the materials. This property is fundamental to all the above mentioned stimuli dependent phenomena, which are related to structural flexibility. Cheetham and co-workers pioneered the investigation of the mechanical properties of dense and porous coordination network compounds and metal–organic frameworks.[64] Various phenomena, like pressure induced amorphization[65,66] or phase transitions to a new high pressure phase,[67] inaccessible by conventional synthetic methods, have been reported. However, these types of structural transformations are not necessarily reversible, while compressions are in any case considered to be fully reversible after the pressure has changed back to the initial conditions.[68–70] Interestingly, some MOFs not only show stress induced reversible deformations, but undergo a complete phase transition, giving rise to an additional stimulus triggering flexibility. ZIF-8 is an interesting example in this context (Fig. 6). Chapman *et al.*[66] showed that the framework is compressed rapidly by 5% when a pressure of 0.34 GPa is applied (under hydrostatic and non-hydrostatic conditions). When the pressure is further increased, an irreversible phase

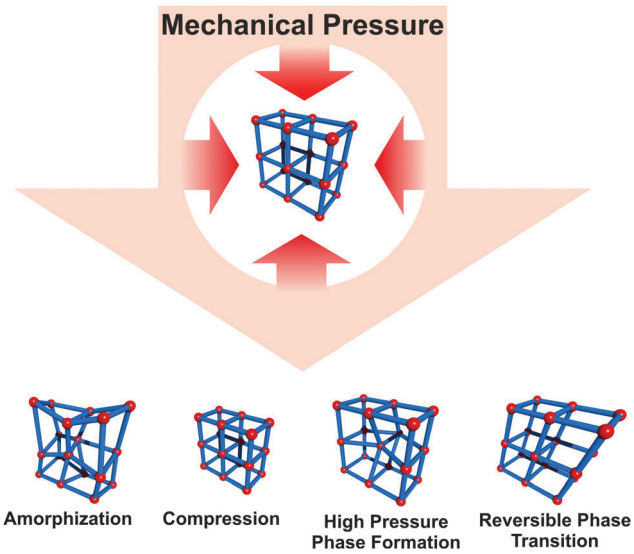

Fig. 6 Depiction of possible transformations MOFs can undergo upon applying mechanical pressure.

transition to an amorphous state is observed, however, N_2 adsorption shows that this state is still highly porous. Moggach *et al.*[67] performed *in situ* single X-ray diffraction on ZIF-8 with increasing pressure (under hydrostatic conditions with EtOH/MeOH as a pressure transducer). The authors show, that the unit cell volume increases first (4900.5 $Å^3$ → 4999.6 $Å^3$) up to a pressure of 0.18 GPa. From that point the unit cell volume decreases until a pressure of 0.96 GPa, and the volume of the unit cell reaches a value similar to the initial one (4893.5 $Å^3$). From this pressure, the cell volume increases again, and a phase transition to a new high pressure-phase occurs at 1.47 GPa. The obtained high pressure-phase of ZIF-8 regains the initial status at a pressure of 0.82 GPa during pressure reduction. It is reasoned that the twisting and reorientation of the linker are responsible for the observed phase transition. Gagnon *et al.*[70] analyzed the behavior of a zinc phosphonate framework $[Zn(BB\text{-}pc)\cdot 2H_2O]_n$ (ZAG-4) (Zinc-Alkyl Gate; BB-pc = 1,4-butanebis(phosphonic acid)) under increasing pressure (hydrostatic conditions, EtOH–MeOH mixture). In this case a steady reduction of the unit cell volume to 27% was observed, while increasing the pressure up to 7.32 bar. Interestingly, all cell parameters shrink until a pressure of 1.65 GPa is reached. From this point on, the length of the *b*-axis slightly increases, while *a* and *c* continue to decrease. After reaching ambient pressures again, the structure goes back to the initial state. The reason for this behavior is attributed to a drastic decrease of the O–Zn–O angle and the distance between the Zn atoms in the SBU.

An example of pressure induced linear elastic phenomena in MOFs is negative linear compressibility (NLC).[71] When a sample is exposed to pressure, usually a compression along all three unit cell axis is expected. However, in some cases the shrinkage is anisotropic and while two cell parameters decrease, the third one might increase. This anisotropic behavior upon compression is labeled as NLC. Since there are only a few examples from the world of metal–organic frameworks, we will not further

stress this nonetheless very interesting example. Yot *et al.*[72] showed that MIL-47(V(IV)) $[V(O)(bdc)]_n$ (the V containing analogue of MIL-53) which is classified as a rigid material, undergoes a phase transition from the activated **lp** phase to the **np** phase when a certain mechanical pressure is applied. The mechanochemical behavior of this material was surveyed using Hg porosimetry and high pressure X-ray diffraction. In the intrusion curve three distinct regions are observed, which can be explained as follows. At the start of the measurement, the material is present in the known **lp** phase and the powder is compressed into the penetrometer (below 2 MPa), afterwards the interparticle volume is filled with Hg (2–3.5 MPa).

Interestingly, at 85 MPa the authors observe an increase of intruded Hg, which they correlate to a switch from the **lp** to the **np**, since they assume that the pore size of MIL-47(V) is too narrow to let the Hg penetrate. In this case, mercury only acts as a pressure transducer. To confirm these findings, high pressure PXRD (powder X-ray diffraction) measurements with silicone oil as a pressure transducer were performed, which fit well to the assumptions made from the porosimetry measurements. Similar experiments on MIL-53(Cr) also show pressure induced phase transitions.[73]

2.5. Nanoscale and memory effects

Downsizing MOF crystallites to the mesoscale regime can alter the gas adsorption properties (kinetics as well as overall uptake).[74–78] However, there have been only a few studies involving nanosized flexible MOFs. For example, the X-ray diffraction patterns of nanosized crystals of the flexible framework CID-1 $[Zn(ip)(bipy)]_n$; ip = isophthalate; (CID = Coordination Polymer with Interdigitated Structure) reveal different interlayer distances as compared to the macrocrystalline state.[77] In a follow up study, Hijikata *et al.* had a deeper insight into the differences in framework dynamics and crystal structure between CID-1 and NCID-1 (Nano CID-1; crystal size: 50 nm × 320 nm). The methanol sorption isotherm already indicates a difference between these two structures: in the NCID-1 no hysteresis is observed contrary to the bulk sample. Activated guest-free CID-1 shows a **cp**, but certain guests trigger a reorientation of the linkers and guests can be adsorbed in the framework.

From the X-ray patterns of the nanosized analogue, a slightly distorted activated **cp** state is observed upon activation, leading to a different packing of the 2D layers. Additionally, NMR measurements showed that the rotation of the aromatic rings of the bipy show a much higher velocity in NCID-1. Hence, this structural and dynamical difference of NCID-1 leads to increased sorption kinetics and the disappearance of the sorption hysteresis.

Sakata *et al.*[76] prepared nanosized samples of the catenated $[Cu_2(bdc)_2(bipy)]_n$. The $[Cu_2(bipy)_2]_n$ 2D layers are bridged by bipy linkers. When the MOF is solvated, the layers are stacked on top of each other and the bipyridine molecules orthogonally connect them. After drying, the layers are shifted to each other and the bipy is tilted (see Fig. 7). This turning of the pillars and shifting of the layers is accompanied by a displacement of the interpenetrated frameworks in regard to each other. Thus, a **lp**

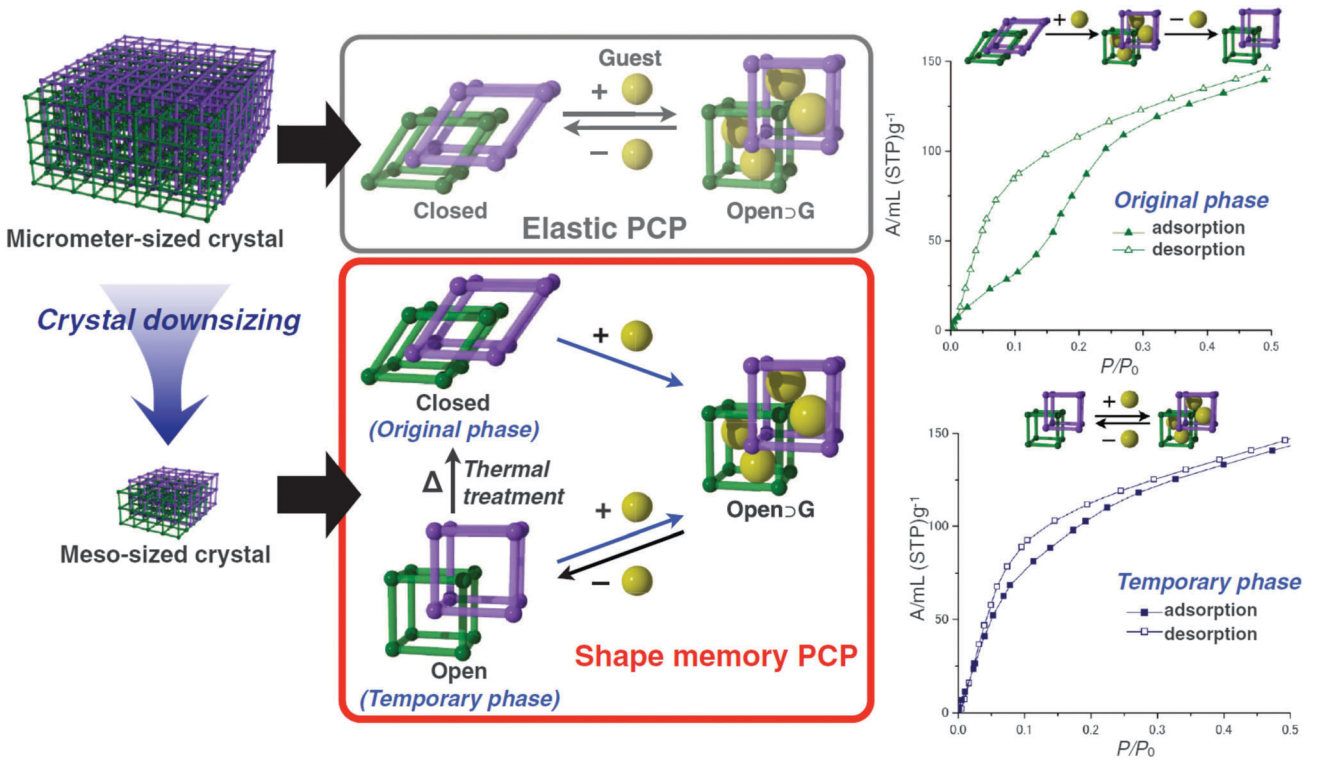

Fig. 7 Schematic depiction of the flexible behaviour of micro-sized $[Cu_2(bdc)_2(bipy)]_n$ in comparison with meso-sized $[Cu_2(bdc)_2(bipy)]_n$. Right – methanol adsorption isotherms of the closed (original phase) and the open (temporary phase) of meso-sized $[Cu_2(bdc)_2(bipy)]_n$. (Reprinted with permission.[76] Copyright 2013. American Association for the Advancement of Science.)

form in the solvated state can be distinguished from a **np** form in the dried state. Interestingly, when the MOF crystallites are downscaled to a particle size below 60 nm, the material does not undergo a phase transition to the **np** anymore after drying. Instead, the material keeps the shape of the solvated form until the material is exposed to temperatures of 473 K. This leads to a material that has different sorption isotherms, determined by its thermal treatment history.

2.6. Deposition on substrates and integration into thin films

The integration of flexible MOFs into thin films or devices has not yet been studied very intensively.[79] There are only rare examples of the deposition of flexible metal–organic frameworks as thin films on suitable substrates. Most likely, the modes of flexibility, which do not involve a change in unit cell dimensions (and pore volume) will not be influenced by surface deposition of MOF crystallites. However, it can be anticipated that the surface anchoring of swelling or breathing MOFs might influence the structural phenomenon. One early example was given by Scherb *et al.*,[80] who deposited thin films of MIL-88B on SAM (Self Assembled Monolayer) functionalized gold surfaces. The SAM triggers an oriented growth of the samples along the [001] axis, this means the hexagonal channels grow parallel to the surface. The sample was loaded with DMF after synthesis, left to dry in air for 24 hours and the diffraction pattern was measured in regular intervals. Interestingly, a shift of the (002) reflection to smaller 2Θ angles is observed during the desorption process, indicating an elongation of the distances between the diffracting centers along this cell axis (along the hexagonal channels).

3. Flexibility and the metal node

The most fascinating flexibility mode is the "breathing". It is a cooperative effect of both, the inorganic node and organic ligand. Up to now, there has been no comprehensive theory established, that provides predicting and full understanding of the key flexibility parameters of MOFs. Although, based on the existing experimental data, G. Ferey and C. Serre have formulated empirical rules that should be satisfied simultaneously to allow the structure to breath.[7] Some of them also concern metal clusters: The inorganic brick should have a mirror plane with the carboxylates ordered in symmetrical positions around it. Another rule concerns the ratio of $C/M \geq 2$ (C: number of carbon atoms of the carboxylic groups surrounding the cluster; M: number of metallic atoms within the cluster). We restrict our discussion to the most relevant examples, the metal nodes of MIL-53, MIL-88, and paddle-wheel based MOFs.

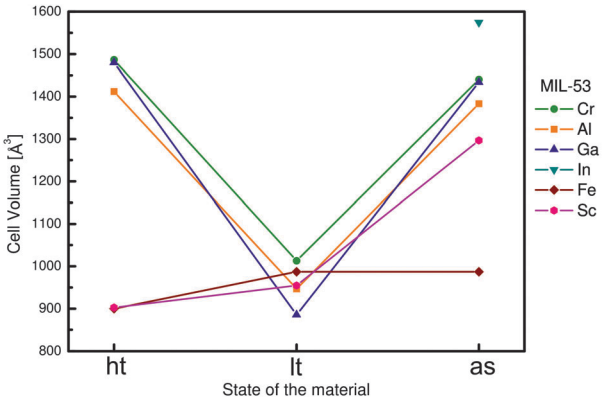

Fig. 8 Depiction of the cell volume evolution in different forms of MIL-53.

3.1. Deformation at the MIL-53 node

Within the MIL-53(M) series (Table 2), the chromium version MIL-53(Cr) is one of the most studied flexible MOFs. It is made of a $[Cr(OH)(CO_2)_2]_n$ chain-like SBU and benzenedicarboxylate as a linker.[19,20] Directly after the synthesis, the solid is isolated in the MIL-53as form containing terephthalate molecules and solvent in the pores. After evacuation at 300 °C the large pore MIL-53ht phase is obtained, which after cooling under ambient conditions transforms to the **np** MIL-53lt phase due to adsorption of water molecules. By considering bdc as a rigid linker, the flexibility of the solid can be explained mainly by changes in the inorganic node or dihedral angle between SBU and the linker. On the one hand, detailed analysis of the MIL-53(Cr) structure shows no significant changes of the SBU that could result in a drastic volume change from 1012.6 Å^3 in the MIL-53(Cr)lt to 1486.3 Å^3 in the MIL-53(Cr)ht (Fig. 9).

The O–Cr–O angles are in all three forms in the range of 88–94°. The Cr–O–Cr angle also does not change dramatically, being in the range of 125–132°. On the other hand, the change in the dihedral angle between O–Cr–Cr–O and the O–C–O planes (177.5° for -as, 180° for -ht and 139° for -lt forms) is indicative of the breathing effect of the framework. The structural transformation upon water adsorption is explained by weak intermolecular interactions between the framework's polar groups and water molecules. Another evidence for the synergetic effect of the inorganic node and the linker during the breathing behavior of MIL-53 is the rigid behavior of DUT-4[81] (Dresden University of Technology) and MIL-69 ($[M(OH)(2,6\text{-ndc})]_n$; M = Al, Cr),[82] which are isoreticular to MIL-53 and contain 2,6-ndc as a linker. Both compounds are rigid, whereas MIL-69 is present in the **np** form and DUT-4 in the **lp** form. An interconversion between these two forms does not take place. DUT-5 has also the same inorganic building

Table 2 Comparison of the unit cell volumes of different MIL-53 derivatives

	MIL-53(Cr)[20]	MIL-53(Al)[22]	MIL-53(Ga)[22]	MIL-53(In)[23]	MIL-53(Fe)[18]	MIL-53(Sc)[21]
V (**ht** form)/Å^3	1486.1	1411.9	1479.7	—	899.6	902.5
V (**lt** form)/Å^3	1012.8	946.7	885.6	—	986.8	954.385
V (**as** form)/Å^3	1440.6	1383.1	1434.1	1574.3	899.6	1296.6

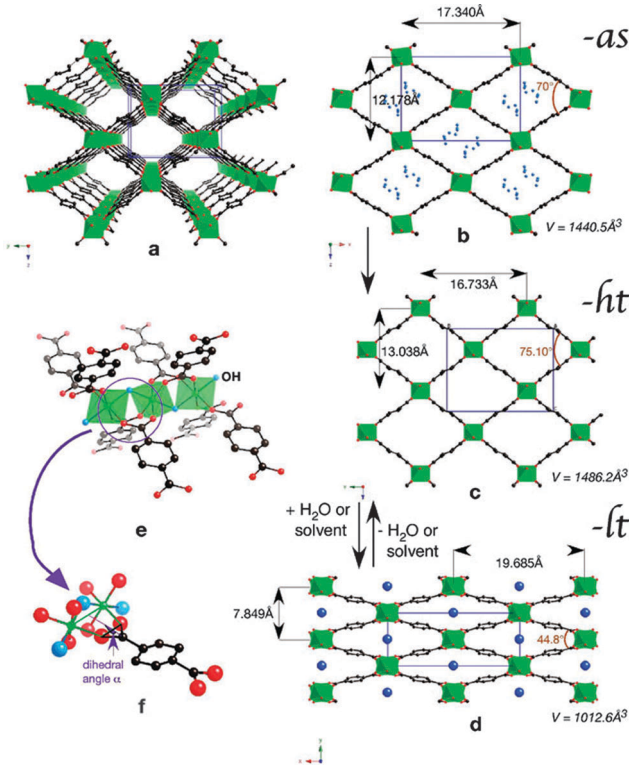

Fig. 9 (a) Perspective view of MIL-53-ht; (b)–(d) Projection along the direction of the channels of: (b) MIL-53-as (with some atoms of the disordered terephthalic acid in blue), (c) MIL-53-ht, and (d) MIL-53-lt with variable parameters; (e), (f) Perspective views of the connection between the chromium chains and the terephthalate ions. Chromium octahedra are depicted in green, water molecules in dark blue, OH groups in pale blue, oxygen in red, and carbon in black. (Reprinted with permission.[7] Copyright 2009 Royal Society of Chemistry.)

unit, but H_2bpdc as a ligand. This material is also rigid with permanent porosity.[81] The MIL-47(V) structure (also isostructural to MIL-53) is constructed by 1D chains of $V^{4+}O_6$ octahedra, interconnected by bdc. The only difference is in the valence of the metal atom that suggests the presence of the protonated μ_2-OH group in the case of MIL-53 series and the μ_2-O group in the case of MIL-47(V). The latter does not show a breathing effect during the adsorption of polar molecules.[83] Leclerc *et al.* were able to prepare a second form of MIL-47(V) which contains bridging OH groups and V(III) metal centers. This material shows again flexible behavior upon sorption of polar guests.[84] From Fig. 8 and Table 2 it is evident that the flexibility of MIL-53 frameworks depends on the metal node. Outstanding examples are the indium, scandium and the iron containing MIL-53 frameworks. For MIL-53(In) no activated phase has been published yet. The iron and scandium analogues show a pore contraction upon activation contrary to the other MIL-53 frameworks. While the remaining materials show an increase in cell volume upon activation (**lp**), the iron and scandium frameworks are in their guest free state even more contracted (**cp**) than the **np** form. The Cr, Al, and Ga show all similar **lp** → **np** transitions when the ht material is exposed to ambient conditions and adsorbs H_2O. In summary, the above mentioned examples show that breathing in MIL-53 materials is a completely cooperative effect of metal node and the linker molecule.

3.2. Deformation at the MIL-88 node

MOFs containing trivalent metal ions often feature the trigonal prismatic SBU $M_3O(COO)_6(H_2O)_2X$ (M = Fe, Cr, Al; X = F^-, OH^-). While hydrothermal synthesis under acidic conditions (HF) yields rigid mesoporous MIL-100[85] and MIL-101[86] frameworks, the utilization of trimeric iron(III) acetate as a metal source and fumaric, terephthalic, 2,6-naphtalenedicarboxylic (2,6-ndc) or 4,4-biphenyldicarboxylic acid (bpdc) as a ligand under basic conditions leads to the formation of flexible solids, namely MIL-88A, MIL-88B, MIL-88C and MIL-88D, respectively.[24,25,87] As synthesized structures of the MIL-88 family show swelling flexibility upon solvent removal, as well as upon adsorption of polar solvent molecules (Fig. 10). By hydrating the evacuated form of MIL-88A, the cell volume increases by 85% from the **np** (1135 $Å^3$) to the **lp** form of MIL-88-H_2O (2110 $Å^3$). The channels contract by activation and can be re-opened when exposed to polar solvent molecules. The driving force is the formation of hydrogen bonds between solvent molecules and the framework.

Although the geometry and connectivity of the SBU itself do not change significantly, the cluster exhibits continuous rotation of the trimers around the [001] direction by a maximum of 30° during the transformation. It became possible due to the knee-cap-like rotational axis, located on the O–O axis of the carboxylate functions, around which the trimer and the phenyl rings can change their respective angular orientations (Fig. 11).

3.3. Deformation at the paddle-wheel node

A paddle-wheel or so called "soft SBU"[88] serves as an inorganic brick for most of the known flexible MOFs (Fig. 12).[31,89–97] It consists of a metal dimer interconnected by four carboxylic groups and represents a four-connecting (square or pseudo-square) SBU. Connection of the paddle-wheels by linear linkers results in $[M_2L_2]_n$ planar grids that are usually interconnected

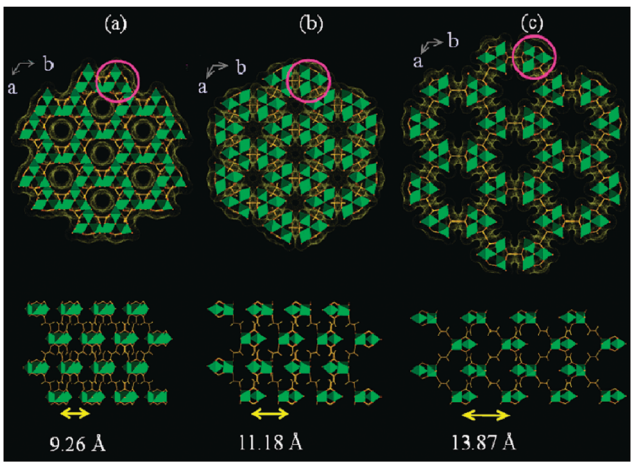

Fig. 10 Simulated crystal structures of the MIL-88A framework in its **np** (a), **as** (b), and **lp** (c) forms. (Reprinted with permission.[87] Copyright 2005 American Chemical Society.)

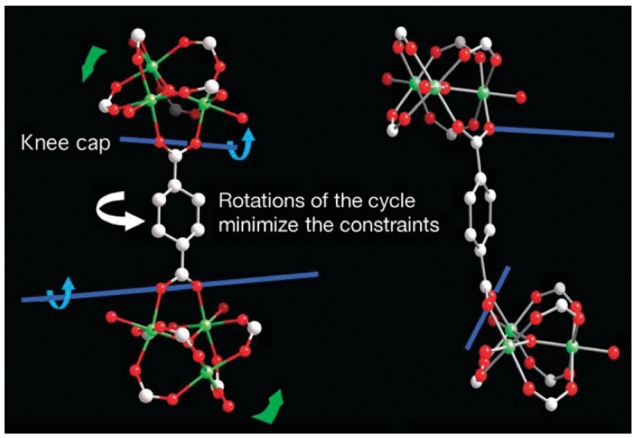

Fig. 11 Depiction of the hinge in MIL-88 around which the rotation that induces the pore swelling occurs. (Reprinted with permission.[133] Copyright 2007 American Association for the Advancement of Science.)

in the third direction by pillar ligands (*e.g.* dabco, bipy, *etc.*) forming a 3-D framework with α-Po topology.

The most representative example of such a system is the MOF $[Zn_2(bdc)_2(dabco)]_n$ (Fig. 12).[98] The planar grid is built by $[Zn_2(COO)_4]$ paddle-wheels and bdc linkers. In the axial positions, the paddle-wheels are interconnected by dabco forming the 3D network. The crystal structure of the as-synthesized phase shows a strong mutual distortion of $[Zn_2(bdc)_2]$ grids in the *c* direction (Fig. 12). Interestingly, the evacuated structure shows ordering of the latter. The contraction of the crystal structure is provoked by adsorption of benzene molecules and is in a good correlation with the adsorption stress model of Neimark.[99] In contrast to MIL-53, where the SBU is not actively involved in the breathing process, in $[Zn_2(bdc)_2(dabco)]_n$ deformation of the paddle-wheel plays a key role in the transformation. Thus, the O–Zn–O adjacent angle in the paddle-wheel changes from 90° in the **lp** structure to 87° in the **np** phase after benzene adsorption. At the same time the "knee-cap" O–Zn–Zn–O and O–C–O dihedral angle, responsible for the breathing of MIL-53, changes from 0° in the evacuated **lp** structure to 9.8° in the **np** one. The same structural transition from the as-synthesized **np** to the evacuated **lp** phase was observed in the case of the isomorphic compound $[Co_2(bdc)_2(dabco)]_n$.[92] In contrast, the X-ray powder diffraction patterns of as-synthesized and evacuated $[Cu_2(bdc)_2(dabco)]_n$ match well indicating the immutability of the framework structures.[89] By expansion of the framework using longer 2,6-ndc instead of bdc in the synthesis, the DUT-8 ($[M_2(2,6\text{-ndc})_2(dabco)]_n$) family with Cu(II), Zn(II), Co(II) and Ni(II) as metal nodes was obtained.[95,96] Similarly to $[Cu_2(bdc)_2dabco]_n$, DUT-8(Cu) shows rigid behavior with no structural changes upon solvent removal. The DUT-8 frameworks, based on Ni, Zn, and Co paddle-wheels, indicate structural changes during the evacuation. In the case of DUT-8(Zn), the changes are irreversible underlining the influence of the metal node. In accordance with nitrogen adsorption isotherms, supported by X-ray powder diffraction patterns it was established that the DUT-8(Ni) structure closes and opens completely showing a unique, and extremely large reversible breathing transition. The flexibility of the Co analogue is less pronounced.

The paddle-wheel related flexibility was also demonstrated by Kitagawa *et al.* on the example of the twofold interpenetrated framework $[Zn_2(bdc)_2(DF\text{-}bpb)]_n$ (DF-bpb = 2,3-difluoro-1,4-bis(4-pyridyl)benzene).[88] During activation, the reversible structural transformation of the paddle-wheel was monitored by single crystal XRD. The structural evolution from **2a** to **2d** (Fig. 13) sequentially shows the contraction of the structure. In the crystal structure of **2a**, the paddle-wheel M–M dimer and the pyridyl based pillar lie on the same axis. In the intermediate structures **2b** and **2c** the pyridyl ligand is tilted, thus decreasing the interlayer distance. Simultaneously, a distortion of the square planar coordination of the bdc linkers around the paddle-wheel is surveyed.

Finally, the structure of **2d** shows partial decomposition of the paddle-wheel with the change in the coordination geometry of Zn from square-pyramidal to tetrahedral.

A similar effect was observed by Rosseinsky *et al.* during dehydration of a Zn paddle-wheel based MOF $[Zn_2(TBAPy)(H_2O)_2]_n$ containing a tetratopic ligand (TBAPy = 1,3,6,8-tetrakis(*p*-benzoic acid)pyrene).[100] As a result of water removal, the framework dimensionality changes from 2D to 3D inducing changes in magnetic and optical properties.

Thus, one can conclude that the paddle-wheel contributes considerably to the flexibility of the framework, but the impact is strongly dependent on the nature of metal used in the

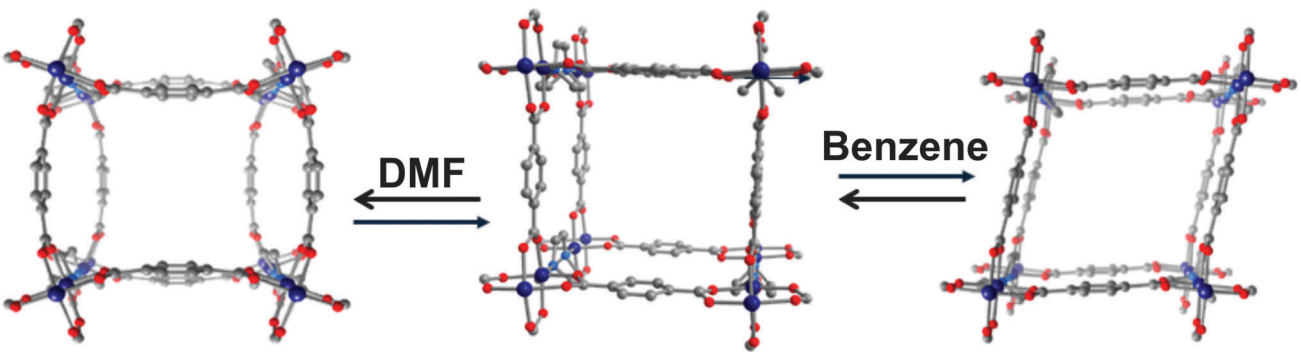

Fig. 12 Crystal structure of $[Zn_2(bdc)_2(dabco)]_n$ (view along *c* direction): left – as synthesized phase; middle – activated phase; right – after infiltration of benzene. Colour code: Zn – blue, O – red, C – grey. H atoms are omitted for clarity.

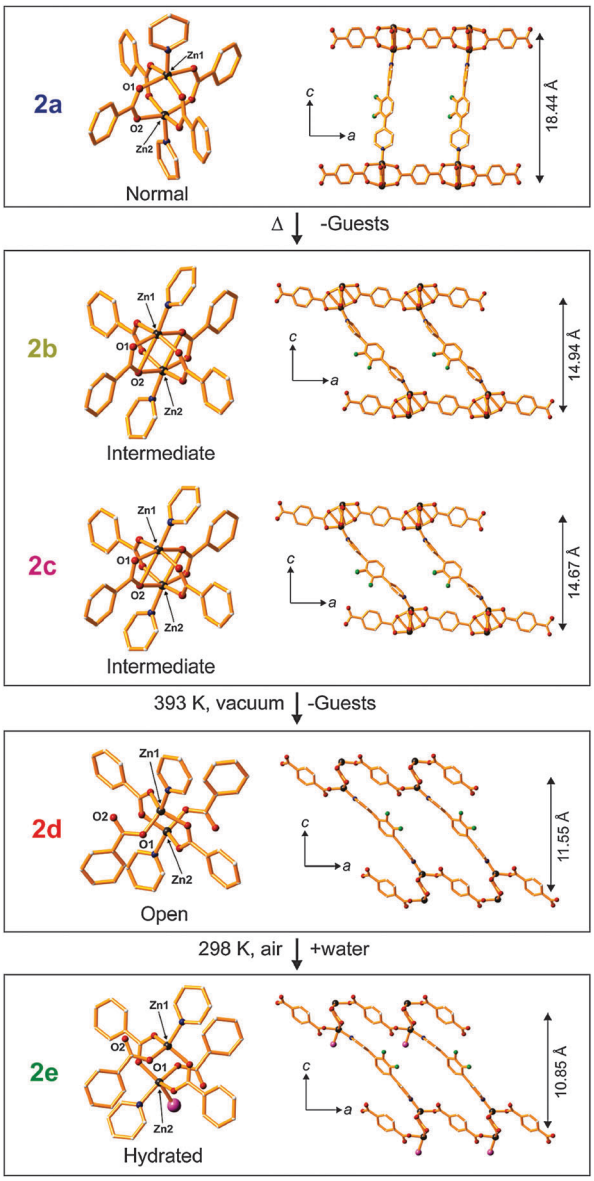

Fig. 13 Crystal structure of $[Zn_2(bdc)_2(DF\text{-}bpb)]_n$ in the forms **2a–2d** showing structural transformations upon desolvation and water coordination. Color code: Zn – gray; F– green; N – blue; O – red,; H_2O – violet (in 2e). Non-coordinated guest molecules and hydrogen atoms are omitted for clarity. Left: coordination environments of the zinc cluster; Right: views of the single framework along the *b*-axis. (Reprinted with permission from ref. 88. Copyright 2011 American Chemical Society.)

synthesis. The Cu based compounds are usually more rigid in comparison to the Zn, Ni and Co analogue.

A more complex type of SBU, however still related to the paddle-wheel structural motif, was observed in $[Zn_2(BPnDC)_2(bipy)]_n$ (BPnDC = benzophenonedicarboxylate), which is a twofold interpenetrated flexible framework also known as SNU-9 (Seoul National University).[101] Later, the intrinsic structural dynamics of SNU-9 were investigated *in situ* during the adsorption of CO_2 and N_2 by Kaskel and co-workers.[102] The structure consists of unusual asymmetric paddle-wheel SBUs (Fig. 14), composed of two Zn atoms coordinated by four carboxylic groups from

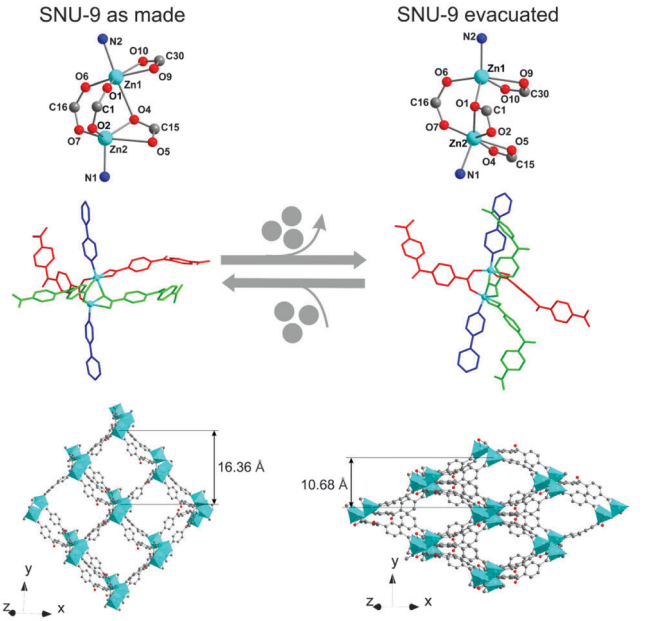

Fig. 14 Crystal structure of SNU-9: as synthesized (left) and SNU-9 activated (right). Top: geometry of the SBU. Middle: ligand arrangement around the SBUs (molecular color code: bipy in blue; crystallographically independent benzophenonedicarboxylate molecules in red and light green). Bottom: view of a single framework along the [101] direction. (Reprinted with permission.[102] Copyright 2014. American Chemical Society.)

BPnDC linkers and two nitrogen atoms from bipy molecules in the axial positions.

Two Zn atoms and bipy molecules are not linearly arranged, as usual for paddle-wheel pillar-layered frameworks. During the activation, a Zn–O bond rearrangement occurs.

Such rearrangement leads to the contraction of the structure in the [010] direction accompanied by decrease in unit cell volume from 10 182 $Å^3$ to 7334 $Å^3$, and accessible void volume from 40.8% to 12.8%. Interestingly, the adsorption of CO_2 at 195 K and N_2 at 77 K proceeds in a different way: the formation of an intermediate phase during the CO_2 adsorption could be postulated, while the transformation from **np** form to the **lp** structure occurs quasi in one step by nitrogen physisorption. The gas loaded compounds have also different final crystal structures at relative pressures around $p/p_0 = 0.9$, depending on the guest molecule. According to the powder diffraction data, the structure of N_2@SNU-9 is identical to the structure of the as synthesized compound. The cell volume of CO_2@SNU-9 is slightly higher.

4. Flexibility and functionalized linkers

A systematic discussion on the various types of framework flexibility based on the motions of the linkers, rather than primarily focusing on the coordination geometry at the metal nodes, was given by Murdock *et al.* in their review article entitled "Approaches for synthesizing breathing MOFs by exploiting dimensional rigidity", as we already highlighted in the introduction.[12]

The categorizing principle was based on conformational properties of the linkers and on the dimensionality of the (cooperative) motions of the framework. The authors analyze twisting, bending, and tilting modes of rigid and (partly) flexible linkers. We refer to this recent article as we want to avoid repeating its content herein. Rather, our focus will be on the opportunities of tailoring framework flexibility by the substituent effects at the linker. *i.e.* by introducing functional groups. An early example for implementing dangling substituents at the backbone of the linker being not involved in framework constructions is the prototypical IRMOF-series introduced by Eddaoudi *et al.*[103] In this, the bdc linker is replaced by analogues containing simple substituents on their benzene core, *e.g.* Br- or NH_2-groups (IRMOF-2 and IRMOF-3, respectively). These functionalities point into the pore and influence the pore shape and metrics, as well as the polarization noticeable. It was shown that by smart linker functionalization the properties, such as sorption selectivity can be tuned in such kind of structurally rigid MOFs. Moreover, the same concept of linker functionalization can be applied to tailor flexibility together with functionality and even to trigger flexibility in otherwise much less flexible or even rigid MOFs.

Several methods have been established in order to introduce functionalities into MOFs. The most straight-forward way is the incorporation of functionalized linkers during conventional solvothermal synthesis.[104–113]

However, this is not always possible, *e.g.* due to steric demand or due to additional ligating groups leading to a different framework topology. This can be avoided by introduction of the functional groups after the MOF synthesis. One method to achieve this is postsynthetic modification (PSM), during which a simple functional group (*e.g.* –OH, $–NH_2$ or N_3) is further reacted under mild reaction conditions (*e.g.* esterification, click reaction).[114–126] For some functionalities it is also possible to protect them with an easily cleavable group ("protection group") before MOF synthesis and set them free after synthesis.[37,38,127,128] Postsynthetic exchange[129,130] (PSE, also known as solvent assisted ligand exchange, SALE[131–134]), a rather new but very powerful method, has also proven to be extremely useful for the introduction of functionalities into a MOF that otherwise would not be possible.[135] When using this method, the MOF is exposed to a highly concentrated solution of a linker molecule at elevated temperatures and the linkers of the MOF exchange with the targeted linker molecules. In the following, we would like to discuss the influence of functional groups on the flexibility of metal–organic frameworks.

4.1. Functionalized bdc-type linkers

Comprehensive studies have been conducted on the functional groups influence on the breathing transitions in MIL-53(Al) and MIL-53(Fe). For the MIL-53(Al) framework the plain bdc linker was substituted with –Cl, –Br, $–CH_3$, $–NO_2$, or $–(OH)_2$ functionalized bdc derivatives.[136] Fig. 16 shows the evolution of the cell parameters in these frameworks from the as-synthesized to the **lp** and to the **np** phase (and to a DMF infiltrated phase). The cell volumes for the as-synthesized phases of the MIL-53(Al) derivatives cover a range between 1375 and 1450 Å^3 representing the **lp** structure. The largest values for the as-synthesized cell volume are observed for rather bulky groups that do not enable hydrogen bond formation with the solvent molecules (–Cl, –Br, $–CH_3$ and $–NO_2$). Smaller cell volumes are observed for groups that can interact *via* hydrogen bonding with the solvent molecules used during synthesis ($–NH_2$, $–(OH)_2$, or $–(COOH)_2$). In these cases, a tighter (energetically more efficient) packing of the solvent and excess linker molecules within the cell is expected. When the pores are filled with DMF, it is observed that the MOF containing the bulkiest non-polar groups has the highest cell volume with the sequence MIL-53(Al)-Br > MIL-53(Al)-CH_3 > MIL-53(Al)-Cl. For the MOFs containing polar side groups, the cell volume of the DMF filled form decreases with decreasing steric demand of these groups (MIL-53(Al)-NO_2 > MIL-53(Al)-$(OH)_2$ > MIL-53(Al)-NH_2). When the material is activated, a guest free high temperature (ht) phase is obtained, which possesses in all cases a **lp** structure. The only exception is MIL-53(Al)-$(OH)_2$, which collapses upon complete removal of all guest molecules.

The differences in the breathing behavior of the MIL-53(Al) derivatives can be attributed to different intra-framework and host-framework H-bonding properties of the material. The μ^2-OH groups and their interactions with guest molecules have been identified as one of the key features during the breathing transitions in MIL-53.

By implementing into the MOFs some functional groups (which to some extent can be considered as guest species), the electronic properties of the μ^2-OH groups get modulated. These side groups may interact directly with the μ^2-OH groups.

Devic *et al.*[137] have performed a very extensive study on the influence of –Cl, –Br, $–CH_3$, $–NH_2$, $–(OH)_2$, $–(COOH)_2$ and $–(CF_3)_2$ functional groups on the flexibility and frameworks' dimensions of MIL-53(Fe) during solvation using a range of different solvents such as H_2O, ethanol (EtOH), pyridine (py), and tetrachlorethane ($C_2H_2Cl_4$). Interestingly, the differences are more pronounced than for the aluminium analogue. It is notably that MIL-53(Fe) shows a different chronology in its phase transitions. The as-synthesized MIL-53(Fe) material has a **lp** form and is filled with guest molecules (excess linker and solvent). After activation and removal of the incorporated guests, the material is unlike the Cr and Al analogue not in a **lp** phase, but contracts even more than the comparable narrow pore forms, giving rise to the closed pored form (**cp**). Interestingly, the degree of contraction of the **cp** is highly dependent on the nature of the functional group attached to the bdc linker and the resulting specific guest–framework interactions (Fig. 15). For the non-functionalized framework and the $(OH)_2$-bdc containing framework the dry ht form has a pore more narrow than the respective hydrated lt **np** phase (V = 917 and 900 Å^3, respectively). All the other materials show a ht phase that has dimensions similar to the lt phase. It is worth mentioning that MIL-53(Fe)-$(CF_3)_2$ already has a high cell volume of around 1318 Å^3 in the dried ht phase. This can be attributed to (i) the bulkiness of the side group or (ii) to the inability of the perfluorated side chains to yield any H-bonding interactions with the μ^2-OH groups and

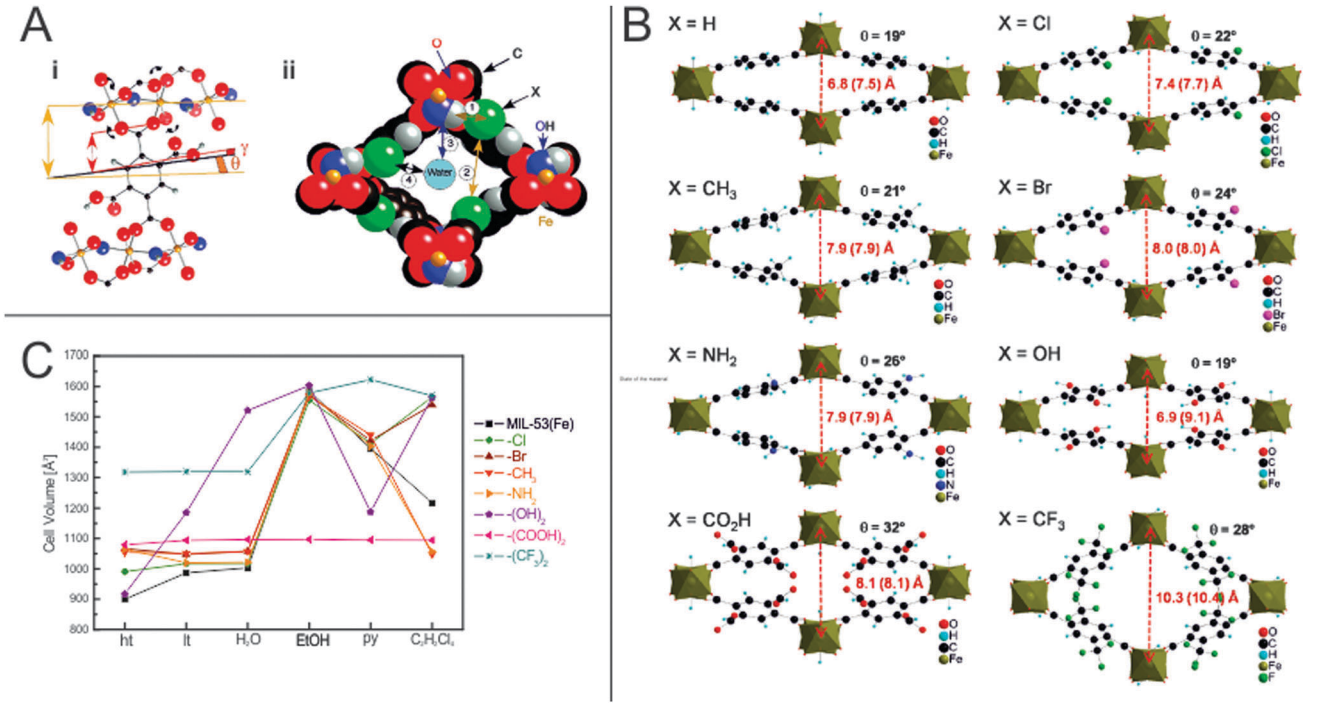

Fig. 15 (A) (i) – Depiction of the O–O rotational axis in MIL-53(Fe), which triggers the phase transition; (ii) – Different interaction sites in the pore of MIL-53(Fe). (B) Calculated crystal structures of differently functionalized MIL-53(Fe)(ht) analogues. Red numbers indicate the length of the *b*-axis, numbers in brackets give the length of the *b*-axis in the hydrated form. (C) Evolution of the unit cell volumes depending on the state of the material. (Reprinted with permission.[137] Copyright 2010 American Chemical Society.)

(iii) to the repulsion of CF_3 groups of adjacent bdc linkers. This conclusion is underlined by the behavior of the MIL-53(Fe)-$(COOH)_2$ framework, which has a bulky functional group attached, but a much lower cell volume (1079 $Å^3$), indicating a strong interaction between the COOH groups with the bridging μ^2-OH. This interaction seems to be so strong that none of the solvents, which are used for exposure, leads to an opening of the pore. When exposed to water, all materials – except the $-(OH)_2$ functionalized analogue – show similar lattice parameters as the lt (**np**) phase (which has water from air adsorbed in the pore space).

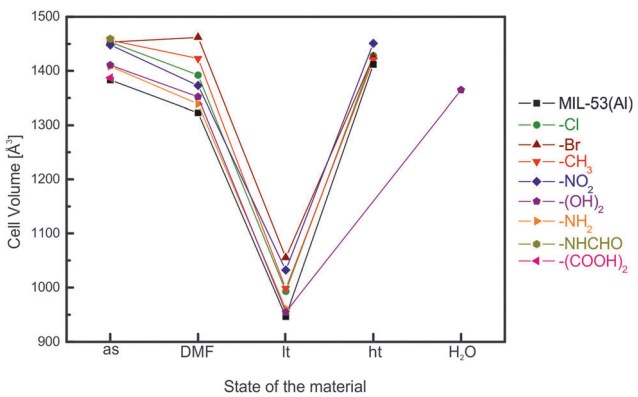

Fig. 16 Evolution of the cell volume in MIL-53(Al) materials depending on the treatment of the material.

Like for MIL-53(Al)-$(OH)_2$ a huge increase in the cell volume is observed when water is offered to the framework. This is reasoned by the polar backbone and by the good ability of the water molecules to form hydrogen bonds with the linkers' OH groups and the polar backbone. Exposing the series of frameworks to ethanol leads to a further expansion up to the maximum cell volume observed in this study for most compounds (except MIL-53(Fe)-$(CF_3)_2$, which has the highest cell volume when pyridine is infiltrated).

Henke *et al.* prepared a series of dialkoxy functionalized linkers and applied them in the synthesis of a series of dabco pillared layered materials of the general formula $[Zn_2(fu\text{-}bdc)_2(dabco)]_n$ (where fu-bdc is functionalized bdc, see Fig. 17 for a listing of the used linker molecules).[138] Depending on the chain length, polarity, and grade of saturation of the added alkoxy chains, the scope of flexibility of the material can be adjusted. Similar to flexible MIL-53 materials, also a rotation around the O–O axis of the carboxylate occurs leading to an increase or decrease of the cell volume. All as synthesized materials are present in the **lp**, when the materials are activated, a contraction to the **np** form is observed. This is due to the interaction of the side chains bound to the framework's backbone. When the solvent is removed, the side chains interact strongly, leading to a complete contraction of the framework. The magnitude of this contraction is strongly dependent on the nature of the substituents. If the side chain is too long, no contraction is observed (*e.g.* fu-bdc = DPe-bdc), since (i) already

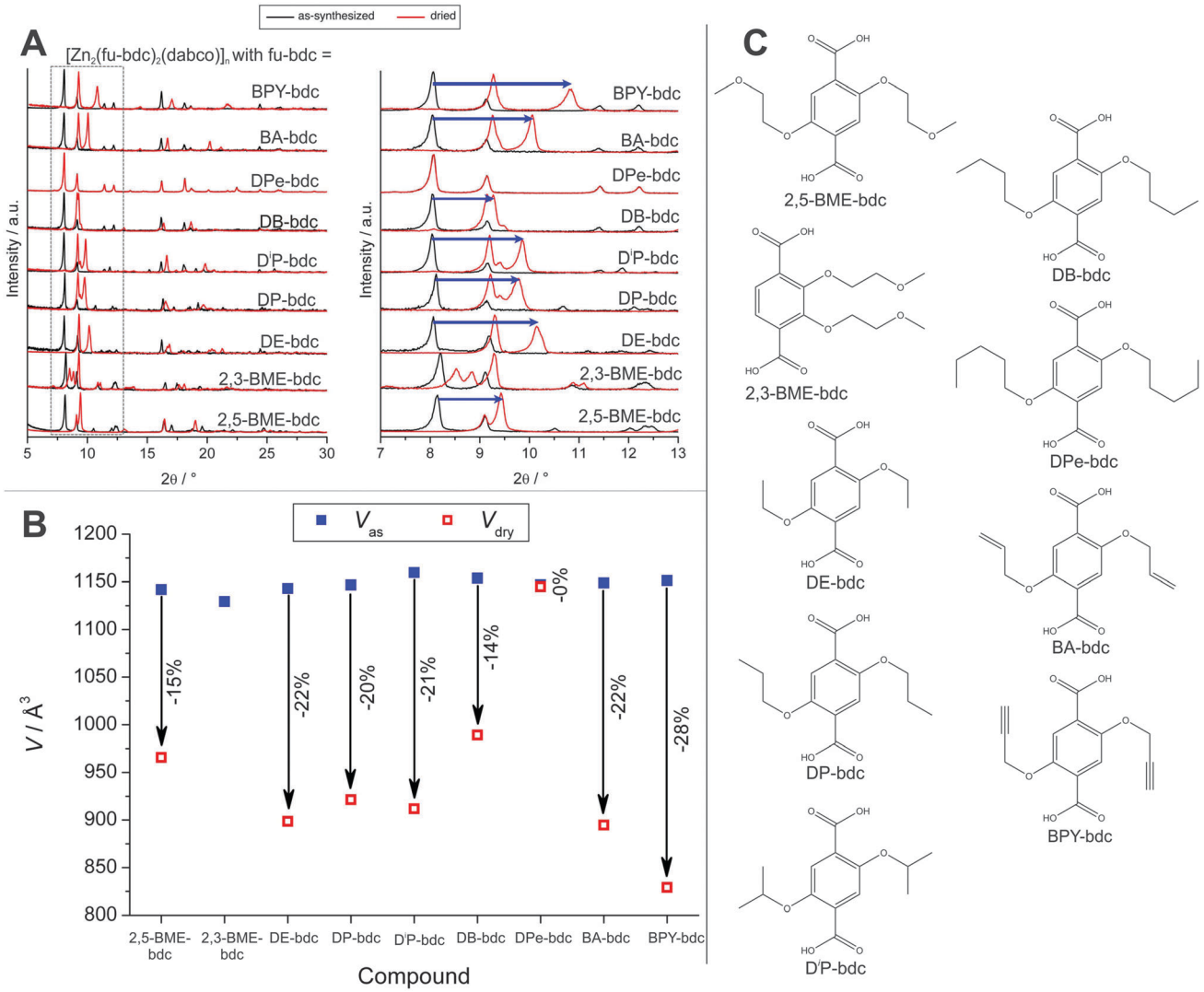

Fig. 17 (A) Powder patterns of as-synthesized (black) and dried (red) $[Zn_2(fu\text{-}bdc)_2(dabco)]_n$. (B) Evolution of the cell paramters during the transitions from the as-synthesized lp to the dried np of the framework. (C) Listing of the linkers that were used to prepare the discussed pillared-layered frameworks. (Reprinted with permission.[138] Copyright 2012. American Chemical Society.)

in the **lp** form beneficial interactions between adjacent side chains can occur or (ii) the chains fill the pore volume and restrict the space necessary for contraction. When the chain length is decreased, a strong contraction is observed for DB-bdc and BME-bdc containing pillared-layered MOFs. Even though the polarity of the materials is different (with BME-bdc containing a oxygen molecule in the fourth position of the side chain), only a slight difference in the pore contraction is observed (for 2,5-BME-bdc – 15%; for DB-bdc – 14%). The difference is more noticeable for side chains with a different grade of saturation. While the framework, built up from DP-bdc linkers possessing completely saturated side chains, contracts by 20% (the respective isomer $[Zn_2(DiP\text{-}bdc)_2(dabco)]_n$ contracts by 21%), the related framework containing unsaturated propynyloxy side chains $[Zn_2(BIPY\text{-}bdc)_2(dabco)]_n$ contracts by 28%.

Cohen and coworkers selected the same parent system for modulation of the flexible properties by applying the concept of post synthetic modification of $[Zn_2(NH_2\text{-}bdc)_2(dabco)]_n$. Reaction of the NH_2 group with carboxylic acid anhydrates of different chain lengths, alters the degree of flexibility of the frameworks. However, this has been so far the only systematic study which focuses on the employment of PSM to trigger and tune flexibility of a MOF.[139]

Apart from the frameworks undergoing breathing transitions, also very interesting studies were conducted on the swelling MIL-88B framework. Horcajada *et al.* exchanged the bdc linkers with a wide variety of different functionalized bdc linkers.[140] A big influence of the type and number of functional groups on the pore swelling of the material was observed. The general trends of the experiments are displayed in Fig. 18. The volume of the unit cell of non-hydrated **np** material is strongly dependent on the type of functionality – the higher the steric bulk of the group, the higher the necessary volume to accommodate the functional groups. It is interesting to see, that by judicious choice

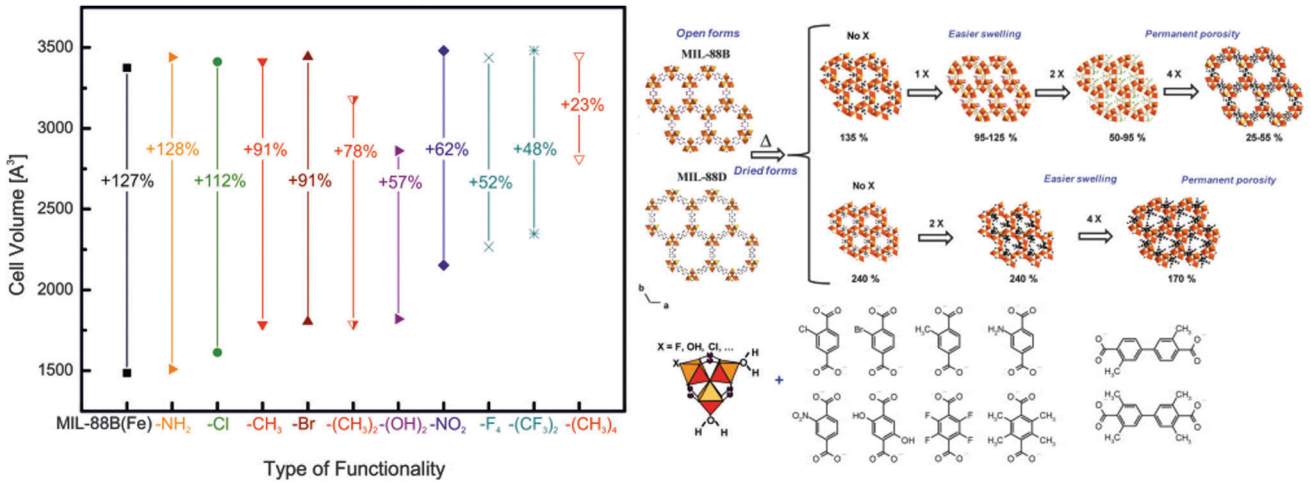

Fig. 18 Left: depiction of the evolution of the cell volumes during the swelling process depending on the functionalities added at the bdc benzene core of MIL-88B(Fe) Right: schematic depiction of the pore swelling in MIL-88B and MIL-88D depending on the number of substituents on the benzene rings. (Reprinted with permission.[140] Copyright 2011. American Chemical Society.)

of substituent, the material's surface area can be tuned. If mono-substituted linkers are used (Cl-bdc, Br-bdc, NH_2-bdc, NO_2-bdc or $(OH)_2$-bdc), the pores are contracted and no significant BET surface area can be determined. If the linker, however, is double or quadruple substituted with sterically more demanding linkers (*e.g.* F_4-bdc, $(CH_3)_2$-bdc, $(CH_3)_4$-bdc, and $(CF_3)_2$-bdc), the permanent porosity can be confirmed by nitrogen adsorption experiments.

So far, there only have been few comprehensive studies that were able to compare differently functionalized MOFs. The flexibility of many systems is however very complex (metal and linker influence) and a generalization of how a certain group –X changes the responsiveness of a MOF to an outer stimuli is according to the literature not possible up to now.

4.2. Elongated linear carboxylate linkers

In two studies Dau *et al.* showed the influence of differently functionalized 4,4′-biphenyldicarboxylic acids on the sorption properties of bipyridine and dabco pillared layered Zn^{2+} frameworks.[141,142] In their first study they prepared 2-phenylpyridine-5,4′-dicarboxylic acid and applied it in the synthesis of different MOFs. Interestingly, for the prepared pillared-layered frameworks distinct differences in the gas-adsorption isotherms were observed compared to the unfunctionalized bpdc, originating most probably from the differences in the framework dynamics upon adsorption. In a second study, nitro and dinitro-functionalized bpdc derivatives were prepared and employed in the synthesis of dabco and bipy pillared layered MOFs. Interestingly, the 2-NO_2-bpdc forms a non-interpenetrated pillared layered framework for both cases, while the 2,2′-$(NO_2)_2$-bpdc linker forms the interpenetrated framework for the bipy pillared version and a 2D-coordination polymer in the case of the dabco pillar. The functionalized linkers have a distinct effect on the sorption properties of the materials. The observed hysteresis in the CO_2-sorption isotherms suggests a dynamic framework behavior.

5. Multivariate flexibility, solid solution MOFs of mixed linkers and metal ions

The integration of different building blocks, which feature the same coordination geometry (structure) and connectivity, can lead to the construction of mixed component MOFs (MIXMOFs),[143–146] sometimes also referred to as multivariate MOFs (MTV-MOFs)[147,148] or solid solution MOFs.[149,150] In these *single-phased* materials at least two types of different metals (a) or differently functionalized linkers (b) are present. However, these different components are not regularly ordered, but rather random or inhomogeneous incorporation occurs. The concept of MIXMOFs (illustrated schematically in Fig. 19) can lead to advanced materials with complex functionalities, unusual and specific properties. Conceptually, by variation of the building block ratios in the synthesis batch, it is possible to control the composition and the resulting pore metrics and

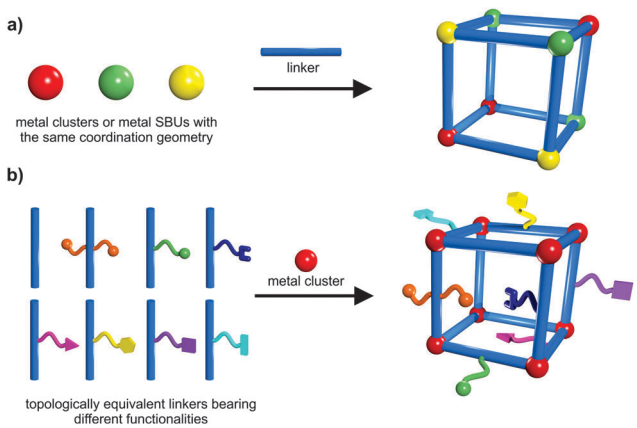

Fig. 19 Schematic depiction of the construction of: (a) solid solutions of mixed metal ions; (b) mixed linkers leading to multivariate flexibility of MOFs.

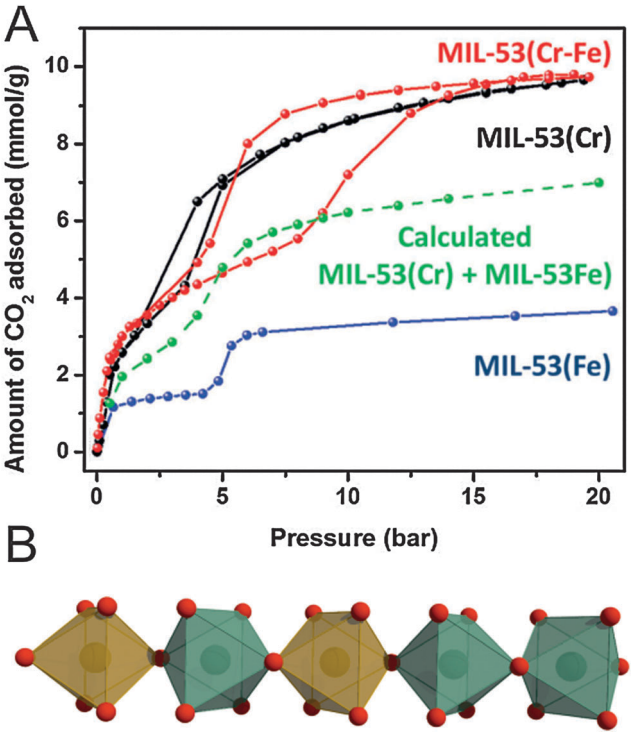

Fig. 20 (A) Comparison of the CO_2 adsorption isotherms of MIL-53(Fe–Cr), MIL-53(Fe), and MIL-53(Cr). (B) One dimensional SBU chains in MIL-53(Fe–Cr). Green and orange polyhedra represent iron and chromium SBUs, respectively. Red spheres represent oxygen atoms. (Reprinted with permission.[151] Copyright 2012. The Royal Society of Chemistry.)

pore functionalities, offering a powerful approach to tailor and adjust the desired physicochemical properties of porous materials. Complexity and combinatorial richness can be introduced, far beyond the limitations of the single-component compounds.

Regarding flexible MOFs, the construction of mixed-component systems is not extensively studied yet and to the best of our knowledge, there are only a few examples of tailoring the breathing behavior in mixed component MOFs. We want to address the most prominent ones in the following. Starting with flexible mixed-metal MOFs, the attention was mainly focused on the MIL-53 system. All MIL-53(M(III)) derivatives feature a **np** structure in their hydrated form. Upon heating, the frameworks start to "breathe" and transform, depending on the metal, either to a **lp** form (*e.g.* M = Cr) or to a **cp** form (*e.g.* M = Fe). Serre and coworkers thus investigated the influence of mixing cations featuring this antagonist flexibility.[151] The prepared solid solution (evaluated metal contents: Cr: 60%, Fe: 40%) shows a structural behavior being completely different from both of the parent compounds, since it initially contracts to a **cp** form at 343 K and re-expands to a **lp** form upon further heating to 463 K. This two-step behavior of contracting and expansion is neither observed in MIL-53(Cr), nor in MIL-53(Fe) and clearly indicates the formation of a single phased solid-solution. Structural differences are also observed from the sorption measurements (Fig. 20). The CO_2 triggered phase transitions in MIL-53($Cr_{0.6}Fe_{0.4}$) $[Cr_{0.6}Fe_{0.4}(OH)(bdc)]_n$ (**cp** → **np** → **lp**, indicated by the stepwise uptake and *in situ* PXRD studies) are distinctly different from the transitions observed for the parent frameworks, as well as from the theoretical calculations, indicating the pronounced effect of the mixed Cr–Fe chains in the network on the structural flexibility. Particularly, the facility of opening a pore might thus be tunable by controlling the Cr/Fe ratio.

Another example describes the formation of solid solutions by doping MIL-53(Al) with vanadium ions, conducted by Fischer and co-workers.[152] The pure guest-free V-analogue of MIL-53 (called (MIL-47(V)) slightly differs in structure, as the metal centers are bridged by μ-O^{2-} instead of μ-OH^- groups, which is related to the higher oxidation state of the V(IV) ions. Notably, MIL-53(Al) features a flexible structure (guest and heat induced oscillation between **lp** and **np** phase), while the V(IV) analogue is rigid, due to the absence of the bridging μ-OH groups. And indeed, incorporation of different amounts of V confirms the expected trend: With increasing molar ratio of vanadium, a gradual change from a highly flexible framework structure to a completely rigid one is observed. 87% of vanadium is enough to suppress the structural transformation from the initial **lp** form to the **np** form upon CO_2 adsorption. Accordingly, the guest pressure required for a subsequent **np** to **lp** transition decreases from 600 mbar to lower values with increasing vanadium content, until it completely disappears (for 87% V^{IV}). Generally, the flexibility is thus strongly dependent on the V^{IV} content in mixed Al/V chains. Worth mentioning, these two examples show that combination of either two flexible MOFs (Cr/Fe), or also of a flexible and a rigid one (Al/V) can lead to flexible solid solutions, which feature a breathing behavior completely different from the parent frameworks and which can be tuned over the whole range of metal ratios.

Besides the mixed-metal MOFs, there are also examples of flexible mixed-linker systems, which will be discussed in the following. Farrusseng and coworkers prepared a series of MIL-53(Al) derivatives containing different mixtures of bdc and NH_2-bdc.[153] They observed that the guest dependent behavior is highly influenced by the molar ratios of the applied linkers in $[Al(OH)(bdc)_{1-x}(NH_2\text{-bdc})_x]_n$ (with x = 0, 0.1, 0.2, 0.5, 0.6 and 1). All samples show a distinct two-step adsorption profile in the CO_2 isotherms, attributable to the **lp** → **np** and **np** → **lp** form transformation at low and high pressures, respectively. The threshold pressure of the second phase transitions (**np** → **lp**) increases (from 665 kPa to 1770 kPa) with increasing NH_2-bdc content. This indicates a more pronounced stabilization of the **np** form in the presence of a high NH_2-bdc content, due to a larger number of stabilizing hydrogen bonds within the pore. Temperature-dependent PXRD studies reveal a **np** → **lp** transition at 60 °C (dehydration) for pure lt $[Al(OH)bdc]_n$, which is not observed for pure lt $[Al(OH)NH_2\text{-bdc}]_n$. The phase transition temperature at intermediate NH_2-bdc contents is spread over a temperature range and **np** and **lp** form can coexist in some cases. Evidently, with increasing amount of NH_2-bdc, much higher temperatures are required for a full **np** → **lp** conversion.

The breathing behavior was also fine-tuned in pillared-layered $[Zn_2(BME\text{-}bdc)_{2x}(DB\text{-}bdc)_{2-2x}dabco]_n$ (x = 0.25, 0.50, 0.75) solid solutions.[138] Henke *et al.* showed that all frameworks

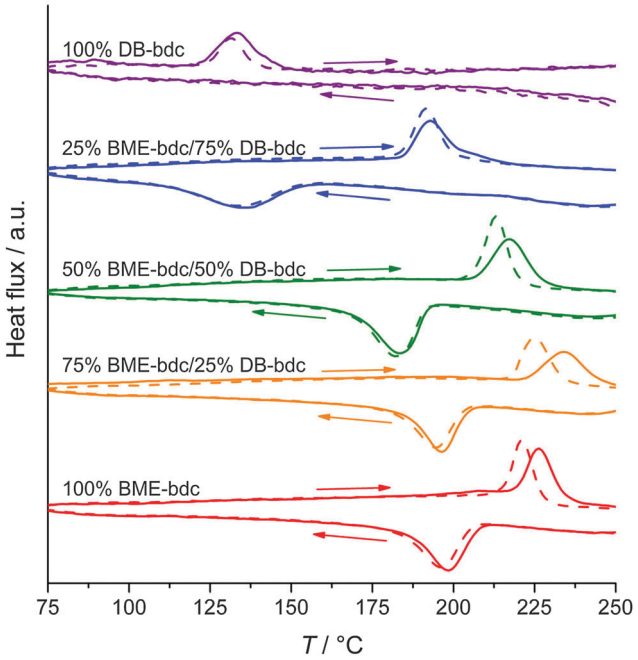

Fig. 21 DSC curves of $[Zn_2(BME\text{-}bdc)_{2x}(DB\text{-}bdc)_{2-2x}dabco]_n$ solid solutions. (Reprinted with permission.[57] Copyright 2013 John Wiley and Sons) and Sons.

feature a distinct **lp** → **np** contraction upon solvent removal and the scope of contraction is linearly enhanced with increasing amounts of BME-bdc. Notably, the CO_2 pressure required to trigger the **np** → **lp** and the width of hysteresis also depends on the BME-bdc/DB ratio, however, non-linearly. $[Zn_2(BME\text{-}bdc)_{0.5}(DB\text{-}bdc)_{1.5}dabco]_n$ shows a much higher transition pressure than pure $[Zn_2(DB\text{-}bdc)_2dabco]_n$. Similar results were obtained for the thermoresponsive pore opening in a related study.[57] The threshold temperature highly depends on the BME-bdc:DB-bdc ratio, but again non-linearly, since the phase transition of $[Zn_2(BME\text{-}bdc)_{1.5}(DB\text{-}bdc)_{0.5}dabco]_n$ occurs at higher temperatures than the phase transition of pure $[Zn_2(BMB\text{-}bdc)_2dabco]_n$, observed in DSC curves and also confirmed by variable temperature PXRD and differential scanning calorimetry (DSC) (Fig. 21).

Concluding, as seen from the above discussed examples, structural adaptivity in solid solutions (guest-dependent or temperature-dependent) can linearly be adjusted, however, non-linear effects are also possible and offer further tuning possibilities of the breathing behavior.

6. *In situ* characterization and computational analysis

The investigations of dynamic structural changes in flexible MOFs require special *in situ* analytical techniques. The application of *ex situ* solid state characterization methods is often not sufficient to understand all the processes occurring in a system. In particular by a multi-step adsorption behavior of MOFs, the probability of the existence of intermediate states and coexistence of several states in a narrow pressure range is high.

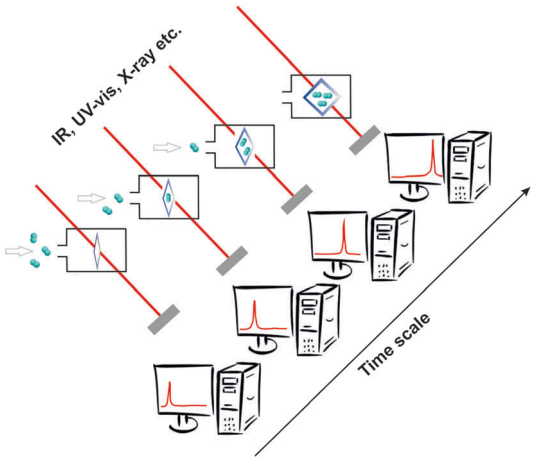

Fig. 22 Representation of *in situ* techniques for the characterization of flexible MOFs.

However, if a gas is used as a trigger molecule, only the starting state (empty framework) can be characterized by *"ex situ"* diffraction and spectroscopic techniques. To gain insight into the structural changes during the gas adsorption, the intermediate state should be stabilized for the time of measurement (*in situ*) and high time resolution during the adsorption process is beneficial (Fig. 22). Due to the crystallinity of MOFs, X-ray diffraction methods are predestinated for structure monitoring during the adsorption. Also *in situ* spectroscopic methods, such as NMR (Nuclear Magnetic Resonance), IR (Infra Red), RAMAN, EXAFS (Extended X-ray Adsorption Fine Structure) *etc.* are extremely useful, especially if the intermediate state is not crystalline or if motions of the framework need to be monitored, which do not correspond to crystallographic changes, such as linker rotations.

6.1. X-ray diffraction methods

The structural transition in flexible MOFs is usually accompanied by enormous changes in the lattice parameters and cell volume. These microscopic changes often lead to macroscopic damage of the single crystals, which makes it often very difficult to use single crystals for *in situ* investigations. However, *in situ* single crystal X-ray diffraction experiments are also possible in some particular cases. For example, the structural transformation of the two-fold interpenetrated $[Zn_2(bdc)_2(DF\text{-}bpb)]_n$ during the stepwise drying of the single crystal was investigated by Kitagawa *et al.*[88] The coordination environment of the Zn-atoms changes from square-pyramidal in the **lp** structure to a distorted tetrahedral in the **np** form. Single crystals of the flexible $[Sc_2(bdc)_3]_n$ were investigated *in situ* with different loadings of CO_2, H_2, CH_4 and C_2H_6 by Filinchuk co-workers[154] The details of framework rearrangements as well as the adsorption mechanisms of the above mentioned gases could be investigated. Moreover, well-defined adsorption sites for CO_2, CH_4, and C_2H_6 were determined.

The thermally induced structural changes in $[Cu_2(OH)(SO_3H\text{-}ip)(H_2O)\cdot 2H_2O]_n$ (Cu-SIP-3; SO_3H-ip = sulphoisophthalate) were also studied by *in situ* single crystal X-ray diffraction at

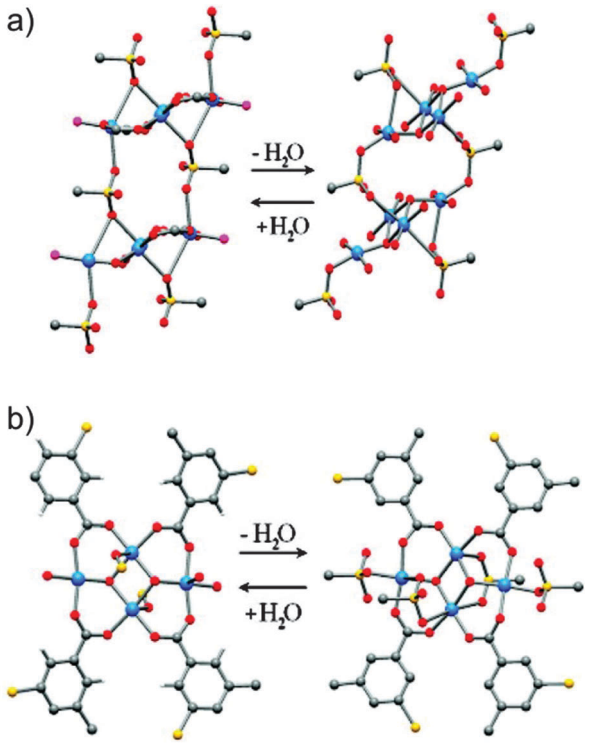

Fig. 23 Structural transformations in Cu-SIP-3 during hydration/dehydration: (a) Chains of the copper tetramers in the low-temperature (left) and high-temperature (right) structures. (b) Copper tetramers in the low-temperature (left) and high-temperature (right) structures. Color codes: Blue balls – copper atoms; red balls – oxygen atoms; yellow balls – sulfur atoms; grey balls – carbon atoms (Reprinted with permission from.[155] Copyright 2010. American Chemical Society.)

variable temperatures.[155] X-ray diffraction data were collected over a temperature range from 150 K to 500 K. Refinements of the data collected in the temperature range 150–365 K yielded the structure of hydrated Cu-SIP-3 (Fig. 23). In the temperature range of 370–405 K, no Bragg reflections were observed in the diffraction images indicating a loss of the long-range order in the crystal. A corresponding increase in the diffuse scattering from the crystal was observed. Obviously, a significant structural movement in this material is caused by water removal and is accompanied by increased movement of all atoms. Above 430 K, a highly crystalline, dehydrated material is formed (Cu-SIP-3), whose crystal structure could be determined. It has been shown that the structural transition can be fully reversed (under retention of the crystallinity) by exposure of the system to moisture.

Very recently, Kitagawa and coworkers were able to investigate the propagation mechanism of structural transformation in $[Zn_2(1,4\text{-ndc})_2(dabco)]_n$ (1,4-ndc = 1,4-naphthalenedicarboxylate) through an entire single crystal for the first time.[156] The contracted shell could be created on the outer surface of the single crystal by adsorption of organic molecules with dimensions, very close to the pore size of the framework. At the same time, the remaining part (the core) of the crystal stays in the original, open state. Using synchrotron grazing incidence single crystal diffraction measurements, the authors show that the structural transformation from the original phase to the deformed one is accompanied by sharing one out of four edges of the crystal cell to maintain the connectivity between the two phases. The obtained results clearly show that propagation of structural transformation and the domain formation is strongly correlated with the diffusion of molecules. Further development of this unique technique would definitely help to explain the mechanism of the structural transformation in other flexible MOFs.

For sensitive crystals, as well as for very small crystallites, powder X-ray diffraction is often the method of choice.[157] In order to collect high quality powder X-ray diffraction data time resolved, high intensity synchrotron radiation is essential,[42,157–160] but in principle, comparable experiments are also possible using the laboratory diffraction system. Often, the sample holder for *in situ* measurements is based on a thin-wall glass capillary (Fig. 24). The adsorption temperature is usually provided by a nitrogen cryostream setup that allows working in the temperature range of 80–500 K only.[161,162] Such type of instrumentation was developed by the group of Llewellyn and implemented at the Swiss-Norvegian beamline (European Synchrotron Radiation Facility). The instrumentation was widely used for *in situ* investigation of MIL-53(M) (M = Al, Cr) materials using carbon dioxide and hydrocarbons as probe molecules.[163–167] The main advantage of the capillary based setup is a possibility to perform *in situ* high-pressure gas adsorption experiments. For instance, pressures up to 100 bar can be achieved if the capillary with 0.5 mm inner diameter is used in the experiment.

To lower the possible working temperature up to 5.5 K and to achieve higher temperature stability, a system based on a closed cycle He cryostat and Be-dome (Fig. 24) was developed by Kaskel and co-workers.[162] However, the use of a Be-dome constricts the operating pressure range to 1 bar only. The gas dosing can be performed in both cases manually or the conventional automated gas dosing system can be adopted for *in situ* measurements.

In recent years, *in situ* powder X-ray diffraction was widely used for the characterization of flexible MOFs. The *in situ* study

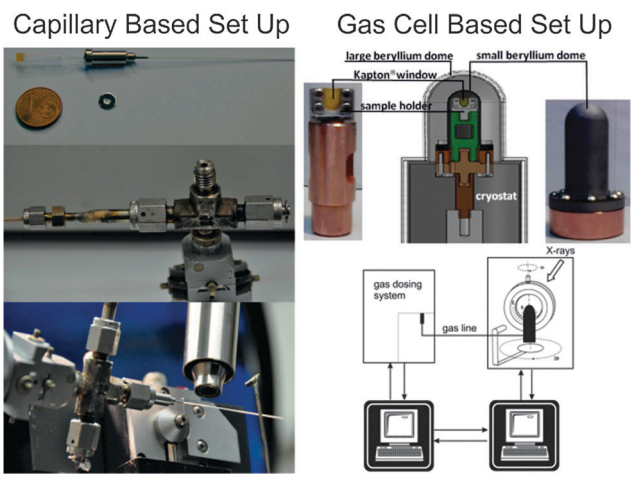

Fig. 24 Capillary based experimental setup (left) (Reprinted with permission[161]) and gas cell, based on closed cycle He-cryostat (right) (Reprinted with permission.[162] Copyright 2014. Elsevier.)

of $[Cu(bipy)_2(OTf)_2]_n$ (OTf = trifluoromethanesulfonate), also known as ELM-12 (Elastic Layer Material), shows no significant structural changes after the first CO_2 adsorption step in the isotherm, that agrees with a solvent accessible void of 17.9% for the activated structure. The second step in the isotherm is followed by a structural transition to the **lp**, leading to an increase of 38% of the unit cell volume.[159] In case of CPL-1[157] (Coordination Polymer with a Pillared-Layer Structure) with the composition $[Cu_2(pzdc)_2(pyz)]_n$ (pyz – pyrazine), the intermediate phase (**ip**) could be identified during the adsorption of acetylene at 270 K. The crystal structure of the **ip** form was solved from powder X-ray diffraction data, explaining the mechanism of acetylene adsorption on the framework. More than ten articles with regard to *in situ* XRD studies were published on MIL-53 materials.[167–176] Combined *in situ* PXRD and Raman spectroscopy experiments were performed on the MIL-53(Cr) material using a CO_2/CH_4 gas mixture as adsorptive, confirming the preferable CO_2 adsorption.[167] In the same manner, the effect of ligand functionalization was investigated using CO_2 high pressure adsorption. This proves the strong relationship between the functional group of the phenyl ring and flexible behavior of the framework. Surprisingly, $-NH_2$ and –COOH functionalized MIL-53 materials show no structural transformation during the CO_2 adsorption, in spite of the strong affinity of the adsorptive to these groups. Oppositely, materials containing –Cl, –Br and $-CH_3$ functionalized bdc linkers show a flexible character.[137] A successful combination of *in situ* PXRD with AIMD (Ab Initio Molecular Dynamics) simulation based approaches was used to explain the CO_2 adsorption related breathing phenomena (in particular, the broadening of the reflections in the powder XRD of the close pored form) of MIL-53(Sc).[170]

The structural dynamics of the partially interpenetrated flexible indium based framework NOTT-202 was investigated by *in situ* PXRD studies using CO_2 as the adsorptive. In this case, *in situ* powder diffraction data reveal the flexibility of the framework in the temperature and pressure range below the triple point of CO_2.[42]

In order to investigate processes with fast kinetics, *in situ* EDXRD (Energy Dispersive X-Ray Diffraction) is the method of choice. Very intense white X-radiation allows to measure PXRD patterns of the sample within a few seconds. Thus, the adsorption process of liquid alcohols on hydrated MIL-53(Fe) was monitored by EDXRD.[174] Also the adsorption kinetics for N/S-heterocycles on MIL-53(Fe) were studied by the same group using the same technique.[171]

Summarizing, the *in situ* powder XRD technique is mainly sensitive to structural changes of the host framework, although due to the physical limitations of X-rays, the method provides sometimes ambiguous information about the ordering of the adsorbed molecules, specifically in the case of light atom adsorbates. To solve this problem, *in situ* neutron diffraction can be used in some particular cases. By using deuterated adsorptives it is possible to determine the preferable adsorption sites. Mulder *et al.* studied the deuterium adsorption on MIL-53(Cr) by combined neutron diffraction and inelastic neutron scattering.[175] It has been shown that the adsorption sites near the Cr–O clusters reach the highest occupations. Thus, *in situ* diffraction methods give significant information about structural changes of the framework and about preferable adsorption sites in the structure.

6.2. NMR-methods

The ^{129}Xe NMR technique with thermally or hyperpolarized Xe as a probe has been widely used for characterization of porous solids, such as zeolites, amorphous silica–alumina, polymers, carbons, peptides, *etc.*[177] In the recent few years, the method was also applied to study the interaction between the adsorbed Xe and flexible MOFs. ^{129}Xe NMR spectroscopy of adsorbed xenon gives detailed information about the pore interior and dynamics, in particular the ^{129}Xe chemical shift, line width, chemical shift anisotropy, and longitudinal relaxation time T_1 are influenced by structural parameters, such as pore size, pore shape, composition of the pore walls, and dynamics.[178] The MOF lattice itself and its changes during the adsorption of NMR active species can be studied. Since the changes in the framework are accompanied by the changes in pore size and/or their pore windows, flexibility can also be explored in an indirect way by using probes like ^{129}Xe sensing the inner surface of the pores.

Springuel-Huet *et al.* have performed *in situ* ^{129}Xe adsorption NMR experiments on the flexible MIL-53(Al) material at different temperatures and pressures.[179] The authors use the chemical shift of Xe as an indicator of the local xenon amount and, consequently, of the extent of transformation from **lp** to **np** form. The hysteresis of the chemical shift variation *versus* xenon pressure observed for the signal corresponding to the **lp** form was explained by an exchange of the Xe atoms through the gas phase, between **lp** form and **np** form particles or by shrinkage of the one-dimensional pores at both ends of the crystal. The isothermal experiment (295 K) shows the adsorption of Xe on MIL-53(Al) even at low pressures confirming accessibility of the **np** form for the Xe atoms.

DUT-8(Ni) ($[Ni_2(2,6\text{-ndc})_2(dabco)]_n$) is a flexible gate-pressure material that was also studied using ^{129}Xe NMR (Fig. 25).[180] Isothermal *in situ* measurements at 237 K were performed in the pressure range from 1 to 19 bar and show only the signal of gaseous Xe within the pressure range from 1 to 12 bar. At 14 bar, a weak broad signal of adsorbed Xe at 227 ppm appears in the spectrum indicating the expansion of the structure. The desorption branch indicates both adsorbed and gaseous Xe in the whole pressure range from 14 to 1 bar, which is in good agreement with previously reported Xe adsorption data.[96,181] The isobaric (15 bar) *in situ* study of DUT-8(Ni) in the temperature range from 237 to 292 K shows almost no adsorption by increasing the temperature to 270 K and higher, confirming the presence of the narrow pore form of the compound. Lower temperatures (at the same pressure corresponding to a higher p/p_0) promote the gate opening, leading to the signal of adsorbed Xe at 225–230 ppm.

Recently, ZIF-8, which shows linker rotation, was explored using the same technique.[181] Although the kinetic diameter of the Xe atom is much higher (4.4 Å) than the pore windows in the MOF structure (3.4 Å), the adsorption of Xe occurs due to

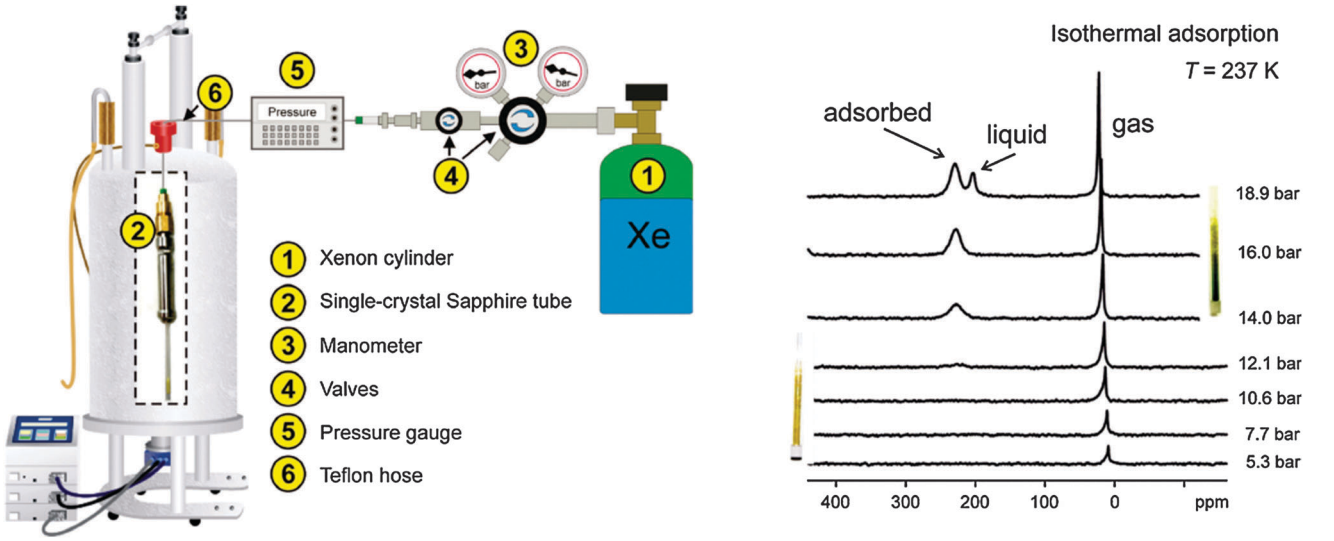

Fig. 25 Schematic representation of an apparatus for high pressure *in situ* ^{129}Xe NMR experiments under variable thermodynamic conditions (left). *In situ* ^{129}Xe NMR spectra recorded during the adsorption and desorption of Xenon on DUT-8(Ni) at 237 K (right). (Reprinted with permission[180] Copyright 2011. American Chemical Society.)

the rotation of the linker. The study was performed at a constant pressure of 10 Torr in the temperature range of 138–323 K. Deriving from the signal position at ~80 ppm, one can state that there is no specific interaction of Xe with the imidazolate moieties at ambient temperature. Low temperature spectra exhibit an abrupt increase in the chemical shift by more than 100 ppm within a narrow temperature range (between 163 K and 170 K). Thus, the chemical shift increases slowly when the temperature decreases from 380 K to 180–190 K, showing that the Xe–Xe interactions are negligible. After the transition that occurred at 166 K, the chemical shift remains constant and equal at around 215 ppm, which is typical for xenon dissolved in organic compounds and suggests that Xe atoms interact specifically with the imidazolate linkers, after the structural change, which occurs at low temperatures.

In summary, *in situ* NMR is a powerful technique that can be used as a complementary tool to X-ray powder diffraction and provides particularly information about host–guest interactions in flexible MOFs. However, the use of this method is still limited, presumably because of the lack of accessibility of the instruments and restrictions on certain probe molecules. Only *in situ* NMR studies with Xe and $^{13}CO_2$[182] as a probe are described in the literature so far.

6.3. Raman/IR-spectroscopy

Vibrational methods are one of the most powerful techniques that provide information about chemical bonding, helping to determine the structure of investigated compounds. Under *in situ* conditions, these methods can provide information about both, structural changes of the host framework and its interaction with the guest molecules. Technically, both *in situ* IR- and Raman spectroscopic experiments were realized using microscopes, connected to the spectrometers. The detailed instrumentation setups are described by Weckhuysen *et al.*[183] Usually Raman microscopes are installed at synchrotron beamlines, dedicated to *in situ* and *operando* investigations of catalysts.[184] For example, *in situ* Raman spectroscopy was used by Kitagawa and co-workers to confirm the COO^- bond rearrangements in the coordination environment of the Zn-based paddle-wheel unit in $[Zn_2(bdc)_2(DF\text{-}bpb)]_n$.[88] At 16 kPa CO_2 pressure, the characteristic double band of $\nu_{sym}(COO^-)$ vibration around 1425 cm^{-1} appears, along with the band from the adsorbed CO_2 at 1374 cm^{-1} (Fig. 26). The peak change indicates that the cluster undergoes a bond rearrangement after the first step of CO_2 adsorption at 195 K. Increasing pressure does not involve any further changes in the Raman spectrum apart from an increase in the intensity of the band related to adsorbed CO_2.

In situ IR spectroscopy during N_2 adsorption at 100 K was used as one of the characterization methods in combination with UV-vis and powder XRD for investigation of the multi-step adsorption behavior in $[Co(bdp)]_n$ (bdp = 1,4-benzenedipyrazolate).[185]

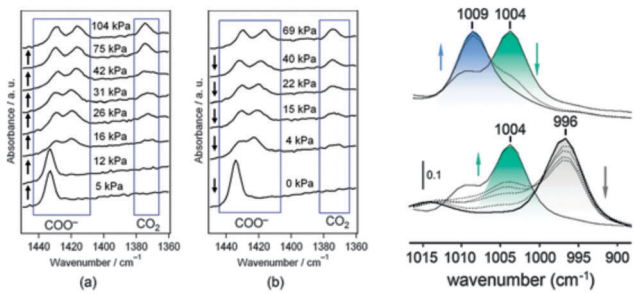

Fig. 26 Left: Raman spectra of $[Zn_2(bdc)_2(DF\text{-}bpb)]_n$ upon (a) adsorption and (b) desorption of CO_2 at 195 K (Reprinted with permission.[88] Copyright 2011 American Chemical Society); right: overlayed *in situ* infrared spectra for the pyrazolate ring stretch vibrations in $[Co(bdp)]_n$, recorded at 100 K with increasing N_2 pressure up to 0.01 bar (bottom) and from 0.01 to 0.023 bar (top). These transitions are coincident with the phase transitions from the dry form (gray) to **ip1** (green) to **ip2** (blue) (Reprinted with permission.[185] Copyright 2010. American Chemical Society.)

It was confirmed that the C–N stretching vibrations for the pyrazolate rings have undergone transitions from **np** to intermediate phase 1 (**ip1**) and from **ip1** to intermediate phase 2 (**ip2**) upon increasing the N_2 pressure to 0.01 and 0.023 bar, respectively (Fig. 26).

In the case of adsorption of a CO_2/CH_4 mixture on MIL-53(Cr), *in situ* Raman spectroscopy was used to provide an estimation of the composition of the adsorbate phase, as well as of the **lp**/**np** ratio.[167] For evaluating the **lp**/**np** ratio, the relative intensities of the characteristic bands at ~1432 and 1444 cm^{-1} were used (ν_{sym}(COO) vibration). The band at 1432 cm^{-1} is characteristic for the **np** form, while the band at 1444 cm^{-1} carries the signature of the **lp** form. The corresponding Raman band intensities were integrated and compared with gravimetric adsorption measurements. It was concluded that only in the case of pure gases, the correlation between the two applied methods was good enough, while in the case of gas mixtures, Raman spectroscopy tends to overestimate the adsorbed amount of methane compared to the gravimetric measurements. Further, *in situ* IR spectroscopy was applied to study the host–guest interactions on MIL-53(Fe)–X (X = Cl, Br, CH_3) solids upon adsorption of CO_2.[173] The experiments show the perturbation of the bands associated with the μ_2-OH group. Both, the ν(OH) and δ(OH) bands are shifted (from 3649 cm^{-1} to 3621 cm^{-1}, $\Delta\nu$(OH) = 28 cm^{-1} and from 842 cm^{-1} to 881 cm^{-1}, $\Delta\delta$(OH) = 39 cm^{-1}) and the ν_2 band of the adsorbed CO_2 is split into two components (651 cm^{-1} and 661 cm^{-1}). The shift of the ν(OH) and δ(OH) bands can be interpreted as a result of the formation of a hydrogen bond between the O atom of the CO_2 molecule and the H atom of the μ_2-OH group. Moreover, the information about μ_2-OH···X (X – Cl, Br) intra-framework interactions can be extracted from δ(OH) band shifts.

Schröder and coworkers used *in situ* DRIFTS (Diffuse Reflectance Infrared Fourier Transform Spectroscopy) for monitoring the adsorption of SO_2 on the partially interpenetrated flexible NOTT-202a framework.[186] The overtone vibrations of SO_2 were monitored in the region 2250–2540 cm^{-1}. In the absence of the MOF, two overtone bands observed at *ca.* 2500 and 2350 cm^{-1} were assigned to overtone and combination bands, respectively. After the sample was introduced into the *in situ* cell, the new bands at 2461 and 2280 cm^{-1}, consistent with adsorbed SO_2 on porous material, appeared in the IR spectra (Fig. 27). Recently, *in situ* RAMAN spectroscopy was used to confirm chemisorption of CO molecules (81.7 K) on the open metal sites of the flexible MOF $[Cu(aip)]_n$ (aip = 5-azidoisophtalate).[187] Pressure increase from 10 Pa to 1 kPa causes the appearance of the absorption band at 2168 cm^{-1}, clearly confirming the formation of a Cu···CO module.

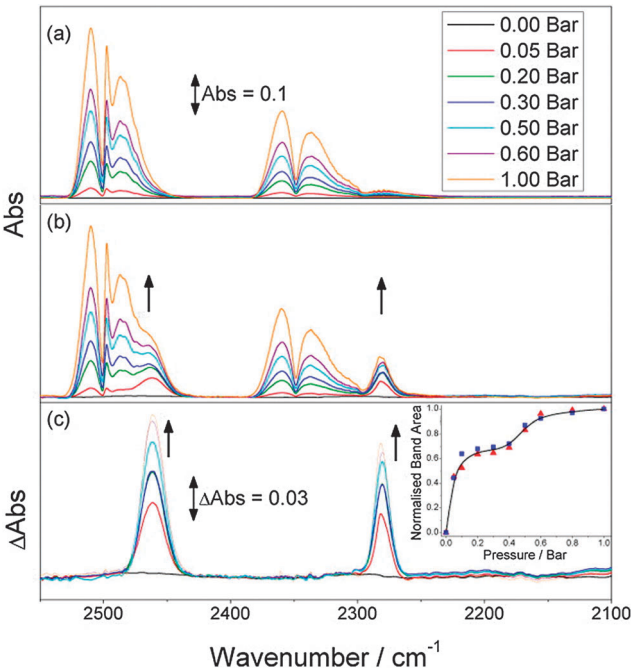

Fig. 27 *In situ* DRIFTS spectra of gaseous SO_2 at various pressures (0–1 bar) in the overtone region at 273 K: (a) KBr + SO_2, (b) KBr + NOTT-202a + SO_2, and (c) the difference spectra, showing the growth of two new bands. Arrows indicate the growth of bands due to adsorbed SO_2 with increasing pressure. Inset: Plot showing the growth of new bands at 2461 (red ▲) and 2280 cm^{-1} (blue ■) as a function of SO_2 pressure. The areas were averaged at each pressure to produce a point-to-point average (black beta-spline line) (Reprinted with permission. Copyright[186] 2013. American Chemical Society.)

6.4. X-ray absorption spectroscopy

EXAFS (Extended X-ray Absorption Fine Structure) is a powerful technique for determining the local structure of the metal cluster, in particular if single crystal X-ray data are not accessible for any reason. The rather simple measurement principle, as well as the rapidity makes the method appropriate for *in situ* measurements. Moreover, usually both *in situ* powder XRD and EXAFS often can be measured quasi–simultaneously on the same sample under the same conditions.[184] Currently, the method is widely used for *in situ* characterization of MOF materials during hydration and dehydration processes.[188] For instance, the local bond rearrangement of the metal clusters of the rigid frameworks HKUST-1 and UiO-66 (Universitetet i Oslo, $[Zr_6(OH)_4O_4(bdc)_6]_n$)[189] upon dehydration was studied. It should be mentioned that the use of XAS (X-ray absorption) is still not widely developed to study the flexibility of MOFs. It could be particularly useful in the cases of changes in coordination geometry during the phase transition. For example, *in situ* EXAFS was used for activation process monitoring of the Co based flexible MOF $[Co(Hoba)_2{\cdot}2H_2O]_n$ (Hoba = 4,4′-oxybis(benzoic acid)).[190] On the one hand, the differences observed in the XANES region (X-ray Adsorption Near Edge Spectroscopy) before and after activation (Fig. 28) are indicative of the local coordination geometry changes at the cobalt sites upon removal of the water molecules. On the other hand, reduction of the degeneracy value of the Co–O scattering pair in the EXAFS fitting from 6 in the as-synthesized phase to 4.2 in the activated phase confirms the expected decrease in coordination number accompanied by nearly complete removal of coordinated water molecules. In some particular cases, peculiarly in the case of crystalline-to-amorphous structural transitions, XAS could be the only method that can provide information concerning changes in the local structure of the metal cluster. For instance, the structural

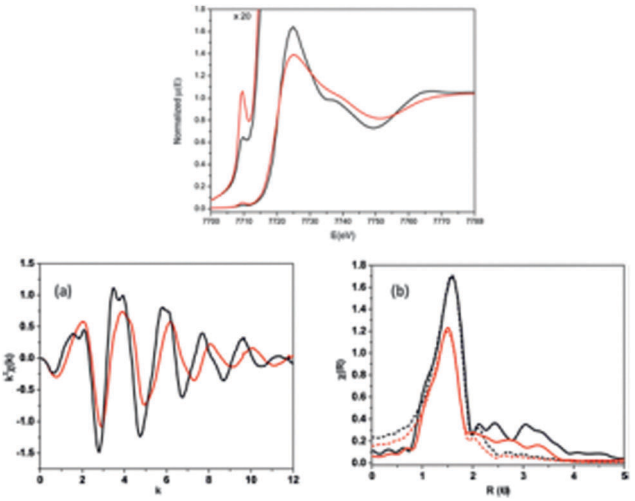

Fig. 28 Top: cobalt K-edge XANES spectra of 1 (black) and 1′ (red) pre edge feature at 7709.5 eV shown with 20× magnification. Bottom: comparison between EXAFS spectra of 1 and 1′ in (a) *k* space and (b) FT R space (also includes the theoretical first shell fits); see text for details of fitting. (Reprinted with permission.[190] Copyright 2012 American Chemical Society.)

changes in DUT-13 $[Zn_4O(BenzTB)_{3/2}]_n$; BenzTB = *N*,*N*,*N*′,*N*′-benzidinetetrabenzoate) cannot be explained by using exclusively *in situ* powder XRD because of amorphization of the sample in a certain range of the isotherm.[191]

6.5. Theoretical description of structural transitions in flexible MOFs

6.5.1. Thermodynamic analysis. A general thermodynamic model describing the adsorption phenomena in flexible MOFs was proposed by Coudert *et al.*[192] The model is based on the calculation of the grand canonical ensemble and the corresponding configurational partition function. By separating variables, the partition function can be expressed as a sum of configurational partition functions for each phase of the solid, finally reducing the flexibility problem to only three key parameters: the free energy of the solid phases, the adsorption isotherm of fluids inside that phase, and the molar volume of the fluid as a function of pressure. This model allows to calculate the relative free energies of the empty solid phases ($F^{(i)}_{host}$) in the absence of the adsorbent from readily available experimental adsorption isotherms, while the specific pore volume of the phases is extracted from crystal structure data. The multi-step isotherms are fitted using Langmuir type equations for each phase, this allows to calculate affinity constants (Henry constants, $K^{(i)}$) for each phase by fitting the corresponding sections in the isotherm. This model allows a qualitative distinction between "gating" and "breathing". Essentially in this model "gating" occurs as a single transition for soft porous crystals, in which the narrow pore phase (**1**, smaller pore volume) is energetically more stable than the empty large pored phase (**2**), both in the absence of the adsorbate, $V^{(2)}_p > V^{(1)}_p$, $F^{(2)}_{host} > F^{(1)}_{host}$. This picture is independent of the values of K and the energy difference $\Delta F_{host} = F^{(2)}_{host} - F^{(1)}_{host}$. Only if ΔF is too large, the energy gain from the adsorption term will not be able to compensate the energy penalty of the structural transformation. The typical "breathing" mode of MIL-53(Al) (two transitions, contraction followed by expansion) is observed if the empty large pore structure **1** is more stable than the narrow pore structure **2** in the absence of adsorbate ($V^{(1)}_p > V^{(2)}_p$, $F^{(2)}_{host} > F^{(1)}_{host}$) but only if the affinity for the adsorbate is higher for phase **2** ($K_2 > K_1$), which should be the case for most of the normal systems, since the adsorption potential in physisorption usually increases with decreasing pore size due to overlapping potentials. To put it very simple, an adsorbed species may interact with several pore walls (K_2) in the narrow pore structure but only with one of the walls (K_1) in the open pore structure, hence $K_2 > K_1$. In the case of MIL-53, adsorption enthalpies for both structures differ only slightly for Xe ($\Delta H_{ads,np}$ = 22.2 kJ mol^{-1}, $\Delta H_{ads,lp}$ = 19.8 kJ mol^{-1}) but the difference is very pronounced for CO_2 ($\Delta H_{ads,np}$ = 38.8 kJ mol^{-1}, $\Delta H_{ads,lp}$ = 26.0 kJ mol^{-1}).[193]

However, a second condition for breathing is that ΔF_{host} should be small enough or ΔK must be large enough,[192] in other words again, the energy gain due to the adsorption in the narrow pore structure (high K_2) must compensate the energy penalty of the structural transition. If this narrow pore form is too narrow, the small pore volume $V^{(2)}_p$ will not adsorb enough gas to compensate ΔF_{host}, only if K_2 is high (for example for CO_2), the transition will occur. Thus, a very subtle interplay between adsorptive interaction and structural bistability makes it difficult to predict novel breathing MOFs *ab initio*.

Valuable outcomes of the theoretical description are free energy differences ΔF_{host} extracted from adsorption data. In most of the guest induced transitions (physisorption) these energy differences fall into the 2–6 kJ mol^{-1} range, for example ΔF_{lp-np} = 2.5 kJ mol^{-1} per unit cell for MIL-53(Al). However, comparing such values for different MOFs may be misleading, since the unit cell is an arbitrary choice for the thermodynamic description and normalization would be needed. The analysis of temperature dependence of the isotherms may be used to calculate enthalpic and entropic contributions. Thus, in the case of Xe adsorption at MIL-53(Al), ΔH_{lp-np} and ΔS_{lp-np} were estimated to be 15 kJ mol^{-1} and 74 J (mol K)$^{-1}$.[194] As a result, the transition free energy was estimated to vanish at a lower temperature boundary of T = 203 (±20) K and the **np** structure becomes more stable below that temperature. On the other hand, entropy driven at high temperature (>300 K) the **lp**-structure is more stable independent of the Xe pressure. A simple estimation of this upper boundary (T_{max}), above which gas adsorption does not induce the **lp** → **np** phase transition, was given as $kT_{max} \approx \Delta H_{ads,lp}$.[193]

A full p-T phase diagram for Xe adsorption in MIL-53(Al) was derived from thermodynamic analysis revealing the regions in which phase transitions occur[195] and the general applicability was demonstrated by extending the methodology to CH_4 and CO_2 adsorption in MIL-53(Al),[193] clearly revealing that the host guest interactions are non-specific and mostly dominated by the differences in adsorption enthalpy of the different gases. Thus, the upper boundaries (T_{max} and p_{max}) above which gas adsorption does not induce the **lp** → **np** phase transition are observed for CO_2 molecules with the strongest host–guest interaction due to their quadrupole moments. The larger stability

domain of the **np** phase during CO_2 adsorption in amino functionalized MIL-53(Al) was attributed to the increased affinity for CO_2 due to the presence of amino groups.[195]

Overall, this phenomenological model is very general and applicable to many cases. The model can be extended for the prediction of structural transitions upon adsorption of gas mixtures, based on experimental pure component adsorption isotherms OFAST (Osmotic Framework Adsorbed Solution Theory), relying on Ideal Adsorbed Solution Theory (IAST) for prediction of co-adsorption and Langmuir fits of the experimental isotherms.[196–198] A restriction may be the limited availability of adsorption data to obtain a good Langmuir fit for both phases or at least for the open phase for "gating" MOFs (K values). On the other hand, the model can also account for small differences depending on the adsorbates, which may cause slightly different degrees of expansion/contraction (small differences in V_p). These intermediate structures correspond to stable states of the guest–host system and can be interpreted as elastic deformations of the empty host system (**np** or **lp**) depending on the adsorbate size. In the continuous deformation model[15] a particular value of deformation exists for which the adsorbate fits exactly into the pore interacting with multiple walls of the framework corresponding to a maximum Henry constant. This point was termed the single particle most comfortable structure (MCS). With increasing adsorbate size, the volume of the **np** form increases, while the volume of the large pore form is almost constant. For large adsorbates, only one form of the material is observed, corresponding to the **lp** structure leading to a first order transition between the empty **lp** structure and an expanded **lp** MCS causing a step in the adsorption isotherm. It should also be stressed that this analysis predicts the thermodynamic stability at full equilibrium and does not take into account (kinetic) hysteresis effects.

6.5.2. Stress-based model. In order to overcome this limitation, a stress-based model and a qualitative scenario for structural breathing was developed[99] by introducing two critical stress constants σ_{np}* and σ_{lp}*, each of them representing a threshold of critical stress the respective phase can withhold. Once the critical stress σ_{lp}* is reached, the MIL-53(Al) **lp** phase becomes unstable, and the first structural transition **lp** → **np** occurs. Since the vapor pressure corresponding to σ_{lp}* in adsorption is larger than the pressure corresponding to σ_{np}* in desorption, a hysteresis results. In this model the coexistence of **lp** and **np** phase observed in some experiments is explained by a broad crystallite size distribution causing a distribution in the critical stress constants. Defects or grain boundary distributions in polycrystalline samples would also cause a broader distribution for the critical stress but were not considered initially. A quantitative estimation of critical stress constants was extracted from mercury intrusion experiments by compressing an evacuated **lp** MIL-53 sample.[199] Thus, critical threshold stress values P^* = 55 and 10 MPa were obtained for the **lp** and **np** phase, respectively, while the regime of elastic deformation was quite limited (2.7% for **lp**, 3.6% for **np**) with an isotropic bulk modulus of 2 GPa (**lp**) and 10 GPa (**np**). Moreover, mercury intrusion reveals the particle size distribution postulated to account for the coexistence of **lp** and **np** phases.

Correlating external pressure in the mercury intrusion experiment with the gas pressure and adsorption stress allows us to predict the adsorption-driven elastic deformation based on compression experiments and thus reveals a unified quantitative picture for "breathing" transitions, characterized by regions of small reversible elastic deformation terminated by large irreversible plastic deformations occurring in a stepwise manner, which lead to hysteretic phase transformations.

An important step towards a better structural understanding of the flexibility was achieved by extending the isotropic stress in the model to a microscopic anisotropic elasticity tensor.[200] Full elastic constant tensors were calculated using *ab initio* mechanical calculations for flexible and rigid MOFs. As key quantities, the Young's modulus, linear compressibility and shear modulus were derived. It was recognized that all flexible MOFs (breathing or gating) show highly anisotropic Young's modulus, typically with high modulus along inorganic chains and linkers ($E_{max} \approx$ 50–100 GPa), but low modulus along the directions of deformation (the lowest value E_{min} typically below 1 GPa) resulting in high anisotropies, $A_E = E_{max}/E_{min}$ of 100–400. The presence of directions of very low Young's modulus indicates flexibility along this direction. They correspond to low energy phonons similar to the way low-frequency vibration modes of a molecular structure are indicators of its conformational flexibility. The occurrence of such soft modes initiating a displacive transition was also suggested from MD simulations of the host structure.[201] Similar features were reported for the shear modulus and linear compressibility resulting as well in high anisotropies for flexible MOFs. In contrast, rigid systems showed A_E values only up to 2.1 (for MOF-5). Many soft porous crystals show extreme linear compressibility including positive and negative lobes. The latter is a result of expansion in one direction as a response to isostatic compression and simultaneous compression along another direction of a lozenge shaped channel. Full tensorial analysis reveals key mechanical features of flexibility especially at the initiation of the deformation, as calculations are limited to the elastic domain with strains of up to ±1%, but will typically not cover the complex plastic structural transition. In order to account for the stepwise deformation, a simplified microscopic model was developed for MIL-53 assuming a layer-by-layer switching mechanism by shearing.[202,203] Thus, the deformation can be reduced to one order parameter only (as characterized by the angle of its rhombus cross section) while linker length and the inorganic chain (orthogonal to the rhombus axes) are essentially invariant. By introducing an energy barrier E_B (Fig. 29), and a coupling constant c, which accounts for the penalty between layers of **lp** and **np** phases (interfacial energy), the hysteresis and size effects can be qualitatively described. If E_B and c are zero, a two-step isotherm is observed due to the free energy difference between the two solids but without any hysteresis.

Both the free energy barrier and the layer–layer elastic coupling can cause hysteretic transitions, since the interlayer coupling penalizes the transformation of a single layer of cells in the material, and thus plays a similar role as the free energy barrier. However, in a strong coupling case, the hysteresis width is markedly widened with the number of layers, while

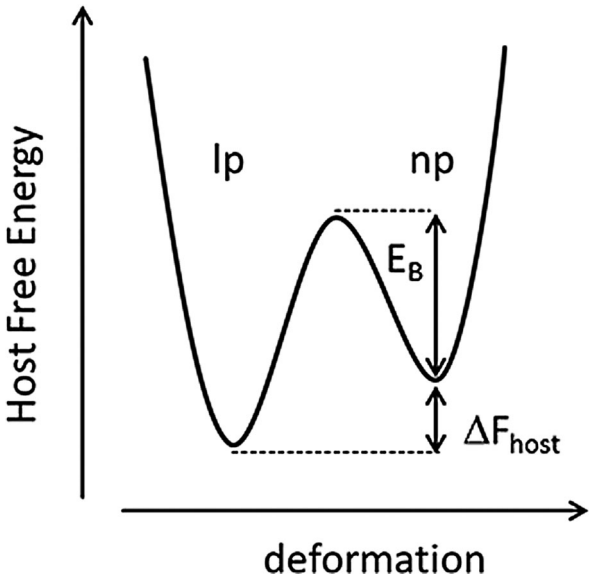

Fig. 29 Schematic of the host free energy landscape for the "dry" bistable framework.

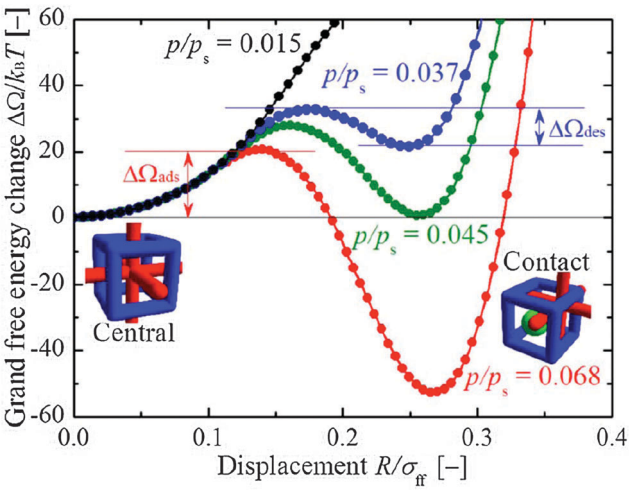

Fig. 30 Grand free energy profiles of the interpenetrated framework along the displacement of one JG relative to the other, calculated for different relative pressures. (Reprinted with permission.[205] Copyright 2009 American Institute of Physics.)

the small size system shows narrow hysteresis. The metastable states caused by interlayer coupling correspond to the simultaneous presence of **np** and **lp** layers in one crystal and are thus an alternative or complimentary explanation for the experimentally in some cases observed coexistence of **np** and **lp** phases. The model accounts for finite size effects and thus would conclude differences in the adsorption branch for powders with a particle size distribution (as discussed above). But two phase coexistence can also be expected in powders with monodispersed size distribution due to the possibility of **np–lp** phase coexistence in the process of breathing transition in one crystal. However, so far the conditions of time and length scales are not clear.[16]

6.5.3. Molecular modeling. The earliest work on modeling adsorption induced lattice transitions was performed by Miyahara and co-workers, focusing on catenated jungle gym structures as an example.[204,205] Grand Canonical Monte Carlo (GCMC) simulations were used to obtain a free energy landscape of the structural transition (Fig. 30). They fixed transition path and the gap distance between two jungle gyms (JGs) and calculated the direct interaction between two JGs and the fluid contribution. In systems composed of benzene rods the *central* configuration corresponding to the closed state is the more stable "empty" ("dry") structure due to the repulsion of the interpenetrating lattice, while the displacement of the interpenetrated structures to achieve *contact* enables the adsorption of gases, such as methane (open state) and for higher pressures a local minimum appears. At p/p_s = 0.045 the free energy profile becomes bistable and at higher pressure the contact configuration becomes more stable. The advantage of this approach is that both, equilibrium data and also energy barriers can be deduced, thus giving information on the equilibrium adsorption isotherm but also predicting hysteresis width. Similar to the thermodynamic analysis, two types of transitions can be distinguished, depending on which empty structure is more stable. The empty central configuration is more stable if repulsion of rods is dominant (for example for benzene linkers), while the empty contact configuration is more stable, if the rods are thinner (carbon rod), as compared to the pore width. In the latter case, the direction of the transition is reversed and the central configuration becomes stable at high pressure because it can accommodate more molecules and due to a high host–guest affinity.

A similar approach was taken to model the step-wise adsorption in $[Cu(bipy)_2(BF_4)_2]_n$ (ELM-11)[206] as a prototype system of a stacked layer MOF. In this case, the closed pored form is stable due to the interlayer attractive forces. By gradually increasing the interlayer width at different pressures free energy landscapes are obtained along a fixed trajectory. At $p/p_0 = 0$ only one minimum is observed corresponding to the closed structure, at p/p_0 = 0.10, a second local minimum appears caused by stabilization due to guest adsorption. Above p/p_0 = 0.013 this becomes the global minimum and the open structure is stabilized by host guest interactions again resulting in a step-wise adsorption isotherm (gating). This approach also illustrates the pressure dependence of the activation energies and thus the width of the hysteresis with respect to pressure and temperature. It was concluded that the gate closing pressure is closer to the equilibrium transition pressure because the gate-closing activation energy is more sensitive to the bulk gas pressure. In general, at the lower temperature regime, the hysteresis width (in absolute pressure) increases with temperature but decreases again at higher temperature and finally vanishes because the energy fluctuation of the system becomes larger than the activation energy. Domain size effects were simulated by constructing a kinetic transition model resulting in pressure and domain size dependent rate constants that increase with pressure by more than 15 orders of magnitude.[206] A smaller domain size produces a transition pressure closer to the equilibrium, whereas for large domain sizes a wide hysteresis is observed. Temperature dependence of the transition pressure was analyzed to deduce the enthalpy differences to reach the transient state.

Despite the deep insights resulting from these studies, they rely on a fixed trajectory of deformation, which is assumed for the simulation. Conventional modeling tools including molecular dynamics (MD) and GCMC techniques are not able to describe the complex interplay of the adsorption process and deformation in flexible MOFs simultaneously. GCMC methods typically allow a fluctuation of number of adsorbate molecules while considering the framework as rigid; MD simulations based on optimized force fields have been successfully applied to predict the structural forms present but for a fixed number of adsorbate molecules.[207] To overcome this limitation, a hybrid osmotic Monte Carlo (HOMC) simulation was proposed combining MD and GCMC techniques.[208] The method successfully reproduces the first **lp** → **np** transition in MIL-53(Cr) (CO_2 adsorption) at p_{calc} = 0.35 bar (p_{exp} = 0.30 bar) but fails to predict the reopening of the structure (**np** → **lp**). The latter was attributed to the difficulty in exploring the full phase space, due to the highly orientational ordered arrangement of the confined CO_2 molecules along the channel axis. To overcome this limitation, a complementary macroscopic "phase mixture" model was included, which allowed to reproduce the full isotherm and both transitions. Such simulations reveal the subtle interplay between structural features of the host and phase transitions, such as translational or orientational ordering of the adsorbate molecules.[201] In this way the microscopic identification of soft modes triggering the displacive transition and the corresponding mode frequency can be connected to the critical stress threshold value proposed in the stress-based model. First principles molecular dynamics simulations based on DFT Car–Parrinello are a powerful tool and were successfully used to model the water adsorption in MIL-53(Cr) by adding a fixed amount of water molecules to the empty framework.[209] Typical hydrogen bond arrangements and structures of the host guest arrangement in the **lp** and **np** structure were illustrated.

Contrary to MIL-53(Al) and MIL-53(Cr) solids, the **np** phase is more thermodynamically stable for the MIL-53(Ga) material. In order to explain the phenomenon, Coudert *et al.* performed a theoretical investigation of both materials using quantum chemical calculations, Density Functional Theory based Molecular Dynamics (DFT-MD) and Thermodynamic Model Based on the Osmotic Ensemble.[210] The energy minimization of both dehydrated frameworks shows that the **np** phase is more stable at low temperatures (Table 3).

The difference in $\Delta\Delta E \sim 4$ kJ mol^{-1} explains why the **lp**/**np** equilibrium temperature T_0 is higher for Ga-MIL-53 (480 K) than for Al-MIL-53 (200 K).

Table 3 Energy and entropy differences between the **lp** and **np** of Al-MIL-53 and Ga-MIL-53, obtained by quantum chemistry calculations. E_{tot} – total energy in kJ mol^{-1}, E_{el} – electronic DFT component in (kJ mol^{-1}), E_{disp} – dispersion correction in (kJ mol^{-1}), E_0 – zero-point energy in (J mol^{-1} K)

Δ (**lp**–**np**)	ΔE_{tot}	ΔE_{el}	ΔE_{disp}	ΔE_0	ΔS_{vib}
Al-MIL-53	35.7	−65.8	101.3	0.25	36.9
Ga-MIL-53	39.6	−53.3	94.5	−1.61	33.8

Another approach was used by the authors to explain the difference in ΔE_{el} and ΔE_{disp} for both materials. The additional calculations were performed on separated clusters, where all –OH groups and carboxylate ions are substituted by F^- anions. It results in a full relaxation of the metal centers to an undistorted octahedral geometry. This relaxation is related to the energetic penalty for the distorted "narrow-pore" conformation of the metal coordination, corresponding to a change in the energy of 97.3 kJ mol^{-1} for Al, and 87.8 kJ mol^{-1} for Ga. The smaller value of the energetic penalty for Ga-MIL-53 is connected with more diffuse electronic orbitals of the latter. This difference was interpreted by the authors as a reason for a higher stability of the **np** form of Ga-MIL-53 at room temperature in comparison with its Al analogue.

In conclusion, the qualitative analysis and partially the quantitative description of thermodynamics in flexible MOFs are well developed. However, a detailed microscopic (atomistic) understanding of switching mechanisms and corresponding time scales is just at the beginning.

7. Applications

Although the industrial application of flexibility in MOFs is still not completely developed, two flexible materials are offered by Sigma-Aldrich under the names Basolite® A100 (MIL-53(Al) analogue) and Basolite® Z1200 (ZIF-8), correspondingly. However, several research papers highlight the potential application of flexibility in MOFs. The most prospective fields of (industrial) application are separation processes, biomedical application, chemical sensing, and catalysis.

7.1. Separation

The dynamic pore system of flexible MOF materials makes them excellent candidates for application in different kinds of separation processes.[150,187,211–222] The separation of gases, especially in energetically favorable pressure swing separation processes, can be one promising application for flexible MOFs, due to the adsorption discrepancy of different gases. Thus, the selective sorption of CO_2 over O_2 and N_2 on flexible porous 2D framework CID-3, constructed from interdigitated $[Zn(2,7\text{-ndc})(bipy)]_n$ layers (2,7-ndc = 2,7-naphthalene dicarboxylate) was discovered by Kitagawa *et al.*[223] Adsorption experiments using $CO_2:O_2:N_2$ mixtures (in composition 1 : 1 : 1 and 1 : 21 : 78) show excellent separation performance of the material (Fig. 31). Although the concentration of CO_2 is low in the last case, clear separation is observed. After reaching the breakpoint, the curve of CO_2 smoothly returns to the initial intensity suggesting that the adsorption rate is relatively fast. The multiple adsorption experiments that were done on the same sample show the reproducibility of the results and reusability of the sample. The MIL-53(Al) material was also subjected to study CO_2/N_2 and CO_2/CH_4 separation.[218,220] In case of CO_2/N_2 separation, the characteristic breathing behavior of amino-MIL-53(Al) for both CO_2 and N_2 in high-pressure gas adsorption measurements can be used for selective adsorption of CO_2.

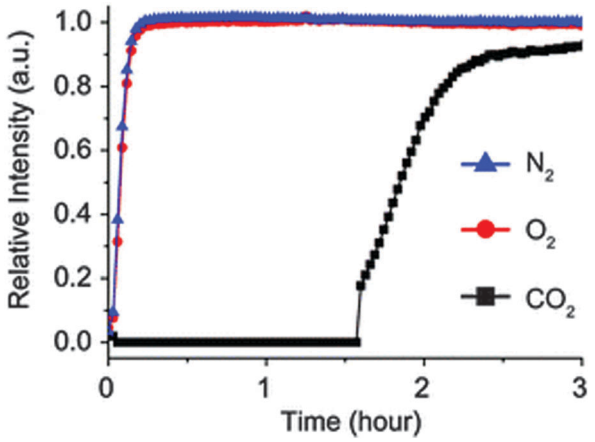

Fig. 31 Breakthrough curve for CID-3 for mixture $CO_2 : O_2 : N_2 = 1 : 21 : 78$ at total pressure of 0.5 MPa. (Reproduced with permission.[223] The Royal Society of Chemistry.)

Pressure swing adsorption–desorption cycles repeated six times between 0.5 and 2.0 MPa at 298 K in all cases showed no deterioration in CO_2 adsorption capacities (291 mg g^{-1} at 2.0 MPa).

In the work of Rodrigue *et al.*, MIL-53(Al) and its amino version were used to prepare MOF-based mixed matrix membranes for CO_2/CH_4 separation. 6FDA–ODA polyimide (6FDA = 4,4′-(hexafluoroisopropylidene)-diphthalic anhydride; ODA = 4,4′-oxydianiline) membranes containing Al-MIL-53-NH_2 particles for CO_2/CH_4 separation display high ideal selectivities up to 77, and a high separation factor up to 53, which is comparable to inorganic filters (zeolite FAU/EMT) for CO_2/CH_4 separation. The same material was subjected to prepare a membrane, supported on macroporous glass for selective hydrogen adsorption from binary H_2/CH_4, H_2/N_2 and H_2/CO_2 mixtures.[224] The membrane demonstrated to be highly selective for H_2 permeation with a separation factor higher than 20, due to its specific sorption affinity and the competitive adsorption effect. Besides the separation of gas mixtures, MIL-53(Al) was successfully tested in liquid phase separation as a stationary phase for HPLC columns. Thus, Millange and coworkers used the flexibility of MIL-53(Fe) to separate a mixture of xylene isomers.[219] In this case, the role of framework flexibility during the process was confirmed by structural analysis. In accordance with powder X-ray diffraction studies, the adsorption of each isomer leads to a fully expanded form of MIL-53(Fe) with a variety of host–guest and guest–guest interactions responsible for stabilizing the structure. The *ortho*- and *meta*-isomers show similar arrangements in the pores, while the *para*-isomer shows completely different host–guest interactions. This fact is underlined by testing the material under chromatographic conditions. As a result, only the *para*-isomer can be isolated at 293 K from the mixture. Remarkably, all components can be desorbed by increasing the temperature to 323 K.

These results are promising, but it should be acknowledged that often the selectivity is calculated from single component gas sorption isotherms. For gas mixtures, however, very complex flexible behavior can be observed. For example, for the MIL-53(Cr) system a high selectivity towards CO_2 over CH_4 was observed for the **np** phase, however the transition to the **lp** at higher working capacities leads to a low selectivity.[167]

Kitagawa and coworkers successfully showed the low energy separation of the strongly related gases CO and N_2 in soft porous crystals.[187] Namely, [Cu(aip)] adsorbs CO in a highly positive cooperative manner, accompanied by a structural transition to the **lp** phase. Oppositely, no structural changes were observed during the adsorption of N_2 under the same conditions. The separation ability was confirmed using mixtures of N_2 and CO (concentration of CO from 10%). A surprising enrichment of CO of 85% and 94% was achieved after the first and second cycles starting from a 1 : 1 mixture of CO and N_2, respectively.

7.2. Biomedical application

Controlled drug release, allowing focused supply of the API (Active Pharmaceutical Ingredient) to the target organ or part of the body, is a challenging task of biomedicine. After discovering the physiological function of nitric monoxide, the problem of targeted delivery was recognized. Exploration of MOFs as drug delivery agents, especially as gas carriers (including NO), was widely studied recently.[225] In particular, a high performance in NO storage under dry conditions was shown for HKUST-1, CPO-27(Ni), and CPO-27(Co) materials, containing open metal sites. Nevertheless, the application of such materials *in vivo* would be dubious, because they contain toxic metals, such as Cu, Ni or Co. Since iron is much less toxic compared to other metals, the iron based porous solids are more suitable for such applications. Recently, the group of Serre tested the iron based flexible MIL-88A as a NO carrier.[226] The loaded structure remains closed, binding NO to the accessible iron metal sites. *In situ* IR adsorption confirms even chemisorption of NO molecules on open metal sites that ensures the loading capacities within the 1–2.5 mmol g^{-1} range. The release of NO in "wet gas" or solution has a prolonged effect, releasing biologically significant quantities (10 parts per billion (ppb)) of NO for up to 16 h after starting from the MOF. Thus, the biomedical application of flexible MOFs is still not developed significantly, mostly because of toxicity and instability of the frameworks under physiological conditions. Beside gas molecules, loading of flexible MOFs with solid APIs was studied by Horcajada *et al.*[227] The ibuprofen was chosen as a model API that has to be adsorbed on biocompatible MIL-53(Fe). The diffraction study of the ibuprofen filled material agrees with the unit cell of MIL-53-lp phases. The delivery of ibuprofen was then performed using a simulated body fluid with inorganic composition similar to that of human plasma, at 37 °C under continuous stirring. Surprisingly, a very slow delivery is observed with clearly two steps in the process (Fig. 32). The slow kinetics of drug release could lead to a stable drug concentration in blood, a minimization of the toxicity effects, as well as a decrease in patient discomfort.

7.3. Sensing

The simplest imaginable sensor property of a flexible framework is a reversible color change upon structural transformation.

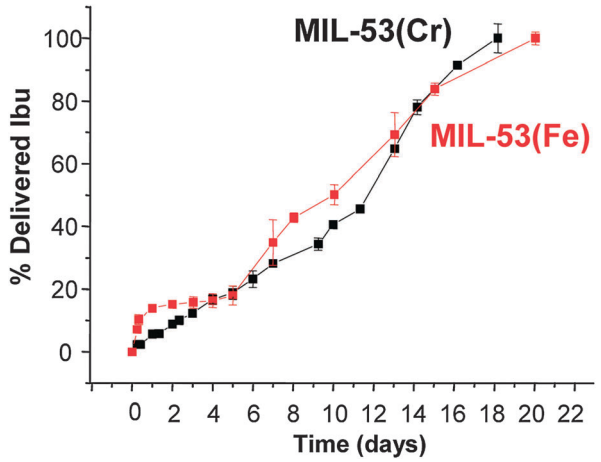

Fig. 32 Depiction of the delivery of Ibuprofen from MIL-53(Cr) and MIL-53(Fe). (Reprinted with permission.[227] Copyright 2008. American Chemical Society.)

For example, DUT-8(Ni) changes its color from yellow to green during the adsorption of CO_2, *n*-butane, N_2 *etc.*[96]

Another flexible ultramicroporous Co based MOF, $[Co_{1.5}(tipb)(SO_4)(bdc)_{0.5}]_n$ (tipb = 1,3,5-tris(*p*-imidazolylphenyl)benzene) involves tetrahedrally coordinated Co atoms in its activated structure.[228] The compound is highly responsive to H_2O and NH_3, showing reversible structural transformation associated with the change in the coordination geometry of Co from tetrahedral to octahedral. This is accompanied by a color change from blue to pink, occurring in a very narrow region of water vapor pressure (Fig. 33). A very promising flexible material, $[Zn_2(bdc)_2(dpNDI)]_n$ (dpNDI = *N*,*N*′-di(4-pyridyl)-1,4,5,8-naphthalenediimide), which is capable not only of detecting, but also of distinguishing between the target molecules was reported recently.[229] Adsorption of aromatic volatile organic compounds (VOCs) leads to the structural transformation of the host framework. Further excitation of the VOCs@$[Zn_2(bdc)_2(dpNDI)]_n$ with 370 nm light leads to the characteristic emission bands over the entire visible region (420–600 nm), allowing to detect the difference with the naked eye. The difference in interactions between dpNDI and VOCs leads to the emission of light with the following wave lengths: 421 nm for benzonitrile, 439 nm for benzene, 476 nm for toluene, 496 nm for *o*-xylene, 503 nm for *m*-xylene, 518 nm for *p*-xylene, and 592 nm for anisole.

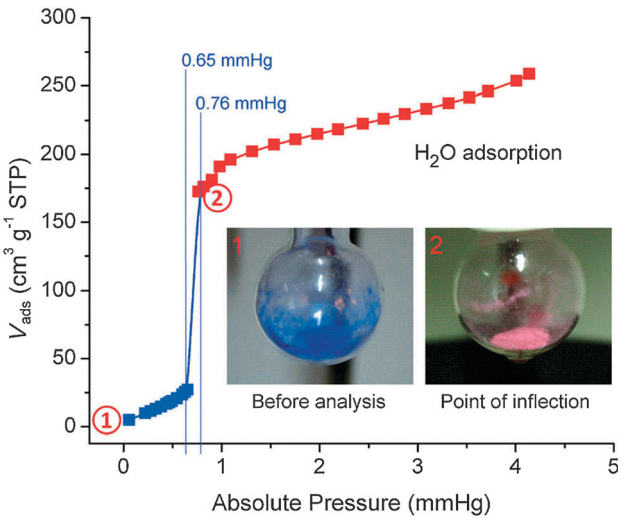

Fig. 33 Color change of $[Co_{1.5}(tipb)(SO_4)(bdc)_{0.5}]_n$ during H_2O adsorption. (Reprinted with permission.[228] Copyright 2012 John Wiley and Sons.)

Another example of possible application of flexible MOFs in sensor technology was shown by Yanai *et al.*[230] The composite material DSB@$[Zn_2(bdc)_2dabco]_n$ (DSB – distyrylbenzene) was used for the selective detection of CO_2 and C_2H_2. Moreover, the composite shows different fluorescence responses to CO_2 and acetylene, molecules that have similar physicochemical properties. In this case, the host–guest interactions play a key role in the sensing mechanism.

If the adsorption on a flexible MOF is accompanied by the size change of the crystallites, this deformation can also be used as a sensor signal.[231]

Moreover, in contrast to the rigid MOFs, the soft porous crystal can serve as a "smart" sensor, for monitoring and simultaneous adsorption of contaminants only when a certain threshold concentration (gate opening pressure) is reached.

7.4. Catalysis

Unfortunately the applicability of flexible MOFs in catalysis is not widely developed yet. Das *et al.* used a Gd based flexible MOF that serves as a heterogeneous catalyst in cyanosilylation and Knoevenagel condensation reactions, proceeding in the pores of the material.[232] In this case, the flexibility of the MOF was used for the first time to monitor the catalytic reaction inside the pore by single crystal X-ray diffraction analysis (Fig. 34). When single

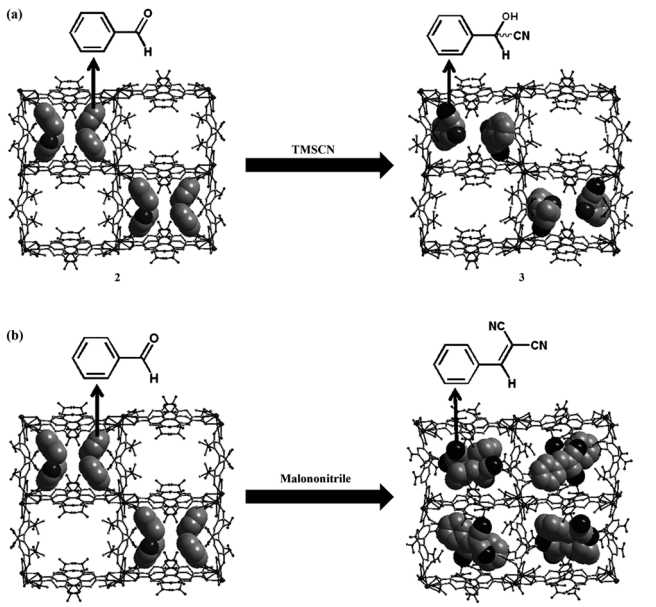

Fig. 34 Single-crystal to single-crystal transition, observed for the cyanosilylation (a) and Knoevenagel condensation reactions (b) of benzaldehyde. The framework is shown as a ball and stick model; guest molecules are shown as CPK models. (Reprinted with permission.[232] Copyright 2012 John Wiley and Sons.)

crystals of the as synthesized compound were exposed to benzaldehyde vapor at ambient temperature for 5 days, benzaldehyde agglomerated inside the pore without a loss in the crystallinity of the framework and preservation of the coordination environment of the Gd_2 dimeric unit and of the overall framework structure (Fig. 34), although the space group changed from $P2_1/c$ to $C2/c$. When a single crystal of a compound loaded with the benzaldehyde was exposed to trimethylsilyl cyanide vapor for 2 h at ambient temperature, 2-hydroxy-2-phenylacetonitrile was formed inside the pores without loss in crystallinity. As a result, the coordination geometry around each metal center remained intact, whilst four trimethylsilylcyanide molecules reacted with the four benzaldehyde molecules to form cyanohydrin trimethylsilylether. The Knoevenagel condensation reaction was performed by exposing a single crystal of the benzaldehyde containing framework to malononitrile vapor for two hours, which yielded a framework containing 2-benzylidenemalononitrile, without loss in crystallinity. Therefore, this study shows a possibility to explore the pore system of (flexible) MOFs for observing chemically important reactions that can also be useful to study their mechanisms.

8. Conclusions

Although a plethora of papers, presenting and discussing flexible MOFs and/or soft porous crystals and various concepts for designing unique functional properties – based on the materials ''softness'' and stimuli responsiveness even beyond simple host–guest interaction during adsorption–desorption – a comprehensive theory that involves all theoretical and experimental aspects of framework flexibility is still at its emerging state. The theory should be developed further, including scale bridging techniques to be able to not only explain, but also to predict the breathing behavior in MOFs and so support the experimental chemists with prospective structural models. Relying on the theoretical and experimental studies, the application potential, in particular in the field of low-energy and high selective gas separation, appears to be promising. A main challenge in the field of experimental chemistry of flexible MOFs guided by theoretical insight (*i.e.* molecular modeling) would be the directed synthesis of materials with pre-defined breathing/gate behavior and functionality. For system integration, thermally, magnetically or electrically switchable flexible materials are ideal for sensing and switching devices. In the field of characterization of flexible materials, sensible *in situ* methods should be further developed in order to identify and characterize the relevant host–host, host–guest and guest–guest interactions that play a key role in the various forms of flexible and dynamic processes.

Acknowledgements

A. S. acknowledges the Research Cluster SusChemSys (http://www.cmt.rwth-aachen.de/projects.html) for a doctoral fellowship. A. S. and I. Sch. acknowledge C. Wiktor for helpful discussions. V. B. acknowledges the German Federal Ministry of Education and Research (Projects 05K10OD3 and 05K13OD3) for the financial support and Helmholtz-Zentrum Berlin für Materialien und Energie for the beamtime, allocated for *in situ* investigation of flexible MOFs. Finally, the authors wish to acknowledge funding by the German Research Foundation *via* the Priority Program 1362 ''Metal–Organic Frameworks'' (http://www.metal-organic-frameworks.de/).

References

1 J.-R. Li, J. Sculley and H.-C. Zhou, *Chem. Rev.*, 2012, **112**, 869.
2 H. Furukawa, K. E. Cordova, M. O'Keeffe and O. M. Yaghi, *Science*, 2013, **341**, 974.
3 A. Schneemann, S. Henke, I. Schwedler and R. A. Fischer, *ChemPhysChem*, 2014, **15**, 823.
4 M. Li, D. Li, M. O'Keeffe and O. M. Yaghi, *Chem. Rev.*, 2014, **114**, 1343.
5 S. Kitagawa and M. Kondo, *Bull. Chem. Soc. Jpn.*, 1998, **71**, 1739.
6 S. Horike, S. Shimomura and S. Kitagawa, *Nat. Chem.*, 2009, **1**, 695.
7 G. Ferey and C. Serre, *Chem. Soc. Rev.*, 2009, **38**, 1380.
8 S. Kitagawa, R. Kitaura and S.-i. Noro, *Angew. Chem., Int. Ed.*, 2004, **43**, 2334.
9 S. Bureekaew, S. Shimomura and S. Kitagawa, *Sci. Technol. Adv. Mater.*, 2008, **9**, 014108.
10 K. Uemura, R. Matsuda and S. Kitagawa, *J. Solid State Chem.*, 2005, **178**, 2420.
11 G. Ferey, *Dalton Trans.*, 2009, 4400.
12 C. R. Murdock, B. C. Hughes, Z. Lu and D. M. Jenkins, *Coord. Chem. Rev.*, 2014, **258–259**, 119.
13 A. J. Fletcher, K. M. Thomas and M. J. Rosseinsky, *J. Solid State Chem.*, 2005, **178**, 2491.
14 L. E. Kreno, K. Leong, O. K. Farha, M. Allendorf, R. P. Van Duyne and J. T. Hupp, *Chem. Rev.*, 2012, **112**, 1105.
15 D. Bousquet, F.-X. Coudert, A. G. J. Fossati, A. V. Neimark, A. H. Fuchs and A. Boutin, *J. Chem. Phys.*, 2013, **138**, 174706.
16 F.-X. Coudert, A. Boutin, A. H. Fuchs and A. V. Neimark, *J. Phys. Chem. Lett.*, 2013, **4**, 3198.
17 T. Loiseau, C. Serre, C. Huguenard, G. Fink, F. Taulelle, M. Henry, T. Bataille and G. Ferey, *Chem. – Eur. J.*, 2004, **10**, 1373.
18 F. Millange, N. Guillou, R. I. Walton, J.-M. Greneche, I. Margiolaki and G. Ferey, *Chem. Commun.*, 2008, 4732.
19 F. Millange, C. Serre and G. Ferey, *Chem. Commun.*, 2002, 822.
20 C. Serre, F. Millange, C. Thouvenot, M. Nogues, G. Marsolier, D. Loueer and G. Ferey, *J. Am. Chem. Soc.*, 2002, **124**, 13519.
21 J. P. S. Mowat, V. R. Seymour, J. M. Griffin, S. P. Thompson, A. M. Z. Slawin, D. Fairen-Jimenez, T. Dueren, S. E. Ashbrook and P. A. Wright, *Dalton Trans.*, 2012, **41**, 3937.
22 C. Volkringer, T. Loiseau, N. Guillou, G. Ferey, E. Elkaim and A. Vimont, *Dalton Trans.*, 2009, 2241.

23 E. V. Anokhina, M. Vougo-Zanda, X. Wang and A. J. Jacobson, *J. Am. Chem. Soc.*, 2005, **127**, 15000.
24 C. Mellot-Draznieks, C. Serre, S. Surble, N. Audebrand and G. Ferey, *J. Am. Chem. Soc.*, 2005, **127**, 16273.
25 S. Surble, C. Serre, C. Mellot-Draznieks, F. Millange and G. Ferey, *Chem. Commun.*, 2006, 284.
26 H. Li, M. Eddaoudi, M. O'Keeffe and M. Yaghi, *Nature*, 1999, **402**, 276.
27 S. S. Y. Chui, S. M. F. Lo, J. P. H. Charmant, A. G. Orpen and I. D. Williams, *Science*, 1999, **283**, 1148.
28 D. Fairen-Jimenez, S. A. Moggach, M. T. Wharmby, P. A. Wright, S. Parsons and T. Duren, *J. Am. Chem. Soc.*, 2011, **133**, 8900.
29 G. Garberoglio and S. Taioli, *Microporous Mesoporous Mater.*, 2012, **163**, 215.
30 D. Fairen-Jimenez, R. Galvelis, A. Torrisi, A. D. Gellan, M. T. Wharmby, P. A. Wright, C. Mellot-Draznieks and T. Dueren, *Dalton Trans.*, 2012, **41**, 10752.
31 J. Seo, R. Matsuda, H. Sakamoto, C. Bonneau and S. Kitagawa, *J. Am. Chem. Soc.*, 2009, **131**, 12792.
32 T. K. Maji, R. Matsuda and S. Kitagawa, *Nat. Mater.*, 2007, **6**, 142.
33 P. Kanoo, R. Matsuda, M. Higuchi, S. Kitagawa and T. K. Maji, *Chem. Mater.*, 2009, **21**, 5860.
34 S. Bureekaew, H. Sato, R. Matsuda, Y. Kubota, R. Hirose, J. Kim, K. Kato, M. Takata and S. Kitagawa, *Angew. Chem., Int. Ed.*, 2010, **49**, 7660.
35 R. Kitaura, K. Seki, G. Akiyama and S. Kitagawa, *Angew. Chem., Int. Ed.*, 2003, **42**, 428.
36 O. K. Farha, I. Eryazici, N. C. Jeong, B. G. Hauser, C. E. Wilmer, A. A. Sarjeant, R. Q. Snurr, S. T. Nguyen, A. O. Yazaydin and J. T. Hupp, *J. Am. Chem. Soc.*, 2012, **134**, 15016.
37 R. K. Deshpande, J. L. Minnaar and S. G. Telfer, *Angew. Chem., Int. Ed.*, 2010, **49**, 4598.
38 R. K. Deshpande, G. I. N. Waterhouse, G. B. Jameson and S. G. Telfer, *Chem. Commun.*, 2012, **48**, 1574.
39 S. Ma, D. Sun, M. Ambrogio, J. A. Fillinger, S. Parkin and H.-C. Zhou, *J. Am. Chem. Soc.*, 2007, **129**, 1858.
40 J. L. C. Rowsell and O. M. Yaghi, *J. Am. Chem. Soc.*, 2006, **128**, 1304.
41 J. L. C. Rowsell and O. M. Yaghi, *Angew. Chem., Int. Ed.*, 2005, **44**, 4670.
42 S. Yang, X. Lin, W. Lewis, M. Suyetin, E. Bichoutskaia, J. E. Parker, C. C. Tang, D. R. Allan, P. J. Rizkallah, P. Hubberstey, N. R. Champness, K. M. Thomas, A. J. Blake and M. Schroeder, *Nat. Mater.*, 2012, **11**, 710.
43 A. Modrow, D. Zargarani, R. Herges and N. Stock, *Dalton Trans.*, 2011, **40**, 4217.
44 J. W. Brown, B. L. Henderson, M. D. Kiesz, A. C. Whalley, W. Morris, S. Grunder, H. Deng, H. Furukawa, J. I. Zink, J. F. Stoddart and O. M. Yaghi, *Chem. Sci.*, 2013, **4**, 2858.
45 J. Park, D. Yuan, K. T. Pham, J.-R. Li, A. Yakovenko and H.-C. Zhou, *J. Am. Chem. Soc.*, 2012, **134**, 99.
46 N. Yanai, T. Uemura, M. Inoue, R. Matsuda, T. Fukushima, M. Tsujimoto, S. Isoda and S. Kitagawa, *J. Am. Chem. Soc.*, 2012, **134**, 4501.
47 K. Uemura, Y. Yamasaki, Y. Komagawa, K. Tanaka and H. Kita, *Angew. Chem., Int. Ed.*, 2007, **46**, 6662.
48 R. Lyndon, K. Konstas, B. P. Ladewig, P. D. Southon, C. J. Kepert and M. R. Hill, *Angew. Chem., Int. Ed.*, 2013, **52**, 3695.
49 Y. Liu, J.-H. Her, A. Dailly, J. Ramirez-Cuesta Anibal, A. Neumann Dan and M. Brown Craig, *J. Am. Chem. Soc.*, 2008, **130**, 11813.
50 A. M. Walker, B. Civalleri, B. Slater, C. Mellot-Draznieks, F. Cora, C. M. Zicovich-Wilson, G. Roman-Perez, J. M. Soler and J. D. Gale, *Angew. Chem., Int. Ed.*, 2010, **49**, 7501.
51 I. E. Collings, A. B. Cairns, A. L. Thompson, J. E. Parker, C. C. Tang, M. G. Tucker, J. Catafesta, C. Levelut, J. Haines, V. Dmitriev, P. Pattison and A. L. Goodwin, *J. Am. Chem. Soc.*, 2013, **135**, 7610.
52 W. Zhou, H. Wu, T. Yildirim, J. R. Simpson and A. R. Hight Walker, *Phys. Rev. B: Condens. Matter Mater. Phys.*, 2008, **78**, 054114.
53 Y. Wu, A. Kobayashi, G. J. Halder, V. K. Peterson, K. W. Chapman, N. Lock, P. D. Southon and C. J. Kepert, *Angew. Chem., Int. Ed.*, 2008, **47**, 8929.
54 J. M. Ogborn, I. E. Collings, S. A. Moggach, A. L. Thompson and A. L. Goodwin, *Chem. Sci.*, 2012, **3**, 3011.
55 L. D. DeVries, P. M. Barron, E. P. Hurley, C. Hu and W. Choe, *J. Am. Chem. Soc.*, 2013, **133**, 14848.
56 C. Yang, X. Wang and M. A. Omary, *Angew. Chem., Int. Ed.*, 2009, **48**, 2500.
57 S. Henke, A. Schneemann and R. A. Fischer, *Adv. Funct. Mater.*, 2013, **23**, 5990.
58 T. D. Keene, D. Rankine, J. D. Evans, P. D. Southon, C. J. Kepert, J. B. Aitken, C. J. Sumby and C. J. Doonan, *Dalton Trans.*, 2013, **42**, 7871.
59 I. Grobler, V. J. Smith, P. M. Bhatt, S. A. Herbert and L. J. Barbour, *J. Am. Chem. Soc.*, 2013, **135**, 6411.
60 A. L. Goodwin, M. Calleja, M. J. Conterio, M. T. Dove, J. S. O. Evans, D. A. Keen, L. Peters and M. G. Tucker, *Science*, 2008, **319**, 794.
61 A. L. Goodwin and C. J. Kepert, *Phys. Rev. B: Condens. Matter Mater. Phys.*, 2005, **71**, 140301.
62 D. N. Dybtsev, H. Chun and K. Kim, *Angew. Chem., Int. Ed.*, 2004, **43**, 5033.
63 T. D. Bennett, D. A. Keen, J.-C. Tan, E. R. Barney, A. L. Goodwin and A. K. Cheetham, *Angew. Chem., Int. Ed.*, 2011, **50**, 3067.
64 J. C. Tan and A. K. Cheetham, *Chem. Soc. Rev.*, 2011, **40**, 1059.
65 K. W. Chapman, D. F. Sava, G. J. Halder, P. J. Chupas and T. M. Nenoff, *J. Am. Chem. Soc.*, 2011, **133**, 18583.
66 K. W. Chapman, G. J. Halder and P. J. Chupas, *J. Am. Chem. Soc.*, 2009, **131**, 17546.
67 S. A. Moggach, T. D. Bennett and A. K. Cheetham, *Angew. Chem., Int. Ed.*, 2009, **48**, 7087.
68 K. W. Chapman, G. J. Halder and P. J. Chupas, *J. Am. Chem. Soc.*, 2008, **130**, 10524.
69 W. Li, M. R. Probert, M. Kosa, T. D. Bennett, A. Thirumurugan, R. P. Burwood, M. Parinello, J. A. K. Howard and A. K. Cheetham, *J. Am. Chem. Soc.*, 2012, **134**, 11940.

70 K. J. Gagnon, C. M. Beavers and A. Clearfield, *J. Am. Chem. Soc.*, 2013, **135**, 1252.
71 A. L. Goodwin, D. A. Keen and M. G. Tucker, *Proc. Natl. Acad. Sci. U. S. A.*, 2008, **105**, 18708.
72 P. G. Yot, Q. Ma, J. Haines, Q. Yang, A. Ghoufi, T. Devic, C. Serre, V. Dmitriev, G. Ferey, C. Zhong and G. Maurin, *Chem. Sci.*, 2012, **3**, 1100.
73 I. Beurroies, M. Boulhout, P. L. Llewellyn, B. Kuchta, G. Ferey, C. Serre and R. Denoyel, *Angew. Chem., Int. Ed.*, 2010, **49**, 7526.
74 H. Uehara, S. Diring, S. Furukawa, Z. Kalay, M. Tsotsalas, M. Nakahama, K. Hirai, M. Kondo, O. Sakata and S. Kitagawa, *J. Am. Chem. Soc.*, 2011, **133**, 11932.
75 T. D. Bennett, S. Cao, J. C. Tan, D. A. Keen, E. G. Bithell, P. J. Beldon, T. Friscic and A. K. Cheetham, *J. Am. Chem. Soc.*, 2011, **133**, 14546.
76 Y. Sakata, S. Furukawa, M. Kondo, K. Hirai, N. Horike, Y. Takashima, H. Uehara, N. Louvain, M. Meilikhov, T. Tsuruoka, S. Isoda, W. Kosaka, O. Sakata and S. Kitagawa, *Science*, 2013, **339**, 193.
77 D. Tanaka, A. Henke, K. Albrecht, M. Moeller, K. Nakagawa, S. Kitagawa and J. Groll, *Nat. Chem.*, 2010, **2**, 410.
78 Y. Hijikata, S. Horike, D. Tanaka, J. Groll, M. Mizuno, J. Kim, M. Takata and S. Kitagawa, *Chem. Commun.*, 2011, **47**, 7632.
79 A. Betard and R. A. Fischer, *Chem. Rev.*, 2012, **112**, 1055.
80 C. Scherb, R. Koehn and T. Bein, *J. Mater. Chem.*, 2010, **20**, 3046.
81 I. Senkovska, F. Hoffmann, M. Fröba, J. Getzschmann, W. Böhlmann and S. Kaskel, *Microporous Mesoporous Mater.*, 2009, **122**, 93.
82 T. Loiseau, C. Mellot-Draznieks, H. Muguerra, G. Ferey, M. Haouas and F. Taulelle, *C. R. Chim.*, 2005, **8**, 765.
83 S. Bourrelly, P. L. Llewellyn, C. Serre, F. Millange, T. Loiseau and G. Ferey, *J. Am. Chem. Soc.*, 2005, **127**, 13519.
84 H. Leclerc, T. Devic, S. Devautour-Vinot, P. Bazin, N. Audebrand, G. Ferey, M. Daturi, A. Vimont and G. Clet, *J. Phys. Chem. C*, 2011, **115**, 19828.
85 G. Ferey, C. Serre, C. Mellot-Draznieks, F. Millange, S. Surble, J. Dutour and I. Margiolaki, *Angew. Chem., Int. Ed.*, 2004, **43**, 6296.
86 G. Ferey, C. Mellot-Draznieks, C. Serre, F. Millange, J. Dutour, S. Surble and I. Margiolaki, *Science*, 2005, **309**, 2040.
87 C. Serre, F. Millange, S. Surble and G. Ferey, *Angew. Chem., Int. Ed.*, 2004, **43**, 6286.
88 J. Seo, C. Bonneau, R. Matsuda, M. Takata and S. Kitagawa, *J. Am. Chem. Soc.*, 2011, **133**, 9005.
89 K. Seki and W. Mori, *J. Phys. Chem. B*, 2002, **106**, 1380.
90 R. Kitaura, F. Iwahori, R. Matsuda, S. Kitagawa, Y. Kubota, M. Takata and T. C. Kobayashi, *Inorg. Chem.*, 2004, **43**, 6522.
91 D. Tanaka, M. Higuchi, S. Horike, R. Matsuda, Y. Kinoshita, N. Yanai and S. Kitagawa, *Chem. – Asian J.*, 2008, **3**, 1343.
92 H. Wang, J. Getzschmann, I. Senkovska and S. Kaskel, *Microporous Mesoporous Mater.*, 2008, **116**, 653.
93 H. Sakamoto, R. Kitaura, R. Matsuda, S. Kitagawa, Y. Kubota and M. Takata, *Chem. Lett.*, 2010, **39**, 218.
94 P. Kanoo, G. Mostafa, R. Matsuda, S. Kitagawa and T. Kumar Maji, *Chem. Commun.*, 2011, **47**, 8106.
95 N. Klein, H. C. Hoffmann, A. Cadiau, J. Getzschmann, M. R. Lohe, S. Paasch, T. Heydenreich, K. Adil, I. Senkovska, E. Brunner and S. Kaskel, *J. Mater. Chem.*, 2012, **22**, 10303.
96 N. Klein, C. Herzog, M. Sabo, I. Senkovska, J. Getzschmann, S. Paasch, M. R. Lohe, E. Brunner and S. Kaskel, *Phys. Chem. Chem. Phys.*, 2010, **12**, 11778.
97 A. Pichon, C. M. Fierro, M. Nieuwenhuyzen and S. L. James, *CrystEngComm*, 2007, **9**, 449.
98 D. N. Dybtsev, H. Chun and K. Kim, *Angew. Chem., Int. Ed.*, 2004, **43**, 5033.
99 A. V. Neimark, F.-X. Coudert, A. Boutin and A. H. Fuchs, *J. Phys. Chem. Lett.*, 2009, **1**, 445.
100 K. C. Stylianou, J. Rabone, S. Y. Chong, R. Heck, J. Armstrong, P. V. Wiper, K. E. Jelfs, S. Zlatogorsky, J. Bacsa, A. G. McLennan, C. P. Ireland, Y. Z. Khimyak, K. M. Thomas, D. Bradshaw and M. J. Rosseinsky, *J. Am. Chem. Soc.*, 2012, **134**, 20466.
101 H. J. Park and M. P. Suh, *Chem. Commun.*, 2010, **46**, 610.
102 V. Bon, I. Senkovska, D. Wallacher, D. M. Toebbens, I. Zizak, R. Feyerherm, U. Mueller and S. Kaskel, *Inorg. Chem.*, 2014, **53**, 1513.
103 M. Eddaoudi, J. Kim, N. Rosi, D. Vodak, J. Wachter, M. O'Keeffe and O. M. Yaghi, *Science*, 2002, **295**, 469.
104 S. Biswas, T. Ahnfeldt and N. Stock, *Inorg. Chem.*, 2012, **50**, 9518.
105 S. Biswas, T. Remy, S. Couck, D. Denysenko, G. Rampelberg, J. F. M. Denayer, D. Volkmer, C. Detavernier and P. Van Der Voort, *Phys. Chem. Chem. Phys.*, 2013, **15**, 3552.
106 S. Biswas and P. Van Der Voort, *Eur. J. Inorg. Chem.*, 2013, 2154.
107 S. Biswas, J. Zhang, Z. Li, Y.-Y. Liu, M. Grzywa, L. Sun, D. Volkmer and P. Van Der Voort, *Dalton Trans.*, 2013, **42**, 4730.
108 S. J. Garibay and S. M. Cohen, *Chem. Commun.*, 2010, **46**, 7700.
109 S. T. Meek, S. L. Teich-McGoldrick, J. J. Perry, J. A. Greathouse and M. D. Allendorf, *J. Phys. Chem. C*, 2012, **116**, 19765.
110 P. Serra-Crespo, E. Gobechiya, E. V. Ramos-Fernandez, J. Juan-Alcaniz, A. Martinez-Joaristi, E. Stavitski, C. E. A. Kirschhock, J. A. Martens, F. Kapteijn and J. Gascon, *Langmuir*, 2012, **28**, 12916.
111 S. Henke, A. Schneemann, S. Kapoor, R. Winter and R. A. Fischer, *J. Mater. Chem.*, 2012, **22**, 909.
112 M. Kim, J. A. Boissonnault, P. V. Dau and S. M. Cohen, *Angew. Chem., Int. Ed.*, 2011, **50**, 12193.
113 P. V. Dau, L. R. Polanco and S. M. Cohen, *Dalton Trans.*, 2013, **42**, 4013.
114 K. Hindelang, A. Kronast, S. I. Vagin and B. Rieger, *Chem. – Eur. J.*, 2013, **19**, 8244.
115 K. Hindelang, S. I. Vagin, C. Anger and B. Rieger, *Chem. Commun.*, 2012, **48**, 2888.

116 K. Hirai, S. Furukawa, M. Kondo, M. Meilikhov, Y. Sakata, O. Sakata and S. Kitagawa, *Chem. Commun.*, 2012, **48**, 6472.
117 G. Tuci, A. Rossin, X. Xu, M. Ranocchiari, J. A. van Bokhoven, L. Luconi, I. Manet, M. Melucci and G. Giambastiani, *Chem. Mater.*, 2013, **25**, 2297.
118 A. D. Burrows, C. G. Frost, M. F. Mahon and C. Richardson, *Chem. Commun.*, 2009, 4218.
119 S. M. Cohen, *Chem. Sci.*, 2010, **1**, 32.
120 T. Gadzikwa, K. Farha Omar, D. Malliakas Christos, G. Kanatzidis Mercouri, T. Hupp Joseph and T. Nguyen SonBinh, *J. Am. Chem. Soc.*, 2009, **131**, 13613.
121 T. Gadzikwa, G. Lu, C. L. Stern, S. R. Wilson, J. T. Hupp and S. T. Nguyen, *Chem. Commun.*, 2008, 5493.
122 Y. Goto, H. Sato, S. Shinkai and K. Sada, *J. Am. Chem. Soc.*, 2008, **130**, 14354.
123 M. Savonnet, D. Bazer-Bachi, N. Bats, J. Perez-Pellitero, E. Jeanneau, V. Lecocq, C. Pinel and D. Farrusseng, *J. Am. Chem. Soc.*, 2010, **132**, 4518.
124 Z. Wang and S. M. Cohen, *J. Am. Chem. Soc.*, 2007, **129**, 12368.
125 J. G. Nguyen and S. M. Cohen, *J. Am. Chem. Soc.*, 2010, **132**, 4560.
126 Z. Wang and S. M. Cohen, *Angew. Chem., Int. Ed.*, 2008, **47**, 4699.
127 C. A. Allen and S. M. Cohen, *J. Mater. Chem.*, 2012, **22**, 10188.
128 K. K. Tanabe, C. A. Allen and S. M. Cohen, *Angew. Chem., Int. Ed.*, 2010, **49**, 9730.
129 M. Kim, J. F. Cahill, H. Fei, K. A. Prather and S. M. Cohen, *J. Am. Chem. Soc.*, 2012, **134**, 18082.
130 M. Kim, J. F. Cahill, Y. Su, K. A. Prather and S. M. Cohen, *Chem. Sci.*, 2012, **3**, 126.
131 S. Takaishi, E. J. DeMarco, M. J. Pellin, O. K. Farha and J. T. Hupp, *Chem. Sci.*, 2013, **4**, 1509.
132 O. Karagiaridi, W. Bury, A. A. Sarjeant, C. L. Stern, O. K. Farha and J. T. Hupp, *Chem. Sci.*, 2012, **3**, 3256.
133 O. Karagiaridi, W. Bury, E. Tylianakis, A. A. Sarjeant, J. T. Hupp and O. K. Farha, *Chem. Mater.*, 2013, **25**, 3499.
134 O. Karagiaridi, M. B. Lalonde, W. Bury, A. A. Sarjeant, O. K. Farha and J. T. Hupp, *J. Am. Chem. Soc.*, 2012, **134**, 18790.
135 S. Pullen, H. Fei, A. Orthaber, S. M. Cohen and S. Ott, *J. Am. Chem. Soc.*, 2013, **135**, 16997.
136 S. Biswas, T. Ahnfeldt and N. Stock, *Inorg. Chem.*, 2011, **50**, 9518.
137 T. Devic, P. Horcajada, C. Serre, F. Salles, G. Maurin, B. Moulin, D. Heurtaux, G. Clet, A. Vimont, J.-M. Greneche, B. Le Ouay, F. Moreau, E. Magnier, Y. Filinchuk, J. Marrot, J.-C. Lavalley, M. Daturi and G. Ferey, *J. Am. Chem. Soc.*, 2010, **132**, 1127.
138 S. Henke, A. Schneemann, A. Wuetscher and R. A. Fischer, *J. Am. Chem. Soc.*, 2012, **134**, 9464.
139 Z. Wang and S. M. Cohen, *J. Am. Chem. Soc.*, 2009, **131**, 16675.
140 P. Horcajada, F. Salles, S. Wuttke, T. Devic, D. Heurtaux, G. Maurin, A. Vimont, M. Daturi, O. David, E. Magnier, N. Stock, Y. Filinchuk, D. Popov, C. Riekel, G. Ferey and C. Serre, *J. Am. Chem. Soc.*, 2011, **133**, 17839.
141 P. V. Dau and S. M. Cohen, *CrystEngComm*, 2013, **15**, 9304.
142 P. V. Dau, M. Kim, S. J. Garibay, F. H. L. Munch, C. E. Moore and S. M. Cohen, *Inorg. Chem.*, 2012, **51**, 5671.
143 A. D. Burrows, *CrystEngComm*, 2011, **13**, 3623.
144 O. Kozachuk, K. Khaletskaya, M. Halbherr, A. Betard, M. Meilikhov, R. W. Seidel, B. Jee, A. Poeppl and R. A. Fischer, *Eur. J. Inorg. Chem.*, 2012, 1688.
145 W. Kleist, F. Jutz, M. Maciejewski and A. Baiker, *Eur. J. Inorg. Chem.*, 2009, 3552.
146 M. I. Breeze, G. Clet, B. C. Campo, A. Vimont, M. Daturi, J.-M. Greneche, A. J. Dent, F. Millange and R. I. Walton, *Inorg. Chem.*, 2013, **52**, 8171.
147 H. Deng, C. J. Doonan, H. Furukawa, R. B. Ferreira, J. Towne, C. B. Knobler, B. Wang and O. M. Yaghi, *Science*, 2010, **327**, 846.
148 X. Kong, H. Deng, F. Yan, J. Kim, J. A. Swisher, B. Smit, O. M. Yaghi and J. A. Reimer, *Science*, 2013, **341**, 882.
149 T. Fukushima, S. Horike, H. Kobayashi, M. Tsujimoto, S. Isoda, M. L. Foo, Y. Kubota, M. Takata and S. Kitagawa, *J. Am. Chem. Soc.*, 2012, **134**, 13341.
150 T. Fukushima, S. Horike, Y. Inubushi, K. Nakagawa, Y. Kubota, M. Takata and S. Kitagawa, *Angew. Chem., Int. Ed.*, 2010, **49**, 4820.
151 F. Nouar, T. Devic, H. Chevreau, N. Guillou, E. Gibson, G. Clet, M. Daturi, A. Vimont, J. M. Greneche, M. I. Breeze, R. I. Walton, P. L. Llewellyn and C. Serre, *Chem. Commun.*, 2012, **48**, 10237.
152 O. Kozachuk, M. Meilikhov, K. Yusenko, A. Schneemann, B. Jee, A. V. Kuttatheyil, M. Bertmer, C. Sternemann, A. Poeppl and R. A. Fischer, *Eur. J. Inorg. Chem.*, 2013, 4546.
153 T. Lescouet, E. Kockrick, G. Bergeret, M. Pera-Titus, S. Aguado and D. Farrusseng, *J. Mater. Chem.*, 2012, **22**, 10287.
154 S. R. Miller, P. A. Wright, T. Devic, C. Serre, G. r. Férey, P. L. Llewellyn, R. Denoyel, L. Gaberova and Y. Filinchuk, *Langmuir*, 2009, **25**, 3618.
155 P. K. Allan, B. Xiao, S. J. Teat, J. W. Knight and R. E. Morris, *J. Am. Chem. Soc.*, 2010, **132**, 3605.
156 M. Kondo, S. Furukawa, K. Hirai, T. Tsuruoka, J. Reboul, H. Uehara, S. Diring, Y. Sakata, O. Sakata and S. Kitagawa, *J. Am. Chem. Soc.*, 2014, **136**, 4938.
157 Y. Kubota, M. Takata, R. Matsuda, R. Kitaura, S. Kitagawa and T. C. Kobayashi, *Angew. Chem., Int. Ed.*, 2006, **45**, 4932.
158 W. Yang, A. J. Davies, X. Lin, M. Suyetin, R. Matsuda, A. J. Blake, C. Wilson, W. Lewis, J. E. Parker, C. C. Tang, M. W. George, P. Hubberstey, S. Kitagawa, H. Sakamoto, E. Bichoutskaia, N. R. Champness, S. Yang and M. Schroder, *Chem. Sci.*, 2012, **3**, 2993.
159 A. Kondo, H. Noguchi, L. Carlucci, D. M. Proserpio, G. Ciani, H. Kajiro, T. Ohba, H. Kanoh and K. Kaneko, *J. Am. Chem. Soc.*, 2007, **129**, 12362.
160 S. Henke, D. C. F. Wieland, M. Meilikhov, M. Paulus, C. Sternemann, K. Yusenko and R. A. Fischer, *CrystEngComm*, 2011, **13**, 6399.

161 T. R. Jensen, T. K. Nielsen, Y. Filinchuk, J.-E. Jorgensen, Y. Cerenius, E. M. Gray and C. J. Webb, *J. Appl. Crystallogr.*, 2010, **43**, 1456.
162 V. Bon, I. Senkovska, D. Wallacher, A. Heerwig, N. Klein, I. Zizak, R. Feyerherm, E. Dudzik and S. Kaskel, *Microporous Mesoporous Mater.*, 2014, **188**, 190.
163 C. Serre, S. Bourrelly, A. Vimont, N. A. Ramsahye, G. Maurin, P. L. Llewellyn, M. Daturi, Y. Filinchuk, O. Leynaud, P. Barnes and G. Ferey, *Adv. Mater.*, 2007, **19**, 2246.
164 T. K. Trung, P. Trens, N. Tanchoux, S. Bourrelly, P. L. Llewellyn, S. Loera-Serna, C. Serre, T. Loiseau, F. Fajula and G. Ferey, *J. Am. Chem. Soc.*, 2008, **130**, 16926.
165 P. L. Llewellyn, G. Maurin, T. Devic, S. Loera-Serna, N. Rosenbach, C. Serre, S. Bourrelly, P. Horcajada, Y. Filinchuk and G. Ferey, *J. Am. Chem. Soc.*, 2008, **130**, 12808.
166 P. L. Llewellyn, P. Horcajada, G. Maurin, T. Devic, N. Rosenbach, S. Bourrelly, C. Serre, D. Vincent, S. Loera-Serna, Y. Filinchuk and G. Ferey, *J. Am. Chem. Soc.*, 2009, **131**, 13002.
167 L. Hamon, P. L. Llewellyn, T. Devic, A. Ghoufi, G. Clet, V. Guillerm, G. D. Pirngruber, G. Maurin, C. Serre, G. Driver, W. van Beek, E. Jolimaitre, A. Vimont, M. Daturi and G. Ferey, *J. Am. Chem. Soc.*, 2009, **131**, 17490.
168 N. Rosenbach, Jr., H. Jobic, A. Ghoufi, F. Salles, G. Maurin, S. Bourrelly, P. L. Llewellyn, T. Devic, C. Serre and G. Ferey, *Angew. Chem., Int. Ed.*, 2008, **47**, 6611.
169 A. S. Munn, A. J. Ramirez-Cuesta, F. Millange and R. I. Walton, *Chem. Phys.*, 2013, **427**, 30.
170 L. Chen, J. P. S. Mowat, D. Fairen-Jimenez, C. A. Morrison, S. P. Thompson, P. A. Wright and T. Duren, *J. Am. Chem. Soc.*, 2013, **135**, 15763.
171 B. Van de Voorde, A. S. Munn, N. Guillou, F. Millange, D. E. De Vos and R. I. Walton, *Phys. Chem. Chem. Phys.*, 2013, **15**, 8606.
172 A. Boutin, D. Bousquet, A. U. Ortiz, F.-X. Coudert, A. H. Fuchs, A. Ballandras, G. Weber, I. Bezverkhyy, J.-P. Bellat, G. Ortiz, G. Chaplais, J.-L. Paillaud, C. Marichal, H. Nouali and J. Patarin, *J. Phys. Chem. C*, 2013, **117**, 8180.
173 T. Devic, F. Salles, S. Bourrelly, B. Moulin, G. Maurin, P. Horcajada, C. Serre, A. Vimont, J.-C. Lavalley, H. Leclerc, G. Clet, M. Daturi, P. L. Llewellyn, Y. Filinchuk and G. Ferey, *J. Mater. Chem.*, 2012, **22**, 10266.
174 R. I. Walton, A. S. Munn, N. Guillou and F. Millange, *Chem. – Eur. J.*, 2011, **17**, 7069.
175 F. M. Mulder, B. Assfour, J. Huot, T. J. Dingemans, M. Wagemaker and A. J. Ramirez-Cuesta, *J. Phys. Chem. C*, 2010, **114**, 10648.
176 S. Bourrelly, B. Moulin, A. Rivera, G. Maurin, S. Devautour-Vinot, C. Serre, T. Devic, P. Horcajada, A. Vimont, G. Clet, M. Daturi, J.-C. Lavalley, S. Loera-Serna, R. Denoyel, P. L. Llewellyn and G. Ferey, *J. Am. Chem. Soc.*, 2010, **132**, 9488.
177 J.-L. Bonardet, J. Fraissard, A. Gédéon and M.-A. Springuel-Huet, *Catal. Rev.: Sci. Eng.*, 1999, **41**, 115.
178 H. C. Hoffmann, M. Debowski, P. Müller, S. Paasch, I. Senkovska, S. Kaskel and E. Brunner, *Materials*, 2012, **5**, 2537.
179 M.-A. Springuel-Huet, A. Nossov, Z. Adem, F. Guenneau, C. Volkringer, T. Loiseau, G. Férey and A. Gédéon, *J. Am. Chem. Soc.*, 2010, **132**, 11599.
180 H. C. Hoffmann, B. Assfour, F. Epperlein, N. Klein, S. Paasch, I. Senkovska, S. Kaskel, G. Seifert and E. Brunner, *J. Am. Chem. Soc.*, 2011, **133**, 8681.
181 M.-A. Springuel-Huet, A. Nossov, F. Guenneau and A. Gédéon, *Chem. Commun.*, 2013, **49**, 7403.
182 X. Kong, E. Scott, W. Ding, J. A. Mason, J. R. Long and J. A. Reimer, *J. Am. Chem. Soc.*, 2012, **134**, 14341.
183 E. Stavitski and B. M. Weckhuysen, *Chem. Soc. Rev.*, 2010, **39**, 4615.
184 W. van Beek, O. V. Safonova, G. Wiker and H. Emerich, *Phase Transitions*, 2011, **84**, 726.
185 F. Salles, G. Maurin, C. Serre, P. L. Llewellyn, C. Knofel, H. J. Choi, Y. Filinchuk, L. Oliviero, A. Vimont, J. R. Long and G. Ferey, *J. Am. Chem. Soc.*, 2010, **132**, 13782.
186 S. Yang, L. Liu, J. Sun, K. M. Thomas, A. J. Davies, M. W. George, A. J. Blake, A. H. Hill, A. N. Fitch, C. C. Tang and M. Schröder, *J. Am. Chem. Soc.*, 2013, **135**, 4954.
187 H. Sato, W. Kosaka, R. Matsuda, A. Hori, Y. Hijikata, R. V. Belosludov, S. Sakaki, M. Takata and S. Kitagawa, *Science*, 2014, **343**, 167.
188 S. Bordiga, F. Bonino, K. P. Lillerud and C. Lamberti, *Chem. Soc. Rev.*, 2010, **39**, 4885.
189 J. Hafizovic Cavka, S. Jakobsen, U. Olsbye, N. Guillou, C. Lamberti, S. Bordiga and K. P. Lillerud, *J. Am. Chem. Soc.*, 2008, **130**, 13850.
190 Y. Chen, J. Zhang, J. Li and J. V. Lockard, *J. Phys. Chem. C*, 2013, **117**, 20068.
191 R. Grunker, I. Senkovska, R. Biedermann, N. Klein, M. R. Lohe, P. Muller and S. Kaskel, *Chem. Commun.*, 2011, **47**, 490.
192 F.-X. Coudert, M. Jeffroy, A. H. Fuchs, A. Boutin and C. Mellot-Draznieks, *J. Am. Chem. Soc.*, 2008, **130**, 14294.
193 A. Boutin, F.-X. Coudert, M.-A. Springuel-Huet, A. V. Neimark, G. Ferey and A. H. Fuchs, *J. Phys. Chem. C*, 2010, **114**, 22237.
194 A. Boutin, M.-A. Springuel-Huet, A. Nossov, A. Gedeon, T. Loiseau, C. Volkringer, G. Ferey, F.-X. Coudert and A. H. Fuchs, *Angew. Chem., Int. Ed.*, 2009, **48**, 8314.
195 A. Boutin, S. Couck, F.-X. Coudert, P. Serra-Crespo, J. Gascon, F. Kapteijn, A. H. Fuchs and J. F. M. Denayer, *Microporous Mesoporous Mater.*, 2011, **140**, 108.
196 F.-X. Coudert, C. Mellot-Draznieks, A. H. Fuchs and A. Boutin, *J. Am. Chem. Soc.*, 2009, **131**, 3442.
197 F.-X. Coudert, *Phys. Chem. Chem. Phys.*, 2010, **12**, 10904.
198 A. U. Ortiz, M.-A. Springuel-Huet, F.-X. Coudert, A. H. Fuchs and A. Boutin, *Langmuir*, 2011, **28**, 494.
199 A. V. Neimark, F.-X. Coudert, C. Triguero, A. Boutin, A. H. Fuchs, I. Beurroies and R. Denoyel, *Langmuir*, 2011, **27**, 4734.

200 A. U. Ortiz, A. Boutin, A. H. Fuchs and F.-X. Coudert, *Phys. Rev. Lett.*, 2012, **109**, 195502.
201 A. Ghoufi, G. Maurin and G. Ferey, *J. Phys. Chem. Lett.*, 2010, **1**, 2810.
202 C. Triguero, F.-X. Coudert, A. Boutin, A. H. Fuchs and A. V. Neimark, *J. Chem. Phys.*, 2012, **137**, 184702.
203 C. Triguero, F.-X. Coudert, A. Boutin, A. H. Fuchs and A. V. Neimark, *J. Phys. Chem. Lett.*, 2011, **2**, 2033.
204 S. Watanabe, H. Sugiyama, H. Adachi, H. Tanaka and M. T. Miyahara, *J. Chem. Phys.*, 2009, **130**, 164707.
205 S. Watanabe, H. Sugiyama and M. Miyahara, *Adsorption*, 2008, **14**, 165.
206 R. Numaguchi, H. Tanaka, S. Watanabe and M. T. Miyahara, *J. Chem. Phys.*, 2013, **138**, 054708.
207 F. Salles, A. Ghoufi, G. Maurin, R. G. Bell, C. Mellot-Draznieks and G. Ferey, *Angew. Chem., Int. Ed.*, 2008, **47**, 8487.
208 A. Ghoufi and G. Maurin, *J. Phys. Chem. C*, 2010, **114**, 6496.
209 V. Haigis, F.-X. Coudert, R. Vuilleumier and A. Boutin, *Phys. Chem. Chem. Phys.*, 2013, **15**, 19049.
210 F.-X. Coudert, A. U. Ortiz, V. Haigis, D. Bousquet, A. H. Fuchs, A. Ballandras, G. Weber, I. Bezverkhyy, N. Geoffroy, J.-P. Bellat, G. Ortiz, G. Chaplais, J. Patarin and A. Boutin, *J. Phys. Chem. C*, 2014, **118**, 5397.
211 B. Chen, C. Liang, J. Yang, D. S. Contreras, Y. L. Clancy, E. B. Lobkovsky, O. M. Yaghi and S. Dai, *Angew. Chem., Int. Ed.*, 2006, **45**, 1390.
212 Y. Hijikata, S. Horike, M. Sugimoto, M. Inukai, T. Fukushima and S. Kitagawa, *Inorg. Chem.*, 2013, **52**, 3634.
213 E. Quartapelle Procopio, T. Fukushima, E. Barea, J. A. R. Navarro, S. Horike and S. Kitagawa, *Chem. – Eur. J.*, 2012, **18**, 13117.
214 S.-i. Noro, Y. Hijikata, M. Inukai, T. Fukushima, S. Horike, M. Higuchi, S. Kitagawa, T. Akutagawa and T. Nakamura, *Inorg. Chem.*, 2012, **52**, 280.
215 S. Horike, Y. Inubushi, T. Hori, T. Fukushima and S. Kitagawa, *Chem. Sci.*, 2012, 116.
216 Y. Inubushi, S. Horike, T. Fukushima, G. Akiyama, R. Matsuda and S. Kitagawa, *Chem. Commun.*, 2010, **46**, 9229.
217 S. Yang, J. Sun, A. J. Ramirez-Cuesta, S. K. Callear, I. F. DavidWilliam, D. P. Anderson, R. Newby, A. J. Blake, J. E. Parker, C. C. Tang and M. Schröder, *Nat. Chem.*, 2012, **4**, 887.
218 J. Kim, W. Y. Kim and W.-S. Ahn, *Fuel*, 2012, **102**, 574.
219 R. El Osta, A. Carlin-Sinclair, N. Guillou, R. I. Walton, F. Vermoortele, M. Maes, D. de Vos and F. Millange, *Chem. Mater.*, 2012, **24**, 2781.
220 X. Y. Chen, H. Vinh-Thang, D. Rodrigue and S. Kaliaguine, *Ind. Eng. Chem. Res.*, 2012, **51**, 6895.
221 T. Remy, L. Ma, M. Maes, D. E. De Vos, G. V. Baron and J. F. M. Denayer, *Ind. Eng. Chem. Res.*, 2012, **51**, 14824.
222 C.-X. Yang, S.-S. Liu, H.-F. Wang, S.-W. Wang and X.-P. Yan, *Analyst*, 2012, **137**, 133.
223 K. Nakagawa, D. Tanaka, S. Horike, S. Shimomura, M. Higuchi and S. Kitagawa, *Chem. Commun.*, 2010, **46**, 4258.
224 F. Zhang, X. Zou, X. Gao, S. Fan, F. Sun, H. Ren and G. Zhu, *Adv. Funct. Mater.*, 2012, **22**, 3583.
225 P. Horcajada, R. Gref, T. Baati, P. K. Allan, G. Maurin, P. Couvreur, G. Ferey, R. E. Morris and C. Serre, *Chem. Rev.*, 2012, **112**, 1232.
226 A. C. McKinlay, J. F. Eubank, S. Wuttke, B. Xiao, P. S. Wheatley, P. Bazin, J. C. Lavalley, M. Daturi, A. Vimont, G. De Weireld, P. Horcajada, C. Serre and R. E. Morris, *Chem. Mater.*, 2013, **25**, 1592.
227 P. Horcajada, C. Serre, G. Maurin, N. A. Ramsahye, F. Balas, M. Vallet-Regi, M. Sebban, F. Taulelle and G. Ferey, *J. Am. Chem. Soc.*, 2008, **130**, 6774.
228 Q. Chen, Z. Chang, W.-C. Song, H. Song, H.-B. Song, T.-L. Hu and X.-H. Bu, *Angew. Chem., Int. Ed.*, 2013, **52**, 11550.
229 Y. Takashima, M. Martinez Virginia, S. Furukawa, M. Kondo, S. Shimomura, H. Uehara, M. Nakahama, K. Sugimoto and S. Kitagawa, *Nat. Commun.*, 2011, **2**, 168.
230 N. Yanai, K. Kitayama, Y. Hijikata, H. Sato, R. Matsuda, Y. Kubota, M. Takata, M. Mizuno, T. Uemura and S. Kitagawa, *Nat. Mater.*, 2011, **10**, 787.
231 A. Kondo, H. Noguchi, S. Ohnishi, H. Kajiro, A. Tohdoh, Y. Hattori, W.-C. Xu, H. Tanaka, H. Kanoh and K. Kaneko, *Nano Lett.*, 2006, **6**, 2581.
232 R. K. Das, A. Aijaz, M. K. Sharma, P. Lama and P. K. Bharadwaj, *Chem. – Eur. J.*, 2012, **18**, 6866.

